TOOLS FOR REAL TIME RELEASE TESTING (RTRt) IN BATCH AND CONTINUOUS TABLET MANUFACTURING

by

PALLAVI PAWAR

A dissertation submitted to the

Graduate School – New Brunswick

Rutgers, The State University of New Jersey

In partial fulfillment of the requirements

For the degree of

Doctor of Philosophy

Graduate Program in Chemical and Biochemical Engineering

Written under the direction of

Fernando J. Muzzio

And approved by

_____

_____

_____

_____

New Brunswick, New Jersey

MAY, 2016

ABSTRACT OF THE DISSERTATION

Tools for Real Time Release Testing (RTRt) in Batch and Continuous Tablet Manufacturing

By PALLAVI PAWAR

Dissertation Director:

Fernando J. Muzzio, Ph.D.

After 50 years of near-stagnation, pharmaceutical manufacturing is experiencing unprecedented scientific and technological innovation. There is a paradigm shift from testing product quality using lengthy off-line (and after-the-fact) assays to quality being tested during the process using online/ at-line measurements. This ability to evaluate and ensure quality of final product based on process data, geared towards making batch release decisions, is known as real time release testing (RTRt). Application of RTRt allows increased assurance of quality, greater manufacturing flexibility, reduced inventory, lesser end product testing, and lower laboratory and manufacturing costs.

In this work, RTR strategies were developed for different critical quality attributes (CQAs) such as Blend and Content uniformity (B.U. and C.U.), and tablet dissolution in

real- time. The utility of different sampling methodologies was investigated with the intention of extracting maximum information and reducing redundancy in data collection.

The first aim of this dissertation investigated the use of Near IR Spectroscopy (NIRS) for online monitoring of B.U. The second specific aim involved developing a RTR strategy to assess C.U. of tablets. NIRS was found to be an effective tool for expedited C.U. predictions enabling interrogation of a greater number of tablet samples. These extensive tablet C.U. studies provided a rigorous basis for assessing and verifying the various thief sampling and PAT methods and determining their relative accuracy and reliability.

A key component of a meaningful RTR strategy for most products is the ability to predict dissolution utilizing the available on/at-line sensing infrastructure. Specific aim 3 focused on using NIRS to develop a RTR strategy for dissolution prediction of tablets made from blends exposed to different levels of mechanical strain in batch processing. This effect of strain was also investigated using traditional approaches such as tensile strength and porosity measurements.

The fourth and final aim focused on using soft sensing combined with at-line Near IR measurements to predict dissolution of tablets manufactured in a continuous direct compaction (CDC) line. Individual dissolution profiles were predicted using this approach with a high correlation between the predicted and the observed dissolution profiles. This concluded the RTRt strategy for solid dosage manufacturing.

ACKNOWLEDGEMENTS

I would like to thank everyone who has been an integral part of my journey at Rutgers as I have worked on this thesis. I would like to extend my deepest gratitude to my thesis advisor, Fernando Muzzio, for his valuable guidance, meaningful insight into my research, and for providing me with wonderful and challenging opportunities throughout the course of my PhD. Fernando, thank you for helping me improve my presentation, communication, and writing skills. I would like to thank my committee members, Alberto Cuitino, Gerardo Callegari, and Ron Snee, for their valuable suggestions and feedback. A special thanks to Alberto Cuitino who guided me through various interesting projects. I would like to thank German Drazer for revising my manuscript in detail.

I would also like to thank National Science Foundation's Engineering Research Center for Structured Organic Particulate Systems (ERC-SOPS) for providing me with opportunities to interact with industry mentors, and help discuss and exchange ideas.

I would also like to thank my friends and colleagues at Rutgers for their immense love and support: Sarang Oka, Krizia Karry, Sara Koynov, Yifan Wang, Sebastian Escotet, Golshid Keyvan, Abhishek Sahay, Wei Meng, James Scicolone, Savitha Panikar, Bill Engisch, Bereket Yohannes, Thamer Omer, Anwesha Chaudhury, Juan Osorio, Athanas Koynov, Sejal Shah, Tushar Saraf, Kellie Anderson, Xue Liu, Koushik Sowrirajan. I would also like to thank Sarang Oka for all the useful discussions. I especially would like to thank Hee Joo, Dheeraj Reddy and Chandrakant Bandi for helping me with the laboratory experiments.

I would like to thank my parents, Dr. Pralhad and Dr. Deepti Pawar for having faith in me, and for motivating me in all walks of life. I wouldn't have been here, and would not have accomplished a tiny fraction of this without you two. I would like to thank my younger brother, Pawan Pawar, who has supported, encouraged, and at times advised me through this process. Growing up with you was so much fun. Last but not the least, a deepest thank you to my beloved husband, Suhas Aithal, for your understanding, patience, and love. You have been a rock-solid support in this journey. The past one year has been amazing thanks to you.

Table of Contents

List of Tables

List of Figures

Chapter 1. Introduction

1.1. Background

The pharmaceutical industry is among the most heavily regulated industries in the world. Because this industry makes products that may entail significant risk to human health, regulations related to drug efficacy and safety are of prime importance. For each product on the market, the relevant regulatory health authorities, e.g. Food and Drug Administration (FDA) in the USA, or European Medicines Agency (EMA) in Europe, define a set of quality criteria (critical quality attributes, CQAs) and their specific limits. Failure to adhere to these limits can lead to product and process failures. For example, in the case of solid dosage forms, tablets must exhibit adequate pharmacological efficacy, which is closely connected to the drug substance content in each tablet [1], to the disintegration properties [2] of the tablet into smaller particles after intake, and to the rate of release of the drug substance from the tablet or particles [3]. Thus, drug content is deemed a critical factor, and blend uniformity, content uniformity, and dissolution constitute some of the CQAs for most tablets.

In the last five years, the field of pharmaceutical process design has advanced rapidly, with an ever-increasing emphasis on materials science and process engineering principles. Continuous manufacturing (CM) has been introduced and embraced by industry, academia and regulatory bodies [4][5]. Distributed closed loop controls, once a distant aspiration, are beginning to be implemented in many solid dosage-manufacturing processes (Figure 1-1), primarily for control of product composition and mechanical

properties of the product such as weight and hardness [6]. However, to achieve full implementation of close-loop process control for all relevant quality parameters, the industry needs to complete the move from off-line product testing to on-line and in-line sensing. For solid dosage forms, the advances in process analyzers (e.g.: different spectroscopy tools) make real time control and quality assurance feasible.

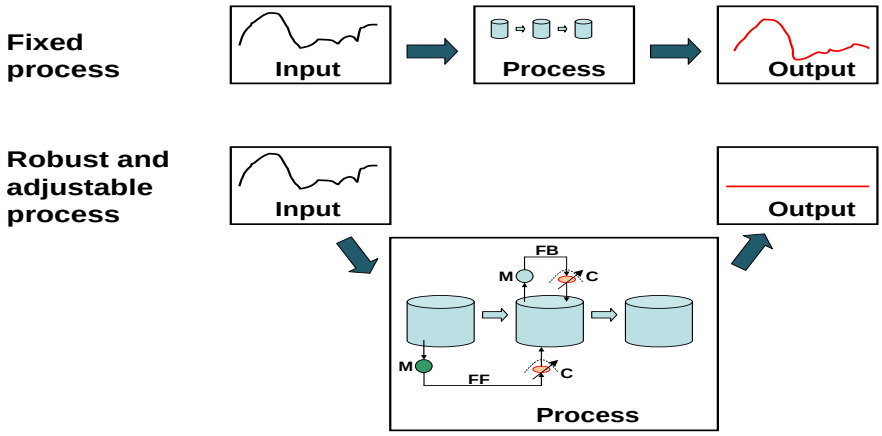

Figure 1-1: Comparison between traditional 'fixed process' pharmaceutical production (upper part of figure) and the PAT- based approach leading to adjustable process (lower part of figure). (M=measurement; C= controller; FB=feedback; FF= feedforward) [7].

Once real-time quality control is achieved in a robust and reliable manner, the same online measurements can be used to make product release decisions. This ability to evaluate and ensure quality of final product based on process data, geared towards making batch release decisions, is known as real time release testing (RTRt, also called RTR or RTRT) [8]. RTRt aims to predict the CQAs during the process, using "a valid combination of assessed material attributes and process control", without requiring lengthy off-line (and after-the-fact) assays. This is supported and encouraged by the Process Analytical Technology (PAT) guidance [9] published by the US Food and Drug

Administration, and the ICH Q8 guideline [8]. Application of RTRt allows greater manufacturing flexibility, reduced inventory, lesser end product testing, lower laboratory costs and better quality. A better quality product can result into higher yields, lower rework and lower rejection rates [10].Generally, an extensive amount of on-line/in-line data is gathered during RTR testing, and its analysis leads to higher assurance in product quality, as opposed to traditional release testing conducted on a limited number of samples [11].

Multivariate Data Analysis supports the real time release testing initiative [12]. For RTRt, product and process information is obtained by measuring different attributes of the intermediates and the final product. This data needs to be gathered from the system at the start of the process, at regular intervals, while it is running and at the end. This approach generates large amounts of data as a function of controlled variables (formulation and process parameters) and uncontrolled parameters (environmental). An example of data collection for a continuous solid dosage system is shown in

Figure **1-2**. Multivariate data analysis can be of use in such situations where the simultaneous and combined effects of more than two variables can be determined statistically.

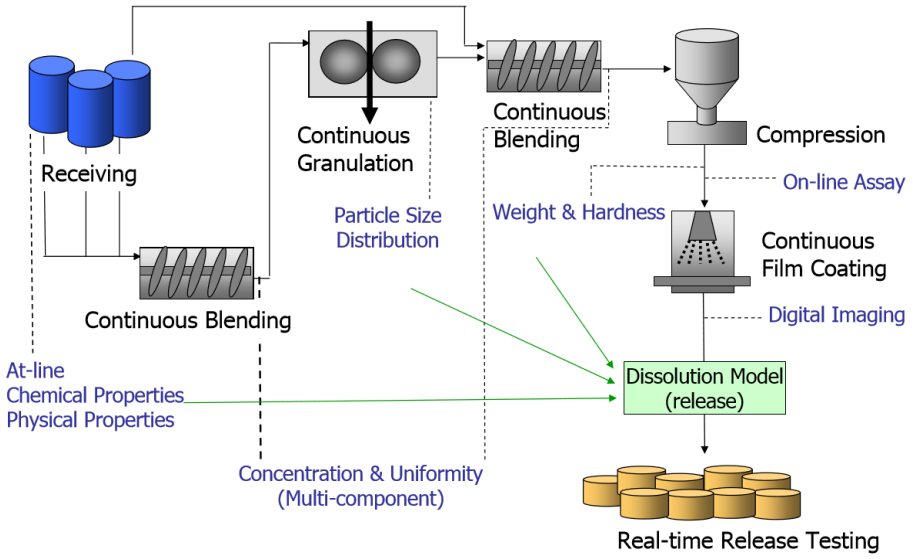

Figure 1-2: Real time release testing control strategy for continuous solid dose manufacturing. Courtesy of Dr. C. Moore (FDA), AAPS Annual meeting, Washington DC 2011

RTRt for different CQAs can be attained by a variety of measurements; online/in-line measurements (e.g.: for B.U.), fast at-line measurements (e.g.: for C.U.), and/or using mechanistic models (e.g.: for dissolution) as surrogate measurements for in-process or end product property (Figure 1-3). While applying the RTRt approach, a scientifically sound sampling strategy should be developed and implemented. Comparing different strategies can help determine the relationship between different sampling methodologies, extracting maximum information and reducing redundancy in data collection.

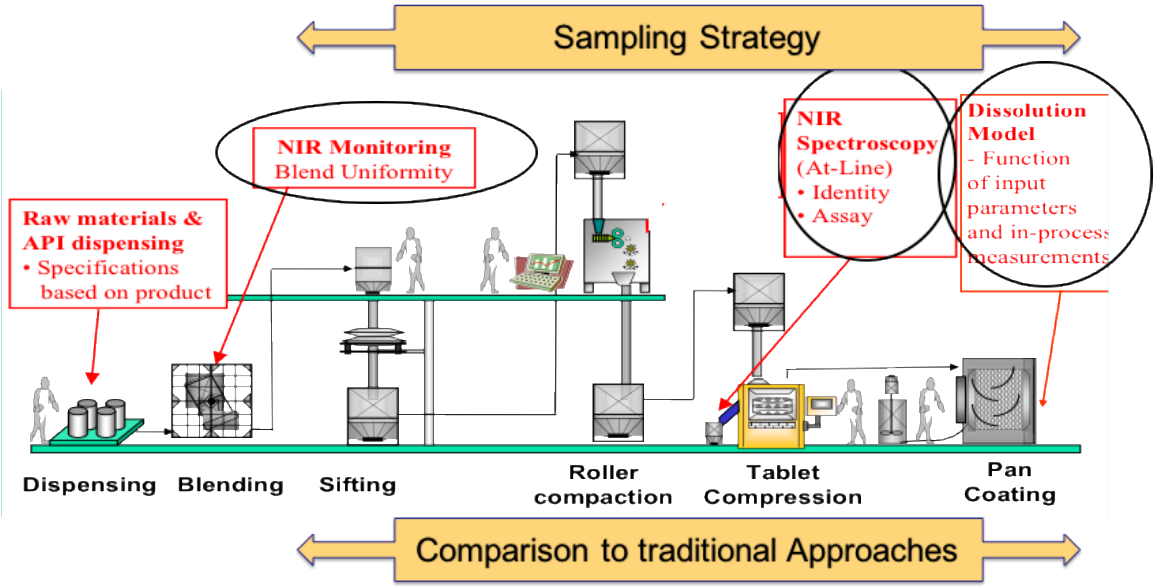

Figure 1-3:Unified approach used for RTRT in this work. Approaches for RTR for Blend Uniformity, Content Uniformity, Dissolution testing were developed for a Direct Compaction system.
Courtesy of Dr. C. Moore (FDA), AAPS Annual meeting, Washington DC 2011

As mentioned, some of the CQAs for direct compaction process includes BU, CU, hardness, and dissolution testing. Powder blending, a crucial unit operation in the manufacture of solid drugs, is instrumental in determining final dose drug content uniformity. Traditionally, the homogeneity of blends has been determined by drawing samples from the blend using various methods such as thief and scoop sampling [13]. Such intrusive sampling leads to errors introduced due to sample thief design, motion of the thief through the blend during sampling, sampling angle, thief orientation in the bed, depth of the powder bed, etc. [14]. In the last decade, the potential of Near IR spectroscopy has been explored for online blend uniformity monitoring [15]. This technique is fast, non- invasive and can provide useful physical and chemical information about the blend in real time. While blend uniformity is an important consideration, the pharmacological action in the body is determined by the attributes of the final dosage form. In fact, it is possible for

blends to de-mix (i.e., segregate) during subsequent processing [16], resulting in finished product of poor quality [17]. Traditional approaches for content uniformity testing employ wet chemistry techniques like High Pressure Liquid Chromatography (HPLC) [18][19], which are time consuming, require solvent and sample preparation, and cannot be used for real time quality control. Tools enabling in-process/at-line C.U. measurement or prediction can help save time, allow fast and extensive quality monitoring, ensure increased quality assurance, and help make batch release decision real time.

The ultimate aim of a tablet manufacturing process is to compress powder into a tablet of desired strength and drug release profile. Pharmaceutical companies are expected to perform *in vitro* dissolution testing to determine the drug release profiles [3]. Different studies have investigated the effect of compression speed [20][21], lubricant concentration [22][23][24][25][26] and nature of excipients [27] and pure drugs [28] on *in vitro* tablet dissolution. The dissolution test is intrinsically slow, time-consuming, expensive, and requires sample and media preparation. As such, this test cannot be used either as part of a Real Time Release strategy or for closed loop process control. Due to the above shortcomings, there has been growing interest in the use of non-destructive prediction of tablet dissolution that would remove one of the remaining obstacles to the widespread implementation of RTR testing[29], [30]. Two different approaches for dissolution prediction were investigated in this work; the first one used information gathered from NIR spectroscopy of tablets to predict dissolution, and the second utilized information gleaned from tablet NIR in combination with drug release mechanistic models to predict dissolution.

1.2. Organization of the dissertation

In this dissertation, approaches were developed for real time release testing of tablets by using knowledge of material attributes, process measurements and information gleaned from PAT sensors to predict the CQAs in real time. Thus, the overall aim of the work was to determine online measurements and sampling techniques that could be used to assure blend and content uniformity for both batch and continuous processes, to use these online techniques to capture the effects of process parameters, including blend shear history, compaction pressure, scale of operation and formulation parameters on the properties of the final dosage form, and ultimately to predict drug release from the tablet. A scientific evaluation of the relative performance of various traditional and modern real-time process monitoring approaches was performed. This will aid in the migration from traditional end product testing approaches to real-time release strategy.

After introducing materials and methods used in this work (Chapter 2), the issues described above were addressed by a research plan comprised of the following specific aims:

Specific Aim 1: Real Time blend uniformity prediction in batch manufacturing (Chapter 3)

Specific Aim 2: RTRt for assessing content uniformity and comparison of different sampling strategies (Chapter 4 and 5)

Specific Aim 3: Towards dissolution prediction of tablets exposed to different levels of over lubrication in batch process (Chapters 6 and 7)

Specific Aim IV: Mechanistic models combined with Near IR spectroscopy for tablet dissolution prediction in Continuous Manufacturing (Chapters 8)

This work represents a first attempt to integrate all of these techniques into a unified strategy to enable RTRt for Direct Compaction formulations (DC). The work described here can be expanded in many directions, including other techniques for RTRt, a broader strategy to consider other dissolution mechanism governing different formulations, expansion of RTRt tools to WG and DG manufacturing processes, etc. These directions are briefly described in Chapter 9, which focuses on conclusions and recommendations for future work (by other students).

Chapter 2. Experimental Platform designs and methodology for enabling Real Time Release testing (Materials and methods)

2.1. Introduction

Achieving real time release goals requires well-designed manufacturing platforms that assure product quality, appropriate fixtures to facilitate PAT testing, and data collection technologies that enable accurate, efficient, relevant, and timely data acquisition. Traditionally, the pharmaceutical industry has developed and manufactured products using batch operations. The reluctance of the pharmaceutical industry to make changes in manufacturing has led to process rigidity, outdated production lines with old equipment designs, resulting into compromised product quality, greater rejection rates, and drug shortages [31]. In an attempt to modernize drug manufacturing, under the FDA's Pharmaceutical Quality for 21st Century Initiative, the industry is slowly shifting gears towards maximally efficient, agile, flexible platforms equipped with modern equipment and effective monitoring technologies [32]. The introduction of continuous manufacturing has shown the potential to achieve higher yields, lower operating, inventory and capital costs, reduced variability, and achieve a more consistent quality [33]. However, shifting to continuous manufacturing requires a complete infrastructure overhaul involving a shift from the extensive existing batch asset- base [34]. Extensive skilled work force training, developing new generations of equipment, installation of sensors and automation to support continuous manufacturing are some of the other key challenges [35]. Keeping this transition in mind, two different platforms were used in this study; a flexible, modular experimental station capable of blending and compressing a

representative range of formulations under multiple conditions, and a direct compression continuous manufacturing platform that is representative of the designs that have been implemented in many industries.

2.2. Materials and Equipment

2.2.1. Materials

The work in this thesis was performed using two APIs; Phenytoin Sodium and Acetaminophen (APAP). The active pharmaceutical ingredients (API) were selected for their representativeness. The first API was Phenytoin Sodium (RIA International, mean particle size 20 microns), an anti- epileptic drug with a narrow therapeutic index and reported history of C.U. issues. This drug was chosen to maximize the public health impact of our studies. Semi fine Acetaminophen (Mallinckrodt Inc. Raleigh, NC, mean particle size 42 μm) was chosen for the later part of the work. It is a representative model drug, and its compaction and flow properties compare well to a majority of the APIs in the industry, allowing extension of the observations across the range of drugs. An abundantly available drug, APAP has poor compressibility and extensive elastic deformation, leading to different structural problems like capping, chipping, etc. Hence, there is a need to study the material in the case of direct compression systems and provide some immediate guidelines on RTR to industry.

2.2.2. PAT Platform

A flexible, modular blending platform (Figure 2.1) was constructed for the first part of the study. It consisted of a 2 cu. feet v- blender (Patterson Kelley) connected to a 36-station tablet press (Kikusui Libra) with the help of an in- house fabricated chute. Brimrose Luminar 5030 handheld NIR spectrometers (Brimrose Corp., USA) were

mounted on each of the arms of the V-blender. At the end of each blending cycle, samples of the blend were taken from the v- blender with the help of a Globe Pharma thief sampler (GlobePharma, New Brunswick, New Jersey). The powder was discharged to the tablet press hopper through the chute. The speed of the tablet press was kept constant at 25 rpm. A JDSU 1700 Micro NIR spectrometer was mounted on the chute to monitor the blend flowing through the chute. The tablets obtained from the tablet press were analyzed using NIR transmission mode as well as content uniformity using traditional HPLC method.

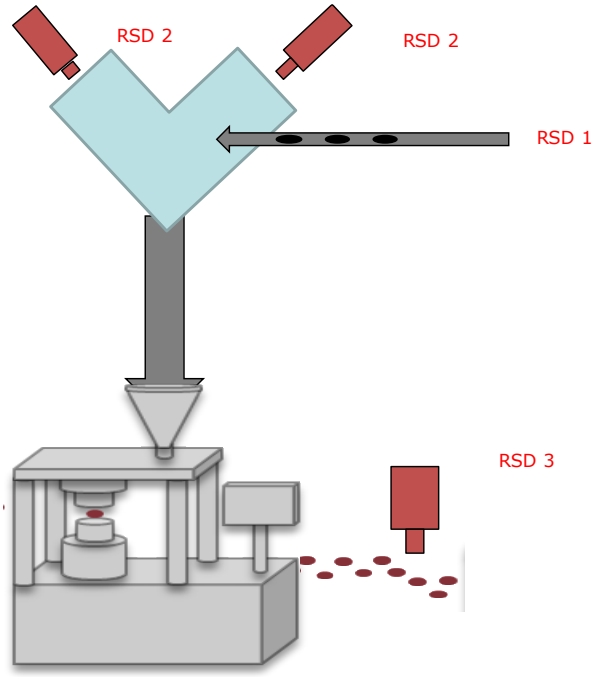

Figure 2.1: Blending platform- Blend uniformity is monitored with two Near IR spectrometers mounted on the blender (RSD2). The thief samples withdrawn from the blend give RSD 1. Content uniformity measured from tablets coming out of the tablet press (RSD 3)

This scale of operation represented an optimum compromise between competing needs – the system needed to be large enough that results were meaningful to the manufacturing scale, but not so large as to make experimentation prohibitively expensive.

A step-by-step approach was taken to develop tools to predict blend uniformity and content uniformity. The calibration and validation approaches for blending and tablet analysis are highlighted in Figure 2.2. A calibration model was constructed from the analysis of small-scale blends of known concentration. The same blends were then compacted into tablets that were analyzed to build a calibration model for content uniformity. The usefulness of a tablet calibration model was that once in place and validated, it was used to scan tablets created from blends of the target formulation and provide information about the distribution of concentration for a large number of tablets. The calibration set was updated using the samples from the pilot scale runs to encompass the effect of the change in scale and process in the final calibration model thus produced.

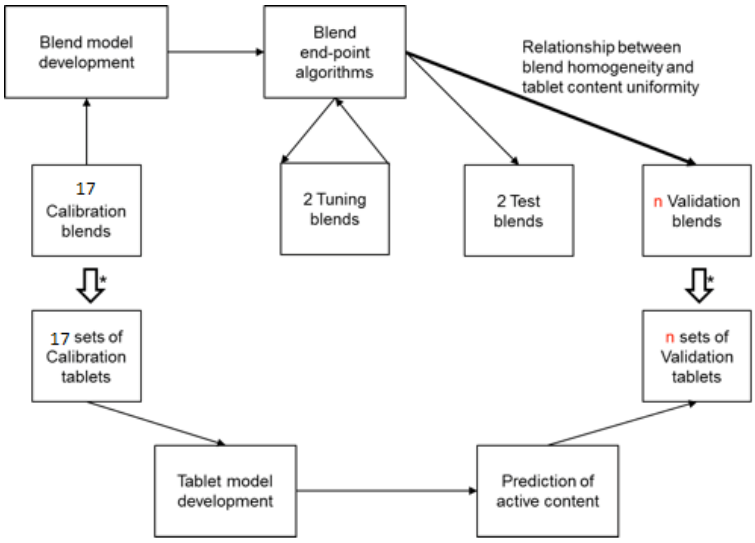

Figure 2.2: Flowchart representing steps taken to generate calibration models, validation approach, and the use of these models to predict BU and CU.

All of the characterization methods (thief sampling, PAT, CU) were used simultaneously in order to minimize experimental error and statistical uncertainty and maximize comparability of the different methods.

2.2.3. Lab Scale Shearing and Tableting Platform

The third aim in this dissertation involved implementing an RTR strategy for tablets made from over-lubricated blends in a lab scale batch process. The first step was to over-lubricate blends by exposing them to a controlled shearing environment, followed by compacting the blends on a tablet press simulator using a Presster (Presster^{TM}, MCC, East Hanover, NJ). The use of the tablet press emulator allowed measuring and recording compaction profiles of individual tablets.

Over-lubrication was achieved by exposing the blend to a uniform and controlled shear environment for a pre-determined amount of time. This was achieved in a modified Couette cell (Figure 2.3), which consisted of two concentric cylinders that rotated relative to each other creating a shearing action. The equidistant baffles were uniformly spaced and the entire setup creates a uniform shear environment on the powder. Mehrotra *et al.* [36] observed that the cell promoted micro mixing of the ingredients by a dispersion mechanism, increasing the blend homogeneity. The amount of energy that was put into the blend was measured by measuring the resistance offered (in the form of torque) by the powder to the motion of the cylinders.

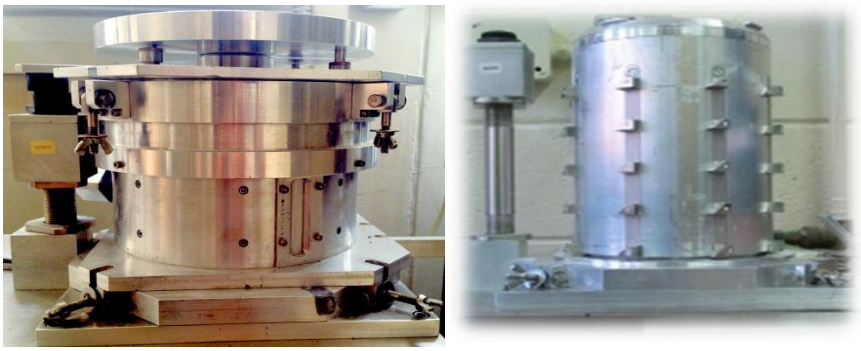

Figure 2.3: Shearing device used to impart uniform shear on blends. Inside cylinder of the Couette shear cell assembly with the baffles (right) The blend is poured in the annular region and the cylinders move relative to each other imparting the shear

Tableting

Blend samples were compressed into tablets using Presster (Figure 2.4), a tablet press emulator (Presster^{TM}, MCC, East Hanover, NJ), which was set to emulate Kikusui Libra2 tablet press. The compaction force, ejection force and dwell time for each tablet was displayed at the end of each tablet compaction. The simulated press was a Kikusui Libra2 with both pre-compression and compression rolls of 200 mm diameter. The speed was kept constant at 20 rpm. Flat-faced punches and round dies were used to obtain round tablets of 10 mm diameter. The dosing position was adjusted and fixed to give tablets of a certain weight. Tablets were made at an average targeted force by changing the compaction gap.

Figure 2.4: Lab Scale blends were compressed using Presster, a rotary press emulator.

2.2.4. Continuous Direct Compaction Platform

The last part of the studies in this work, aimed towards the development of RTR methods for dissolution prediction, were conducted in a continuous direct compaction line at Rutgers University (Figure 2.5). The aim was to predict the dissolution performance of tablets exposed to different processing and formulation conditions in the continuous direct compaction line. The manufacturing line consisted of two feeders from Coperion-KTron (Sewell, NJ), a KT20 and a KT35 used for feeding APAP and Lactose, respectively. Magnesium stearate was fed through a MT12 feeder (K-Tron). The production rate was kept constant at around 20kg/hr. The feed rate in the feeders was adjusted to obtain the desired concentrations of individual raw materials. The APAP and the Lactose were fed into a Quadro S197 Comil, which was used to delump the active and the excipient. Magnesium Stearate was fed directly into the blender near its inlet to avoid over-lubrication in the mill.

These ingredients were then fed into a Glatt GCG 70 mixer with 24 blades arranged in the "1/3 forward + 1/3 alternate + 1/3 forward" blade configuration. In this blade configuration, only the middle 1/3rd (or blades 9-16) are alternated forward 45° and backward 45°. This blade pattern was chosen based on a previous study, which concluded that, the "1/3 forward" configuration yielded improved mixing performance without sacrificing throughput [37][38].

After passing the blend through the mixer, the blend passed through a chute into a tablet press. A 36-station Kikusui Libra2 tablet press was used in a single layer configuration. The press was fitted with a type B flat tooling to make tablets of 10 mm diameter. The fill depth was adjusted to obtain 350 mg tablets. The press was operated at a variable feed-frame speed but a constant turret speed of 20 rpm for the 20kg/hr flow rates. After each step change, the system was allowed to reach steady state. The time required to attain steady state depended on the targeted mass flow rate in the line and the residence time of the blend in each unit operation. The experiments corresponding to the three different API concentrations were run on three separate days. After switching the processing conditions to a new design, tablets were collected after a time interval of 15 minutes. Point. 10 tablets were collected each condition.

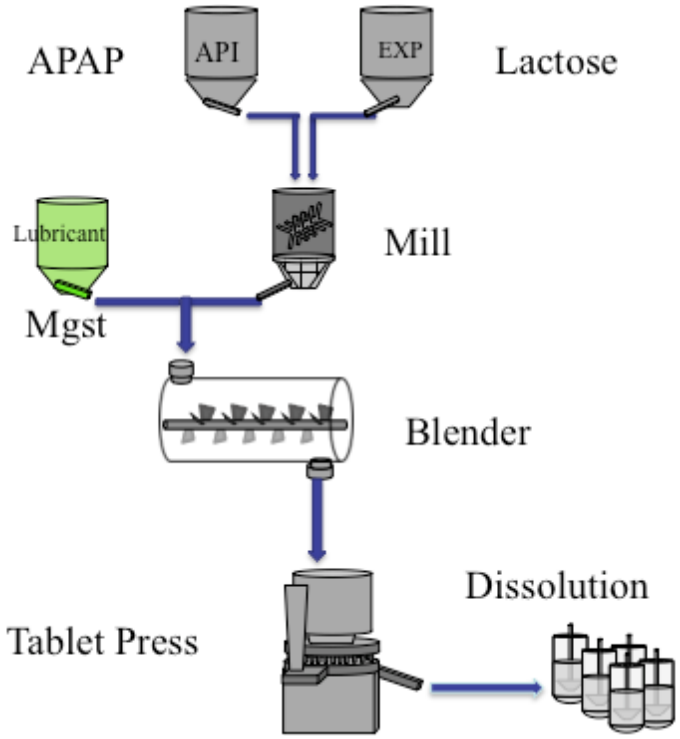

Figure 2.5: Continuous direct compaction manufacturing line

2.3. Methodology

Information obtained from a process is often contained in different types of data, including spectral output from different types of spectroscopic analyzers; point measurements (i.e., thermocouples), and instantaneous values of process parameters (impeller speeds, compression forces). Interpreting this complex data is difficult, unless multivariate methodologies are employed to reduce dimensionality, eliminate redundancies, and extract critical process knowledge. Multi Linear Regression (MLR), Principal Component Analysis (PCA), and Partial Least Square Regression (PLS) are the most commonly used tools for extracting usable information from process data.

2.3.1. Multi Linear Regression

Multi linear regression attempts to model the relationship between more than one regressor variables (X) and response variable (Y) by fitting a linear equation to the observed data.

$$\boldsymbol{Y = \beta_0 + \sum_{i=1}^{n} \beta_i x_i + \varepsilon} \qquad \textbf{Equation 2-1}$$

where β is the regression coefficient and ε is the error term. MLR has several advantages. MLR methods are relatively simple to construct, easy to understand and communicate, since each *x* variable in the model can often be related to certain physical or chemical property of the sample [39]. The disadvantage of MLR is that the regressor variables may be collinear and over fitting can result into poor predictive power of the model. In this work, care has been taken to ensure that the regressor variables are orthogonal to each other and that no collinearity exits between them.

2.3.2. Principal Component Analysis

Principal Component Analysis is a data compression algorithm that reduces a data set (*X*) collected on *M* variables over *N* samples to a simpler lower dimensional set of compressed variables (*K*<<*M*) designated as principal components (PCs) [40]. The mathematical model for the data set *X* can be written in terms of a set of scores (*T*) and loading (*P*) of *K* principal components, and the remaining variability is expressed as the residual noise (*E)*.

$$\boldsymbol{X = TP^t + E} \qquad \textbf{Equation 2-2}$$

The scores represent the intensities of each of the *K* new variables for the *N* samples; loadings *P* can be thought of as the weight of the new *K* variables in terms of the *M* original variables. The first extracted principal component captures the highest amount of variability in the data set, followed by subtraction of that component's contribution from

the data set for the calculation of the next PC. The principal components thus extracted are orthogonal to each other. The number of PCs are chosen such that the key information from dominating sources of variability is captured. The NIR data obtained for a sample carries information about the processing and formulation history that the sample has been exposed to. In this work, PCA has been used as an exploratory tool to look for features/ patterns / clusters in the data set obtained from Near IR Spectroscopy and to extract information about the sample history.

2.3.3. Partial Least Squares regression

PLS is the most commonly used multivariate regression method used for quantitative determination of the attribute of interest (*Y*) from the observations (*X*), and has been found to be a very robust technique [41]. In this work, PLS is applied to the spectroscopy data to obtain measurements that enable real time release testing [12]. Like PCA, PLS method follows exact same mathematical models for describing the *X* data. The only difference is that the data compression in *X* and *Y* data set is attained such that maximum variance in both *X* and *Y* is explained. The Principal Components are selected as those directions that explain the largest amount of variance in *X* that is directly related to the variance in *Y*, and are often called as Latent Variables (LV). PLS is susceptible to data over fitting and as such, the number of latent variables are carefully chosen based on testing the capability of the model to predict independent data sets. PLS, however, has a limited advantage for qualitative interpretation, since the information conveyed by the latent variables is abstract and rarely expresses pure physical or chemical phenomena. The beauty of PLS lies in the fact that the LVs are more relevant to prediction of the response *Y* than the previous discussed methods.

2.4. Conclusions

Three different platforms used for carrying out the experiments aimed towards real time release testing were described. These platforms ranged from lab scale batch setup to pilot scale batch tablet production to direct compaction of tablets using continuous manufacturing line. The lab-scale shearing and tableting setup was used for carrying out over lubrication experiments for developing the RTR strategy for batch samples. The lab scale platform allowed optimal utilization of the limited quantity of the available APIs. The pilot-scale PAT platform was used for developing RTR strategy for B.U. and C.U. The lab-scale blending- compaction platform combined with the pilot scale PAT platform was used to obtain calibration samples used for building the B.U. and C.U. calibration models. This included a step-by-step approach for model building and validation, starting from the samples obtained from the small scale setup moving to the pilot scale samples. The inclusion of samples made at different scales helped to capture the variability arising due to differences in scale of operation during model building (Figure 2.2).

Different data analysis algorithms used to process the vast amount of data generated during the different studies were explained. Tools to extract qualitative (PCA) and quantitative (MLR and PLS) information from the spectroscopic data can help reduce the dimensionality of the problem, reduce noise and predict the responses of interest. The choice of the data analysis method depends entirely on the expected outcome. The methods in this work were carefully chosen keeping in mind the problem statement and the target goal.

Chapter 3. Real Time Blend Process Monitoring and Blending End point detection using Near-Infrared Spectroscopy

3.1. Introduction

Phenytoin is a narrow therapeutic index (NTI) active pharmaceutical ingredient (API), widely prescribed for the treatment of epileptic seizures. Intuitively, achieving target and acceptable content uniformity of such NTI drug products is a public health priority. In case of severe or debilitating diseases (epilepsy), any change in efficacy or safety may result into serious or fatal complications. Studies around Phenytoin have focused on enhancing the drug solubility with salt formation [42], developing sustained release formulations [43], and studying and improving its bioavailability [44] [45] [46]. Phenytoin Sodium, a Phenytoin salt with enhanced drug solubility, is the active ingredient in commercially available oral extended release formulations. Problems have been reported about blend and content uniformity (CU), and about bio equivalence studies for the generic manufactured Phenytoin Sodium formulations [47] [48] [49]. This makes the study of Phenytoin sodium blends and tablets extremely important.

Powder blending, a crucial unit operation in the manufacture of solid drugs, is instrumental in determining final dose uniformity. The ultimate goal of a blending operation is to yield a homogenous blend. Achieving blending and content uniformity is highly important for formulations containing Narrow Therapeutic Index (NTI) drugs. Thief sampling is generally used for the analysis of blend uniformity [13]. Different groups like Harwood and Ripley [14], and Muzzio *et al.* [50] found that the analysis was

affected not only by the thief geometry like thief probe tip, but also by the powder properties. It has been observed that the selection of one sample affects the selection of other samples from the lot. This can be the main source of variability, and can also introduce systematic deviations (i.e., non-existent but nonetheless detected sub- or super-potency) usually termed as bias. Bias could arise from disturbances of the powder bed by the insertion of a sampling probe, also leading to localized segregation. Carstensen and Rhodes [51] verified this fact. Berman *et al.* [13] compared performance of two designs of thieves and demonstrated that the insertion of the thieves caused bed disturbances leading to size segregation. Muzzio *et al*. [50] used glass beads of different sizes to compare three different sampling thieves. Garcia *et al.* [52] suggested that the choice of the thief should depend on the type of the formulation. The thief samples are usually analyzed chromatographically or spectroscopically, which often are slow, labor-intensive techniques and require the use of solvents and reagents.

In the last decade, the use of Near IR spectroscopy has been explored for online blend uniformity monitoring [15]. This technique is fast, non- invasive and provides useful physical and chemical information about the blend in real time. This is in accordance with the FDA PAT guidelines, which encourage analyzing blend samples at-line, on-line or in-line [53] [54]. Some of the earlier efforts have focused on predicting the concentration of the active in a binary and multi- component system [55] [56]. Wu *et al.* used NIR to quantify different ingredients of the blend using a laboratory scale Turbula mixer [57]. Different algorithms have been employed to test the blending end point. Qualitative methods estimate the difference between two spectra recorded during a process; blend end- point is reached when no further evolution is observed between the

spectra over time [58], [59]. Quantitative approaches rely on developing multivariate regression models to predict concentration of constituents in the blends [60] [61]. The advantage of the quantitative approach is that the changes in homogeneity over time, and the deviation of the predicted values from the target concentration, can be quantified. While developing quantitative models, the choice of reference samples and values becomes important. HPLC/ UV values for samples withdrawn from powder beds using thief samples have been used as reference values [62]. However, with the problems associated with thief sampling, assigning these reference values to NIR blend scans can be misleading. Berntsson *et al*. demonstrated that recording the multiple spectra for calibration blends and averaging them was representative of the actual chemical content in the blend [25].

In this work, a PAT method was developed to monitor the blending operation and achieve dynamic control (e.g., operational endpoint determination) of blends containing Phenytoin Sodium, a NTI drug. This is a first reported attempt to characterize blend uniformity for Phenytoin Sodium using PAT methods. A DoE approach was undertaken to encompass the effects of excipient concentration variability on NIR spectra. The effects of scale changes were given due attention during model building. The data generated from monitoring the operational control was fundamental in 1) evaluating the progress of blending, and 2) predicting manufacturing performance.

3.2. Materials and methods

3.2.1. Materials

A drug with a narrow therapeutic index, Phenytoin sodium, was chosen to maximize the public health impact of this study. Different blends were made with Phenytoin sodium (RIA International) as the active pharmaceutical ingredient (API), microcrystalline cellulose (Vivapur PH 102, JRS Pharma, Germany), and lactose monohydrate fast-flo NF (Foremost) as the excipients and Magnesium Stearate NF (Mallinckrodt) as the lubricant. The target formulation consisted of 15% API, 40.5% MCC and lactose, and 4% MgSt

3.2.2. Experimental design

An experimental design for the lab scale blending was built around the target formulation- 15% API, 40.5% of Lactose, 40.5% MCC and 4 % MgSt (blend O). The target formulation was blended for 60 min. The 3-factor inscribed central composite experimental design contained 17 calibration blends (Table 3-1). The variables selected were concentration of the API (12% to 18%), lactose and MCC (28.35 to 52.65%), and MgSt (2 to 6%). Three repeats of the center point were included.

Table 3-1: DOE for calibration blends. 3 factor inscribed central composite design with API ranging from 12% to 18% and three replicates of center point.

Run ID	Trial ID	Phenytoin	MCC 102	Lactose Monohydrate	MgSt
15	A	13.22	33.28	50.69	2.81
5	B	13.22	33.28	48.31	5.19
17	C	13.22	47.72	36.25	2.81
13	D	13.22	47.72	33.87	5.19
16	E	16.78	33.28	47.13	2.81
11	F	16.78	33.28	44.75	5.19
12	G	16.78	47.72	32.69	2.81
4	H	16.78	47.72	30.31	5.19
8	I	12	40.5	43.5	4
14	J	18	40.5	37.5	4
10	K	15	28.35	52.65	4
9	L	15	52.65	28.35	4

2	M	15	40.5	42.5	2
6	N	15	40.5	38.5	6
1	O	15	40.5	40.5	4
7	P	15	40.5	40.5	4
3	Q	15	40.5	40.5	4

Six formulations, I, J, N, M, O1 and O2 from table 1 were run on the pilot-scale. Blends O1 and O2 contained the same ingredient concentration but differed with respect to mixing time, where O1 was blended for 30 min and O2 was blended for 60 minutes. The first five batches were a part of the calibration set, whereas blend O2 was the test set.

3.2.3. Blending

Lab Scale Blending: Small-scale calibration blends (150g) were made for each design point in plastic containers (fig 1a). The blending was carried out for 30 min at 15 rpm using a small-scale V-blender. The containers were placed along the mixing axis of the blender (Figure 1) to simulate the V-blender mixing dynamics. This setup ensured appropriate use of the limited quantities of available API. This was followed by acoustic mixing (30 g's, 30% intensity, 20 seconds) using a Resonant Acoustic Mixer (Resodyn Acoustic Mixers, Butte, Montana, USA) to break down any agglomerates in the powder mixture. Osorio *et al*. characterized the blender and determined its efficiency for micro-mixing of cohesive ingredients [64]. The mixing time was determined from a PCA analysis of previously collected NIR data, where after mixing for 30 minutes, minimal difference in the spectral data was observed (based on PCA score analysis).

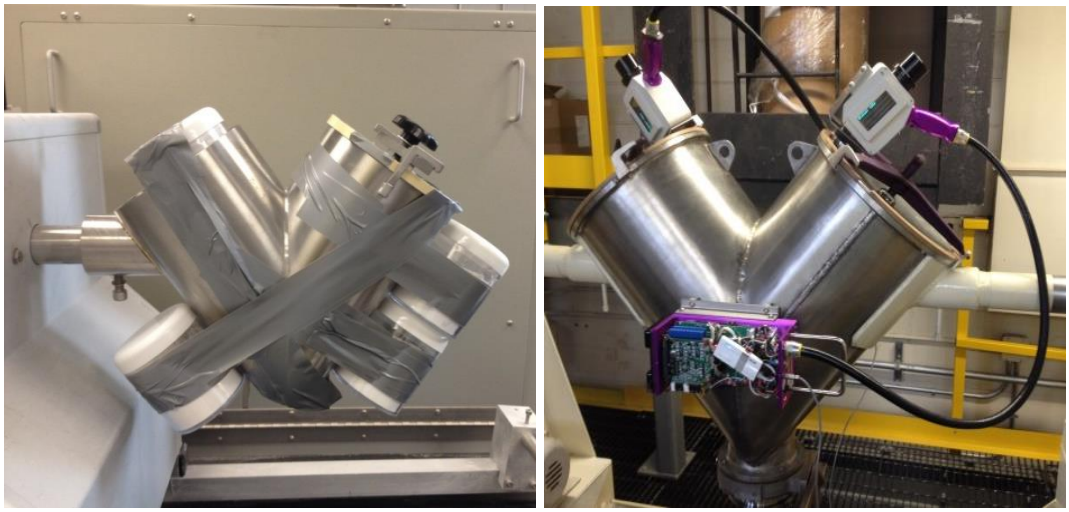

Figure 3-1: a) Small scale calibration blends (left figure). Each container represented a unique blending design point. b) Pilot-scale blending operation with NIR mounted on the blender lids.

Pilot plant scale blending:

The pilot-scale blending operation involved a 50 % fill volume of a 56- liter V-bender (Figure 1 b). The powder bulk density was 0.62 g/ml and a batch size of 18 kilos was used. The blender had a fixed rotational speed of 25 RPM. The amount for individual components was calculated based on the design concentrations and the batch size. The powders for the formulations were loaded from the lower opening of the blender in a bottom to top fashion and blended for 30 minutes. The target formulation, O2, was blended for 60 minutes.

3.2.4. Near IR Spectroscopy data collection

Post-blending, the seventeen lab-scale calibration blends were scanned offline using two Brimrose 5030 spectrometers. The calibration blend was poured on the window of the first spectrometer and a total of ten NIR spectra were acquired over a wavelength range

of 1100 nm to 2200 nm, with a 1 nm step. The spectra were collected using two different data collection configurations (dynamic and static). In the dynamic configuration, 2 scans were averaged to get a spectrum, whereas, in static configuration, 64 scans were averaged to get one spectrum. The powder was then scooped out and poured back onto the same window, to collect a second set of ten spectra each configuration, for the same blend. Thus, a total of twenty spectra per blend per spectrometer, per design point, per data collection configuration were obtained. Later, this strategy was used to collect data at the second spectrometer, and followed for all the remaining design points. This gave rise to a total of 340 (17 design points X 20 spectra) dynamic configuration spectra and 340 static configuration spectra per spectrometer. During data collection, enough powder was poured on the window to achieve an optically infinite medium, in order to avoid light leakage for reflectance spectroscopy. For the purpose of calibration, gravimetric values (from DOE) were used as the reference values.

In the pilot-scale process, Near IR spectrometers mounted on the blender lids collected real-time data for the blends I, J, N, M, O1 and O2. Based on the data collection and the blender rotation speed a trigger period of 200 milliseconds was used. Each spectrum was averaged over 2 scans (similar to the dynamic configuration).

3.3. Results and Discussions:

The samples used for calibration development were unique samples from the small scale blending effort. A global calibration approach was utilized, where the data collected from the two spectrometers was combined to yield a global calibration matrix. Figure 3-2 represents the raw spectra collected for each blend; unique baselines are apparent for the

two spectrometers (red and blue). A greater scan averaging (64 co-adds) led to a decrease in the unstructured noise in the spectra obtained using static configuration. A superior signal- to- noise ratio was observed for the 680 static spectra (right figure) and were used for calibration modeling.

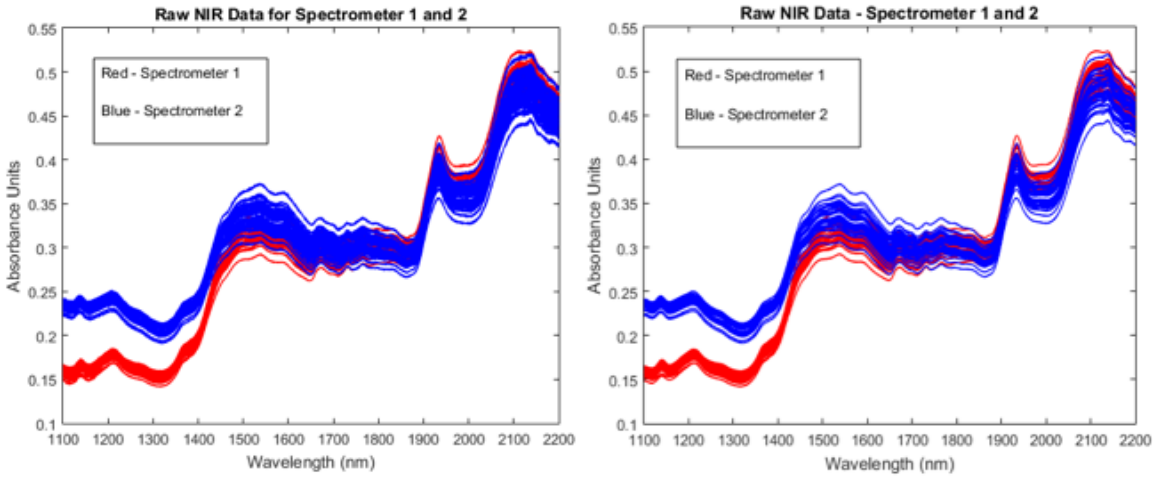

Figure 3-2: Raw Calibration data is depicted (left-dynamic configuration, right-static configuration). The static configuration spectra were observed to be less noisy. The two colors represent the NIR data corresponding to the two spectra collected using different spectrometers.

The NIR spectra was pretreated using the Savitzky-Golay (SG) Smoothing and Derivative (15-point window, 2nd order polynomial, 1st derivative) and mean centering algorithm to minimize the slope and baseline differences. Figure 3-3 represents the data after the pretreatments were applied.

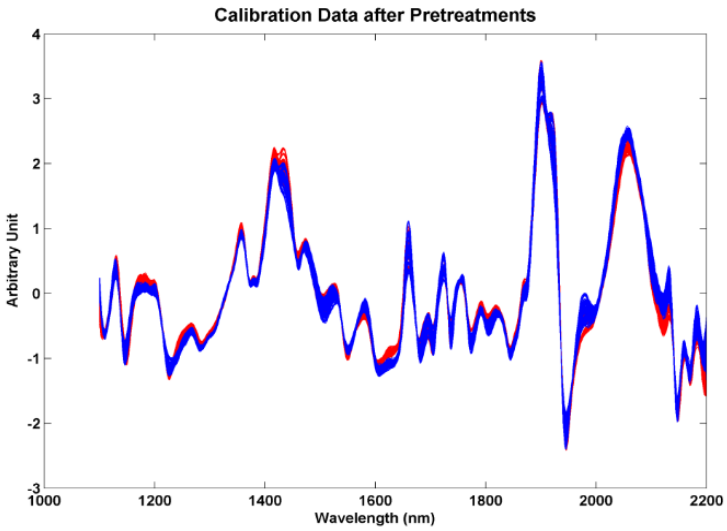

Figure 3-3: Pretreated Calibration Data; SG first derivative and mean centering. Baseline and slope differences were minimized.

Principal Component Analysis

To better understand the sources of variation, the NIR data was subjected to a Principal Component Analysis (chapter 2, section 2.3.2). The other objective of using the PCA was to compare the spectral spaces of the two data collection configurations, static and dynamic. For this, the static configuration spectra were used as the calibration set and the dynamic configuration spectra was used as the test set.

The PCA was observed to capture 96.48% of the total variability in the calibration data set. PC1 captured 51% of the total variance, which was attributed to the differences in the spectrometers (Figure 3-4 (a)). This residual variability associated with the differences in the spectrometers was observed in the form of peak shifts at 1150 nm and 2150 nm (Figure 3-4 (b)).

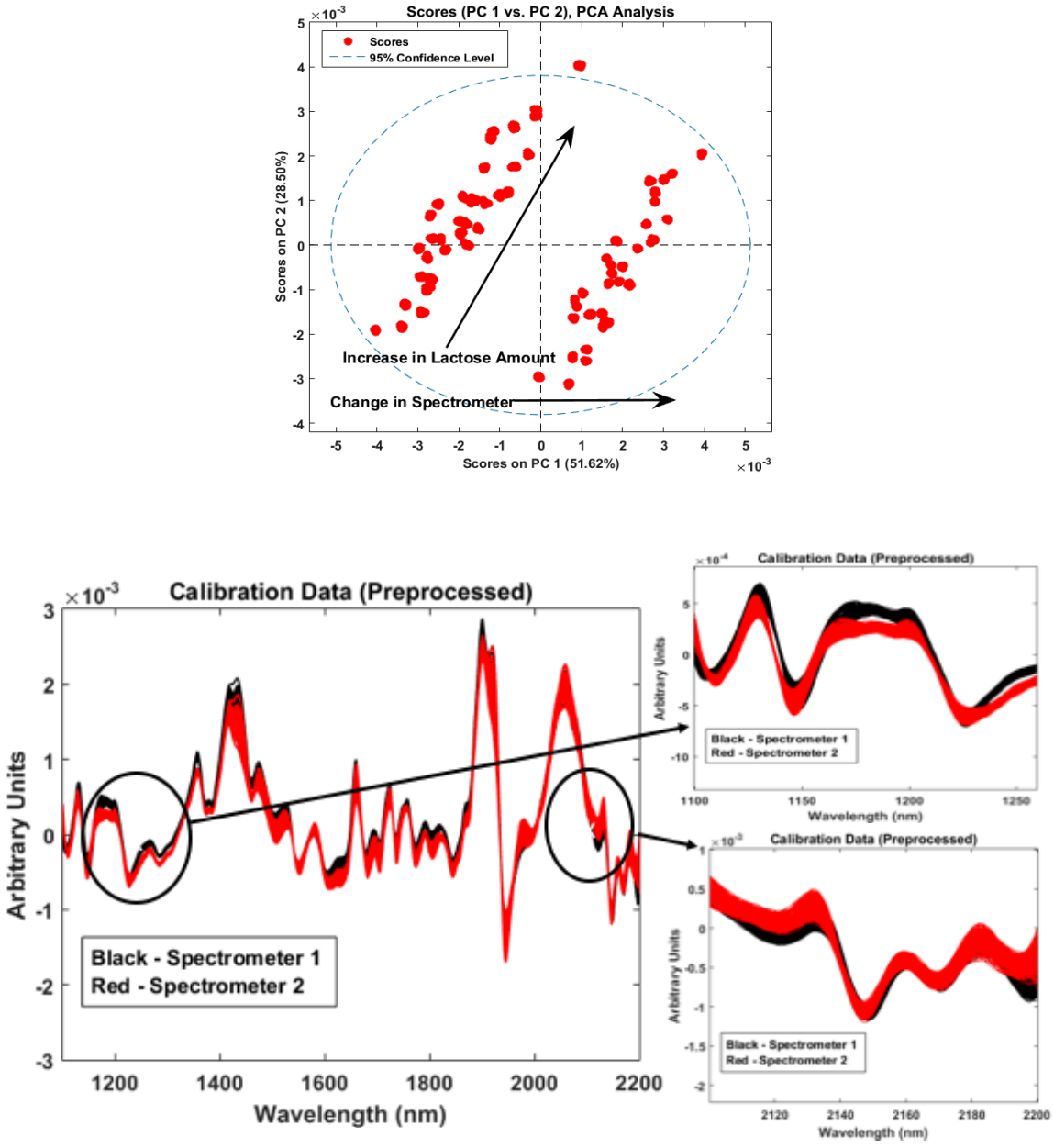

Figure 3-4: a) Scores (PCA) - PC 1 majorly sensitive to differences in spectrometers. PC 2 was majorly sensitive to Lactose. b) Peak shifts between two spectrometers at 1,150 and 2,150 nm.

The second PC was observed to be sensitive towards changes in lactose concentration. The loadings plot for PC2 (Figure 3-5) showed higher intensity in the 1400 nm and 1920 nm wavelength range specific to the lactose -OH band vibrations.

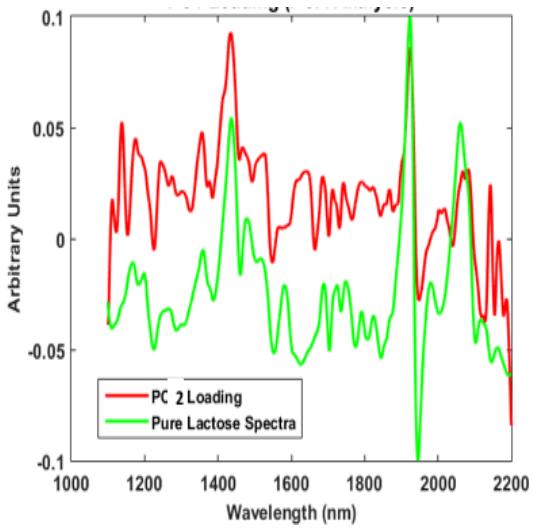

Figure 3-5: PC 2 shows specificity to Lactose, 1,400 nm and 1,920 nm – OH band vibrations

The third PC was observed to capture the effects of changes in Phenytoin Sodium concentration (Figure 3-6 (a)). This was confirmed by the spectral similarity between PC3 and the pure Phenytoin Sodium spectrum (Figure 3-6 (b)). The peaks in the range of 1150 nm and 1170 nm are the characteristic peaks for Phenytoin Sodium. Thus the PCA was able to capture and distinguish the variabilities arising from spectrometer, and the concentration of lactose and Phenytoin Sodium.

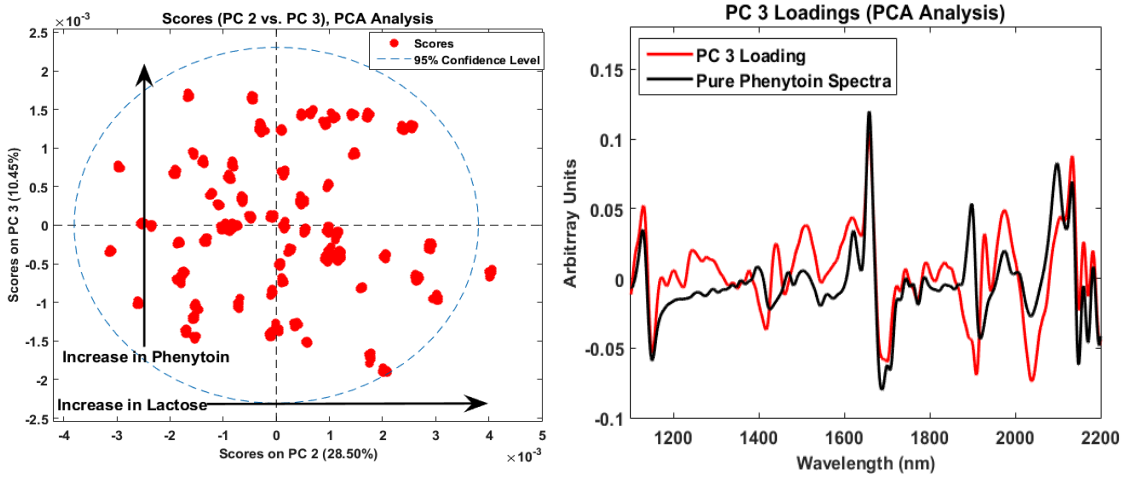

Figure 3-6: PC 3 is majorly sensitive to Phenytoin. Spectral similarity between PC 3 and pure spectra of Phenytoin

The other intention of using PCA was to compare the variance space of the two data collection strategies (static and dynamic).

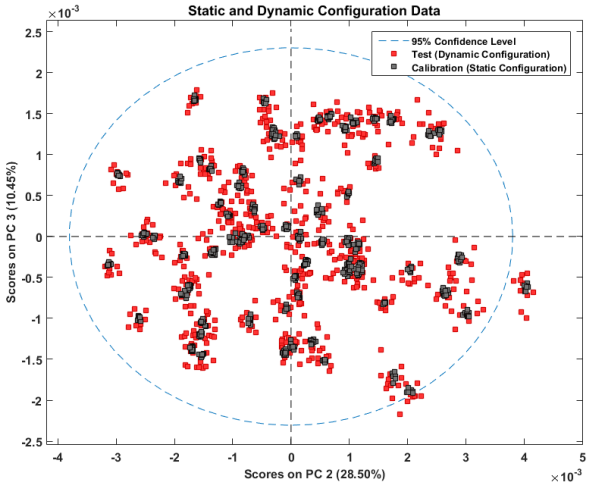

Figure 3-7: Calibration (Static Configuration) and Test (Dynamic Configuration) Data – PCA Scores

The data obtained from the dynamic configuration was projected onto the PCA obtained using the static configuration spectra (Figure 3-7). The scores from the dynamic spectra analysis were observed to overlap the scores obtained from the static configuration data. The preprocessing steps of smoothing and derivative were observed to help the data convergence by minimizing the baseline differences. This allowed the justification of the model building strategy, where a PLS model was created using lab-scale static data and updated by pilot-scale dynamic data.

Lab scale model building for API

Post-pretreatment, a global Partial Least Squares model (refer to chapter 2, section 2.3.3) was developed on the combined static configuration spectra from the two spectrometers.

Gravimetric (nominal) API concentration levels were used as the reference values. The PLS model was built using 6 latent variables, which explained 87.95 % of the total Y-variability. The sources of variability were observed to be the concentration of Phenytoin, Lactose, MCC, differences in spectrometer, and two sets of static configuration data sets (10 spectra each), justifying the use of 6 latent variables.

Table 3-2: Calibration Model Statistics

Model Statistics	
Latent Variables	6
RMSEC (% w/w)	0.55
RMSECV (% w/w)	0.58
Calibration RSD	9 %
R^2	0.87
X-Variance (%)	97.40
Y-Variance (%)	87.95

The predicted vs reference plot for API concentration (Figure 3-8) obtained from the PLS model building obtained using the static configuration showed an R^2 value of 87%, with a RMSEC of 0.55% (w/w) and RMSECV of 0.58% (w/w).

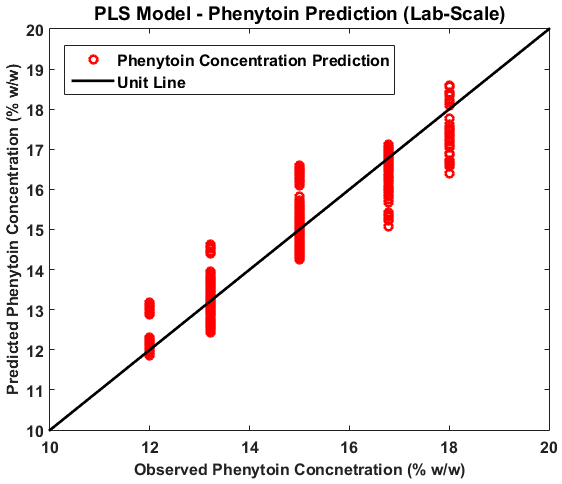

Figure 3-8: Prediction plot is depicted. There exists specificity to the API

Blend Model Update from Pilot-Scale batches: To encompass the effect of scale changes, the lab scale calibration model was updated by adding NIR data from the pilot scale batches O1 (center point of DOE) and I, N, M, J (extreme points of DOE). The five batches were used for model update, and the test batch O2 (calibration centre) was used for testing blend end-point algorithms. The choice of the pilot scale blend data (spectra) to be included in the calibration model development depended on the extent of homogeneity achieved towards the end of the blending process. The following strategy was used for sampling the appropriate data from the real-time blends spectra: The original calibration was used to predict the concentration of API at different time points in the pilot scale blends**.** The prediction residuals were calculated and the original calibration was updated by the last 10 spectra in the real-time blending data that yielded a residual lower than ±1% w/w. This strategy was applied to data collected from both spectrometers**.** Thus a total of 100 spectra were selected (10 spectra x 5 design points x 2 spectrometers). The new calibration thus set contained 780 spectra (680 static configuration spectra+ 100 pilot scale dynamic configuration spectra).

PLS modeling was carried out using the same pretreatments as mentioned earlier. Table 3-3 summarizes the statistics of the updated calibration model. 6 latent variables were used for model building, which explained 86.21% of the total variability in the data set. The prediction vs reference plot (Figure 3-9) showed a specificity for API, with an R^2 of 0.86 and a RMSEC and RMSECV of 0.61 and 0.64% (w/w) respectively.

Table 3-3: Calibration Model Statistics for the updated model

Model Statistics	

Latent Variables	6
RMSEC (% w/w)	0.61
RMSECV (% w/w)	0.64
Calibration RSD	10 %
R^2	0.86
X-Variance (%)	90.09
Y-Variance (%)	86.21

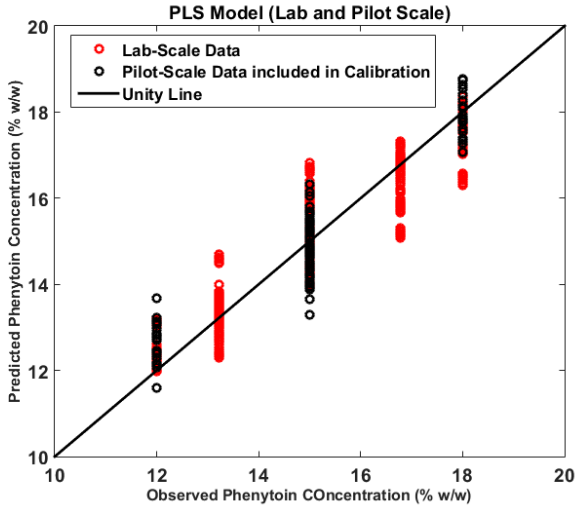

Figure 3-9: Prediction plot for the updated model with an R-square of 0.92

Blending End-Point: The updated calibration model was used to predict the API concentration real-time in blend O2 (targeted API-15%). From the predictions, moving window mean concentration and standard deviation were obtained. Sekulic *et al*. demonstrated the use of moving block standard deviation as a blend end-point criterion, where the variance converges to a low value, indicating the end-point [65]. The moving block window involved one minute of mixing. The spectrometer collected one spectrum every two rotations (empirical observation); therefore, a moving block of 15 was used. Figure 3-10 (a) and (b) displays the moving mean and standard deviation, respectively. A

blending time of 30 minutes (360 revolutions) appeared to provide blend uniformity in terms of standard deviation, the mean API content, was within 10% of the target dose, the standard deviation was around 0.4- 0.6 (%w/w). Closeness of the mean to the target value, and the stability of the standard deviation signified homogeneity at the target concentration.

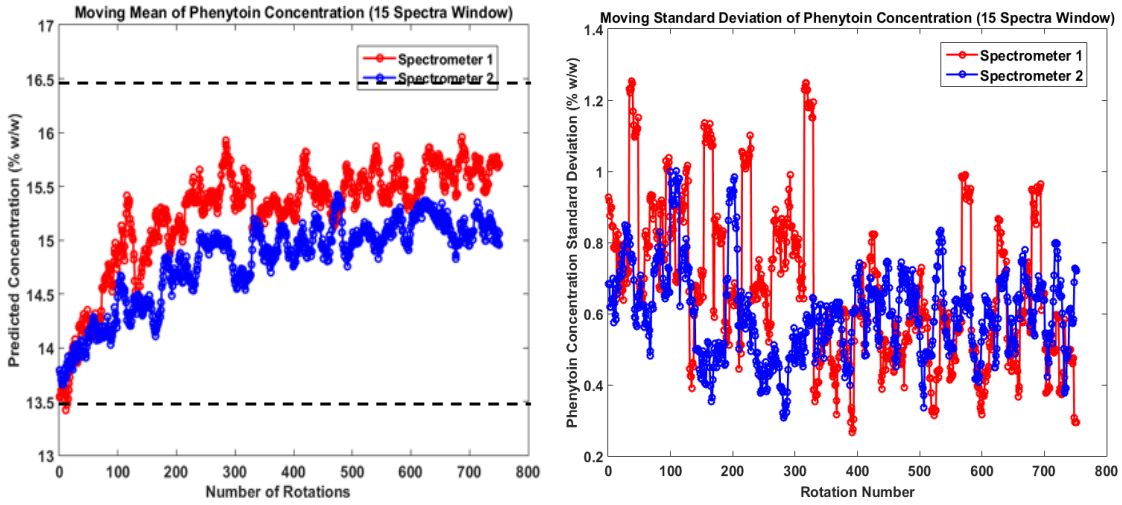

Figure 3-10: (a) Moving window mean shows that the blend approaches the targeted concentration of 15% with blending. (b) Moving window standard deviation is depicted.

A slight bias was observed in the mean API content across the two arms of the blender, however the average was close to the target (15% w/w). A cyclic pattern depicted in both plots was could be because of multiple reasons. A possible reason could be the segregation and desegregation tendency of the blend. Presence of agglomerates in the blend can move throughout the blend in a cyclic pattern presenting themselves to the sampling window at regular intervals. This is investigated in subsequent work.

3.4. Conclusion:

In summary, the development of an analytical platform for on-line blend monitoring and control provided an opportunity to investigate the challenges associated with implementing PAT methods for BU. Determination of the end-point of a pharmaceutical blending operation using online monitoring is an important step towards assuring quality of the final product in real time. A DoE approach helped capture the effects of changes in API and excipient concentrations on the blend NIR spectra. Efforts were taken to minimize the baseline effects owing to differences in spectrometers by different pretreatments. The effect of differences in scale was accommodated in the calibration model by updating the lab-scale calibration model with pilot scale data. The mean concentration after 30 minutes of blending was within 10% of the target dose (15%). This approach can help circumvent the issues arising because of thief sampling and is a step towards real time release testing. The blends obtained from this work were used for content uniformity analysis in the subsequent chapter. A considerable amount of work has been accomplished in this area by different researchers, however, the work in this chapter is a first attempt to develop a methodology for on-line blend uniformity for Phenytoin Sodium. A successful implementation of this strategy will help address the reported blend uniformity issues associate with this NTI drug.

Chapter 4. Near-Infrared (NIR) Spectroscopy-based Content Uniformity (C.U.) Method Development for Phenytoin Sodium Formulation

4.1. Introduction

The Food and Drug Administration (FDA) and European Medical Agency (EMA) emphasizes the role of strict guidelines around tablet Content Uniformity to ensure safety and efficacy of the final product. Stringent regulations around the 'Good Manufacturing Practice' guidelines require interrogation of greater number of samples to assure batch quality. Problems like blend segregation, API agglomeration, API sticking to the walls of the blending or storage containers can worsen the finished product quality. In such cases, there is a need for analyzing greater number of tablets to increase the confidence in the assessment of batch quality post compaction. The need for such extensive and effective sample testing is amplified further when the drug under investigation is a NTI drug. Traditional approaches for content uniformity testing employ wet chemistry techniques like High Pressure Liquid Chromatography (HPLC) [18] [19], which are time consuming, require solvent and sample preparation, and cannot be used for real time quality control.

Near IR Spectroscopy has been found to be a reliable technique for fast and non-destructive C.U. determination. Merckle *et al.*[66] used both reflectance and transmittance NIR on tablets containing acetylsalicylic acid (ASA), ascorbic acid, and paracetamol to determine the C.U. for ASA. The differences arising because of scale of operation must be considered while building calibration models using NIR spectroscopy. Otsuka *et al*. [67] studied and incorporated the effect of scale on tablet hardness and coefficient of variation during NIR

spectra model building. Blanco *et al.* [68] expand the calibration range for the production scale C.U. model by incorporating lab scale samples. Variations between scale can arise from differences in blend shear. The NIR spectroscopy has been successfully employed to capture the effect of shear when the powder is exposed to different levels of strain in the presence of magnesium stearate [69][70]. Thus, including all these potential sources of variability that could arise during actual production runs has been observed to be a good model building practice.

A calibration model is as accurate as the reference method used [71]. Florey *et al.* highlighted different HPLC columns and mobile phases used by different researchers to detect Phenytoin concentrations [72]. Atwell *et al*. used a mixture of chloroform dioxane-isopropanol- acetic acid as mobile phase for simultaneous determination of phenobarbital and diphenylhydantoin from blood plasma [73]. The United States Pharmacopeia, USP 35, stated the guidelines for the assay of Phenytoin Sodium, which uses monobasic ammonium phosphate buffer (pH 2.5)-acetonitrile- methanol solution as the mobile phase. The prime requirement for using HPLC assay is that the entire amount of the drug should be released in the mobile phase. However, the solubility of the drug in the HPLC solvent can be affected for different reasons. Over blending and shearing in the presence of Magnesium stearate in powder blends has been observed to affect the rate of drug release from tablets and granules [24]. Magnesium Stearate is a hydrophobic, shear sensitive lubricant with a tendency to form nano- layers on API and excipient surfaces, affecting the drug release from the dosage form [23]. In such cases, the selection of the mobile phase used for dissolving the samples becomes critical before proceeding to the NIR model building.

Using the technique for blend monitoring developed in the previous chapter, NIR spectroscopy was employed to perform extensive content uniformity studies of tablets obtained from the "experimental station" described in chapter 2. The existing USP HPLC methodology was tweaked by changing the mobile phase composition. The blends obtained from chapter 3 were further used for compaction and model building for C.U. predictions. The experimental design developed previously helped incorporate variability attributed to tablet production scale, formulation parameters, and tableting process parameters during model building. To the best of my knowledge, this was a first attempt reported in the literature to use NIR to predict Phenytoin Sodium C.U. real time, enabling faster investigation of C.U. issues, if any.

4.2. Materials and Methods:

The materials used in the experiments reported in this chapter were listed in chapter 3, section 3.2.1. The experimental design was explained in section 3.2.2. The lab scale and pilot scale blending were explained in section 3.2.3. The compaction of the blends into tablets is given in the following sections.

4.2.1. Laboratory scale tablet manufacturing:

The 17 lab scale blends (Chapter 3, section 3.2.2) were compacted into tablets using a Presster, a tablet press emulator (Presster^{TM}, MCC, East Hanover, NJ), set to emulate Kikusui Libra2 tablet press (refer chapter 2, section 2.2.2). 500 mg tablets were made at five different compaction forces such that the tablet crushing strength varied from ~ 4 kP to 10kP, encompassing the variability encountered during compaction of a pilot scale

batch. One tablet per compaction force per blend was picked for further analysis resulting into a total of 85 tablets.

4.2.2. Pilot scale tablet manufacturing:

The tablet compaction was achieved in the Kikusui tablet press, which was a part of the blending platform described in section (chapter 2, section Figure 2.1). After pilot scale blending operation, the butterfly valve on the blender was opened to dispense the blend through a chute to the tablet press (figure 1-1).

Figure 4-1: Pilot- scale compaction setup. Post- blending. the blend was dispensed to the tablet press through a chute. 6 tablets were collected every minute for the entire duration of compaction.

Five pilot scale blends were blended and compressed to different targeted hardness. Blend O1 was subjected to higher compaction force yielding tablets of an average crushing strength of 18 kP. The average crushing strength for the rest of the four blends I, J, N, and O2 was around 8-9 kP. 600 mg tablets were made using 10 mm diameter flat punches. The

tablets thus produced were stream sampled every minute for the entire duration of compaction.

4.2.3. NIR data collection:

A Bruker Optics Multi-Purpose Analyzer (MPA) FT- NIR spectrometer (Billerica, Massachusetts) was used to obtain transmission spectra for the tablets obtained from the lab scale and pilot scale runs. The spectral range was from 12500 to 550 cm^{-1} with a resolution of 8 cm^{-1}. Each spectrum was averaged over 256 sample scans. A total of 85 lab scale tablets were scanned using NIR. In the case of pilot scale operation, 6 tablets were analyzed each time point and the total number of tablets analyzed per batch depended on the duration of compaction.

4.2.4. Reference Method, High Performance Liquid Chromatography (HPLC)

The tablets were analyzed for their API content using an in-house validated HPLC method. Two different mobile phases were tested. The first mobile phase was a 45:40:15 mixture of Ammonium Phosphate buffer (50mM pH 2.5), methanol and acetonitrile. This method was adapted from the one described for Phenytoin Sodium in USP 35 [74]. Initial method development for tablets highlighted the inadequacy of this method to quantify the API content in the tablets. This called for a further modification in the mobile phase, where the buffer (and hence the pH) in the new mobile phase was changed from Ammonium Phosphate (pH 2.5) to Sodium Borate (pH 9). The new mobile phase consisted of a 45:40:15 mixture of Sodium Borate buffer (pH 9), methanol, and acetonitrile. Tablets

obtained from the lab scale blends were dissolved in the two different mobile phases and the average drug released at each design point was compared.

Mobile phase 2 (containing borate buffer, pH 9) was chosen for further analysis. Each tablet was ground and dissolved in 40 ml of mobile phase (pH 9). The solution was sonicated for 30 min at 30ºC and left overnight for dissolution. The API content was determined using HPLC (Agilent 1100 series) by injecting a 20µL injection aliquot of the dissolved, filtered and diluted tablet solution into a 250 X 4.6 mm 5µm Sonoma C18(2) column held at 25 ºC, at a flow rate of 1.5 ml/min. The elution time for the API was 6 min and was detected at a wavelength of 220 nm using a diode array detector. The API content was reported as weight percent of the total tablet weight for individual tablets.

4.2.5. Multivariate data analysis

The calibration set consisted of tablets obtained from 16 lab scale blends (A to P) and 3 pilot scale blends (O1, I and J). For the lab scale blends, one tablet was selected per force setting (total of 5 compression forces) per design point, resulting into a total of 80 tablets (16 blends x 1 tab each force x 5 force conditions). A total of 22 tablets from three pilot scale tablets were included in the calibration set to account for the variability owing to scale differences. Random subsets consisting of 20 segments were used for cross validation. An internal test set consisting of two blends, lab scale blend Q (5 tablets) and pilot scale blend N (5 tablets), was used to the evaluate model performance for independent tablets. The resulting model was used to predict the tablets obtained from blend O2 (validation set), the center point of the pilot scale runs (Table 4-1).

Table 4-1: Calibration, test set and validation set used in model building and evaluation.

Category	No.	Scale	Blends (No. of blends)	Number of tablets/ blend	Total tablets	Hardness (kP)
Calibration set	1	Small Scale	A to P (16)	5	80	4-10
	2	Pilot Scale	O1, I, J (3)	10, 6, 6	22	18, 10, 8
Test set	3	One small scale and one pilot scale	Q and N	5, 5	10	4-10
Validation set	4	O2	15	234	234	10

The data analysis was performed using Unscrambler X 10.2 (Camo, Oslo, Norway). The NIR data was subjected to different preprocessing combinations, and the treatment that offered maximum predictability was chosen. A Partial Least Squares model was developed to predict the drug content in each tablet from NIR transmittance spectra (X-variable). The tablet calibration model was built by taking the drug concentration obtained from HPLC for each tablet as a reference value. The effect of choosing different variable ranges (wavelength range) was investigated on the model effectiveness.

The predictive capability of the model was evaluated from the correlation coefficient, bias, and the root mean square errors of calibration (RMSEC), cross validation (RMSECV) and prediction (RMSEP). The bias and the root mean square error for calibration and prediction were defined as

$$bias = \frac{\sum_{i=1}^{N}(\hat{y}_i - y_i)}{N}$$

$$RMSEC = \sqrt{\frac{\sum_{i=1}^{N}(\hat{y}_i - y_i)^2}{d.o.f.}}$$

$$d.o.f. = (N - w - 1)$$

$$RMSEP = \sqrt{\frac{\sum_{i=1}^{N}(\hat{y}_i - y_i)^2}{N}}$$

where $\hat{y}_i$ is the model- estimated property value for test sample i, y_i is the measured property value of test sample i, N is the number of samples, w is the number of PLS factors. For the cross-validation and test sets, the number of degrees of freedom is takes as the total number of samples, i.e. N.

4.3. Results and Discussion

4.3.1. Modification of reference HPLC method:

A PLS model is built such that it maximizes the covariance between the dependent variables (Y) and the independent variables (X). The variability associated with the reference method is propagated to impact the accuracy and robustness of the PLS model. The USP recommended method was observed to release less API and bias was observed between the amount of drug released and the actual amount of the drug present. The amount of the API released was observed to depend on the amount of MgSt in the tablet (Figure 4-2 a). As the Magnesium Stearate concentration increased from 2% to 6%, the average % API released from the tablets decreased. This was true for all concentration levels of the API. On the other hand, the amount of MCC present did not affect the drug release. MgSt is a hydrophobic, shear sensitive lubricant with a layered structure [75]. With an increase in blend shear during prolonged mixing, MgSt is capable of forming films on other ingredients in the blend, delaying or reducing contact of the solvent with the API, leading to a prolonged drug liberation time [22][76][77].

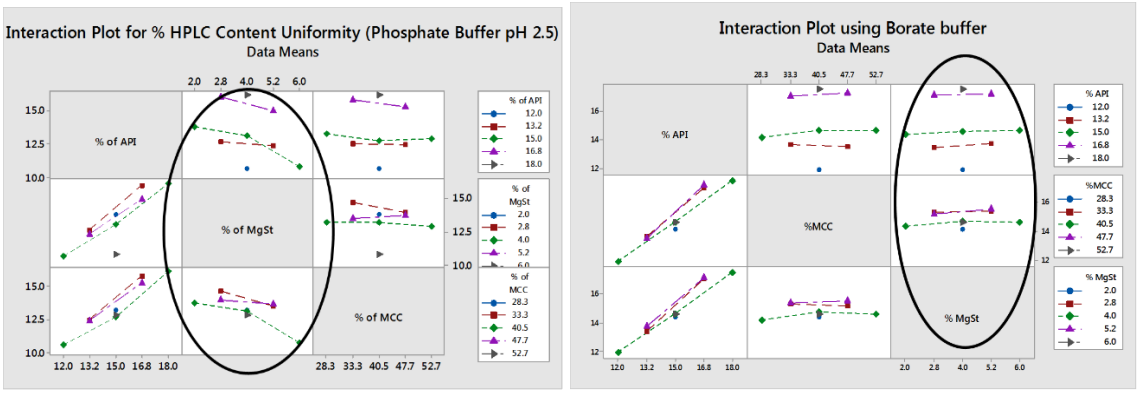

Figure 4-2: Interaction plots to study the effect of magnesium stearate on the drug released (and detected) from the tablets. a) For Phosphate buffer, the levels of MgSt affected the amount of drug released, with increasing MgSt decreased the API detected. b) For Borate buffer, the amount of drug released was independent of levels of MgSt.

In an effort to increase the amount of API released from the tablet, the pH of the mobile phase was increased. Phenytoin sodium is an acidic salt. Serajuddin *et al.* [78] reported a low solubility for phenytoin and phenytoin sodium salt between pH 1 (solubility= 0.035 mg/ml) to pH 6 (solubility= 0.04 mg/mL), and the solubility gradually increased as the pKa (pKa=8.3) of the compound was approached. With an increase in pH of the mobile phase (borate buffer, pH =9), the average drug released increased and was not observed to depend on the level of magnesium stearate (Figure 1-3b). Morin *et al.* studied the mechanism of film formation of MgSt around two excipients and found that MgSt first fills the irregularities on the surface of excipients before forming a continuous layer [79]. The hypothesis is that the increase in the pH, though did not affect the MgSt layer, increased the solubility of Phenytoin Sodium, increasing the concentration gradient across the permeable MgSt layer. This lead to the release of all of the drug into the solution. The reference HPLC values of the API concentration in the remainder of this work were thus measured using the mobile phase containing borate buffer at pH 9.

4.3.2. Tablet Calibration modeling and model evaluation:

NIR transmittance spectra were acquired for the tablets obtained from the lab and pilot scale batches. The Figure 4-3 (a) highlights the NIR transmittance spectra for the calibration set (102 tablets) and the test set (10 tablets). The absorbance values for wavenumbers from 8600 cm^{-1} to 5500 cm^{-1} were observed to be noisy due to high absorbance of low energy radiation, and hence this range was truncated. The resulting wavenumber range spanned from 12489 cm^{-1} to 8609 cm^{-1} (variable set 1). The other region (variable set 2) spanned from 11772 to 11301cm^{-1} and 9041 to 8647 cm^{-1}, which was observed to be the characteristic band for Phenytoin Sodium, as shown in Figure 4-3(b). The pretreatment used in Figure 4-3 (b) was a combination of baseline (BL) correction followed by Savitzky-Golay (SG) first derivative fitted to a second order polynomial. The use of the pretreatments helped enhance the API peak resolution by removing overlapping peaks.

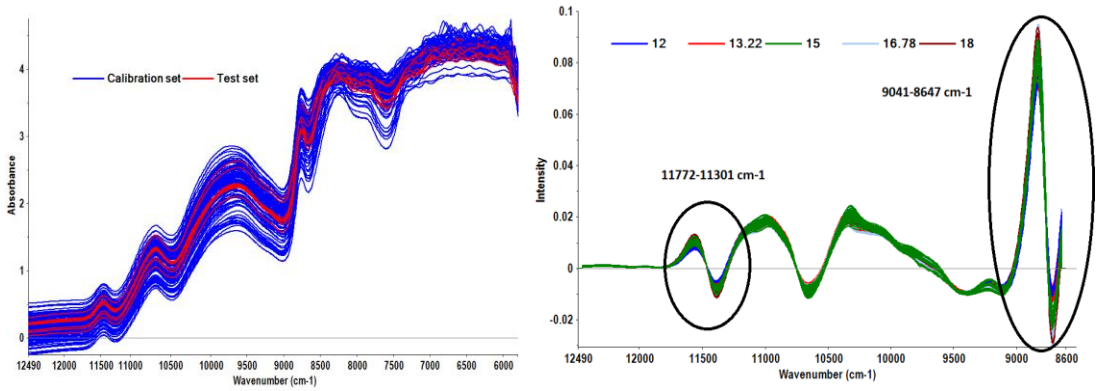

Figure 4-3: a) Raw Calibration and test tablet NIR spectra. The absorbance values for wavenumbers from 8600 cm^{-1} to 5500 cm^{-1} were noisy and hence truncated. b) Preprocessed NIR spectra. The data was subjected to a baseline correction and Savitzky Golay first derivative to minimize the Baseline and slope differences.

Calibration models were built for content uniformity of tablets included in the calibration set. The NIR data was subjected to a range of different pretreatments including a second derivative, and a Standard Normal Variate (SNV) followed by first derivative. The models

were evaluated over different wavenumber ranges (Table 4-2). The model that exhibited the lowest RMSEP and bias for the test set (blend Q and N) was selected. The pretreatment involving baseline correction followed by Savitzky Golay first derivative (fitted to a second order polynomial, 11 segments) over a range of 12489 cm^{-1} to 8609 cm^{-1}, exhibited an R^2 of 0.91, and RMSEP and bias of 0.548 and -0.08 respectively, and was chosen.

Table 4-2: Calibration Model Statistics. Baseline+ Savitzky Golay (SG 11(1)) first derivative was found to be the best pretreatment for 12489 to 8609 cm^{-1} with lowest bias and RMSEP. RMSEC- root mean square of calibration, RMSECV- root mean square of cross validation, RMSEP- root mean square of prediction

	BL-SG11(1)		SNV-SG15(1)	
	12489-8609	11772 n 9041 cm-1	12489-8609	11772 n 9041 cm-1
factors	4	6	5	6
Elements	99	98	99	97
R-sq	0.91	0.9	0.887	0.92
RMSEC	0.545	0.57	0.61	0.527
RMSECV	0.66	0.62	0.68	0.59
RMSEP	0.548	0.552	0.637	1.080
Bias	-0.08	0.16	-0.17	0.6

The predicted vs. reference plot is depicted in Figure 4-4 for an API concentration of 12-18%. An R^2 of 0.91 and a RMSEC of 0.54% was observed, indicating a good fit. Table 4-3 summarizes the model evaluation statistics for 1 to 5 factors. No appreciable increase was observed in the Y-variance explained by the model with addition of the 5^{th} factor (0.42% increase in the explained variance). A RMSECv of 0.66% was observed for model built with 4 factors. Hence, 4 factors were chosen to build the final model.

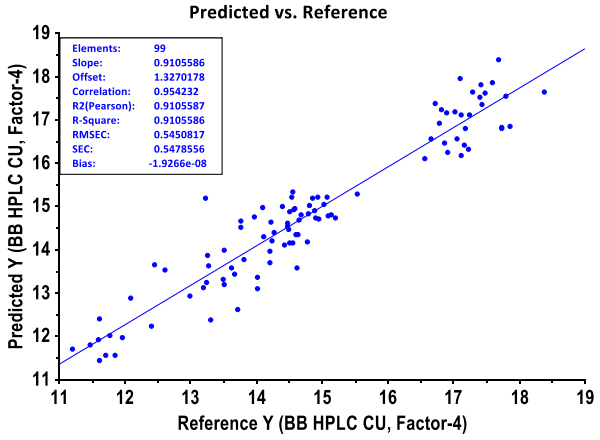

Figure 4-4: Prediction plot is depicted. An R-square of 91% and a low root mean square error of calibration of 0.54 was observed.

Table 4-3 Calibration Model Statistics. 4 factors were chosen to build the final mode. A total of 91.06% Y-variance was captured by the PLS model

Percent Variance Captured by Model					
factors	1	2	3	4	5
Y variance LV	64.25	72.12	74.3	91.06	91.48
Y variance cumulative	64.25	7.87	2.18	16.76	0.42
RMSECV	1.11	1.03	0.98	0.66	0.6

The latent variables obtained from the PLS regression are a linear combination of the original manifest variables. To understand the sources of variation, the contribution of each of the latent variables was investigated. The first latent variable (LV) explained 61% of the observed variation in the NIR data and grouped with increasing API concentration along the LV1 axis (Figure 4-5a). This was confirmed by plotting the loading plot of LV1 and the pretreated spectrum of pure Phenytoin Sodium (Figure 4-5 b). The loadings plot showed higher intensity in the range of 11772-11301 cm^{-1} and 9041-8647 cm^{-1} corresponding to the API peaks.

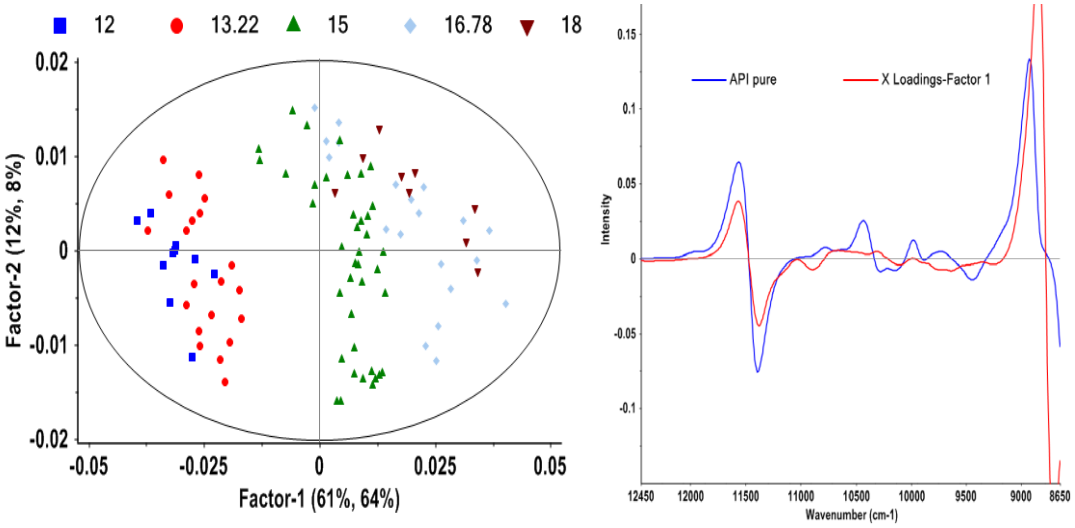

Figure 4-5a) Scores plot shows increasing API concentration along latent variable (LV) 1. b) Loadings plot- spectral similarity between LV 1 and Phenytoin Sodium spectrum. Latent variable 1 shows specificity to Phenytoin peaks for the range: 11772-11301 cm^{-1} and 9041-8647 cm^{-1}.

The second LV explained 12 % variability in the data set (Figure 4-6) and captured the effect of tablet hardness (crushing strength). The tablets with highest compaction force and hence highest hardness (15 kP for pilot scale tablets O1) exhibited negative scores on LV2.

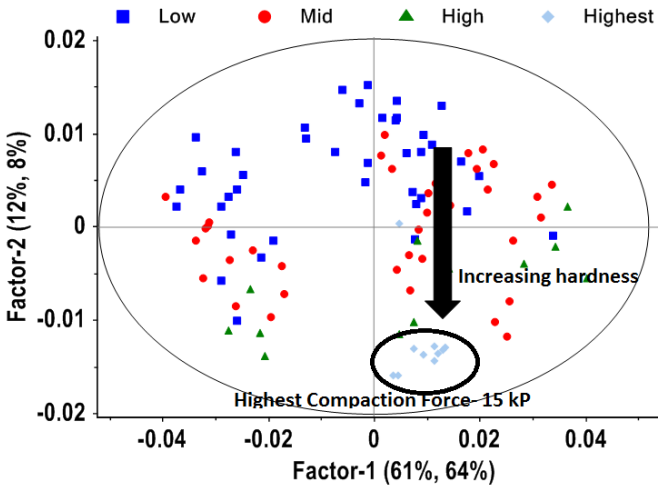

Figure 4-6 Interpretation of latent variables from scores plot. Effects of decreasing compaction force and hence hardness from 15 kP to 5 kP observed along latent variable 2

The third LV, explaining 13% of the total variability, captured the effect of scale of operation (Figure 4-7a). The pilot scale tablets exhibited positive eigenvalues along latent

variable 3 (Figure 4-7b) One major difference between the two scales was the weight of the compressed tablets. The effect of tablet weight was confounded with the effects arising from the scale of operation along the LV3 axis. Including samples from pilot scale was an important exercise to build a robust model extending its predictive power to predict concentration of pilot scale tablets.

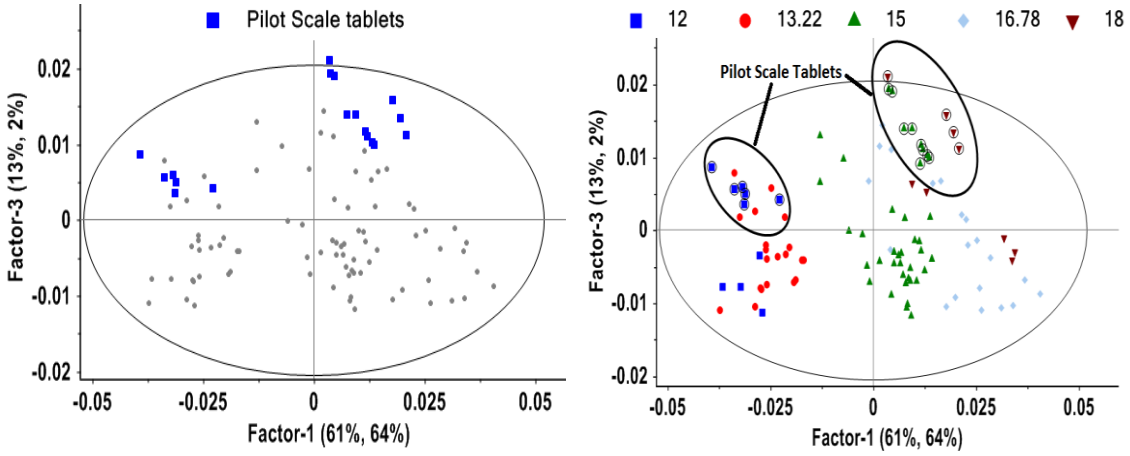

Figure 4-7 Interpretation of latent variables from scores plot. Latent variable 3 captures the differences arising from scale with pilot scale blend I, J and O1 showing highest score on PC3

The model developed in Figure 4-4 was used to predict the API concentration for the pilot scale tablets (blend O2) made at the center point of the CCI design, consisting of 15% drug. The scans of these tablets were projected on the calibration space. The projected data was contained within the 95% confidence interval shown by the hoteling's ellipse in Figure 4-8.

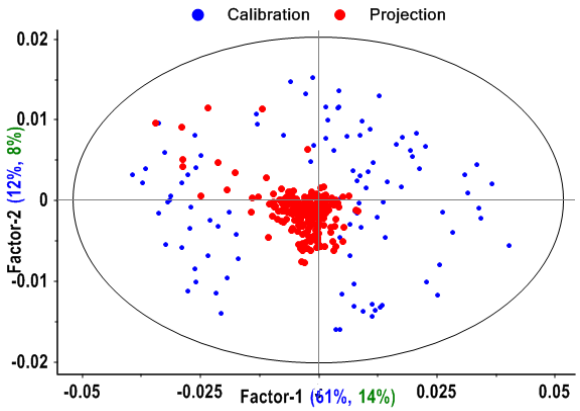

Figure 4-8 Prediction set O2 projected onto the calibration scores plot. The projected data lies within the 95% hoteling's ellipse.

The control chart for the predicted concentration of these tablets over time is exhibited in Figure 4-9.

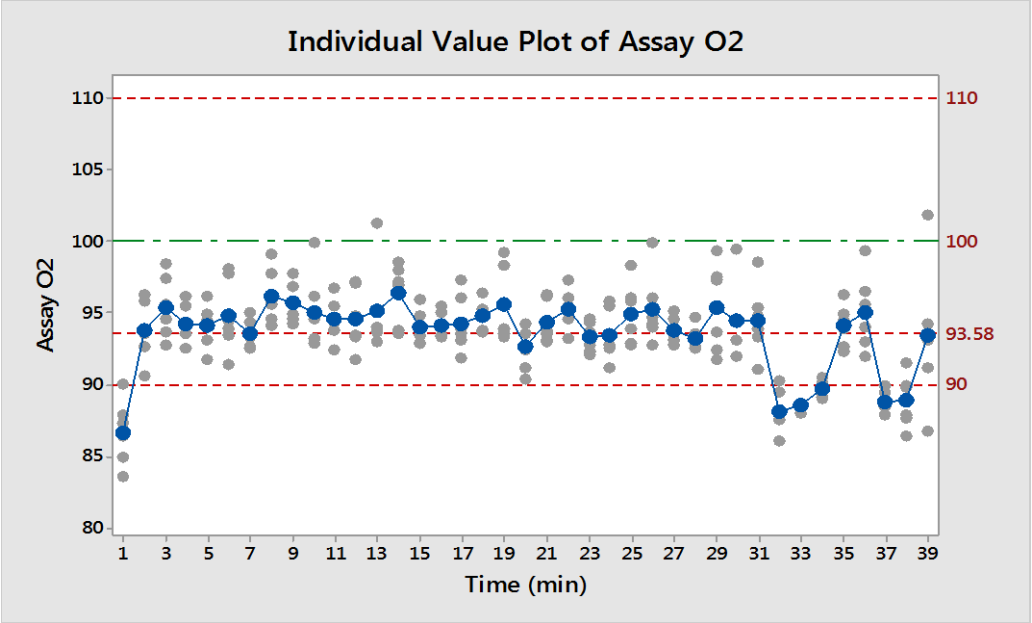

Figure 4-9: Concentration predictions from tablet NIR for blend O2 (targeted 15% API concentration

Each solid data point represented API concentration averaged over 6 tablets. The scatter at each time point was represented as grey dots. The average for the interrogated samples was observed to be around 93.58%. Some under potent tablets were observed at the beginning

and the end of the process where the average API concentration was below 90%. 20 samples were randomly picked from these tablets and subjected to HPLC analysis. A RMSEP of 0.7 was obtained, with a bias of 0.4%. With a successful model and method development for C.U. of phenytoin sodium tablets, the issues with content uniformity were investigated and are reported in the following chapter.

4.4. Conclusions:

Near IR spectroscopy was observed to be an effective tool for expedited content uniformity predictions for a large number of tablets for Phenytoin Sodium formulation. The effects arising because of scale of operation, process parameter variability, and formulation differences were incorporated during calibration model building. The HPLC method was tailored to overcome the issue of API release in the solvent. Changing the pH of the mobile phase allowed for the release of the drug from the tablets, enhancing the reliability of the reference method. With a method in place for tablet C.U. analysis, the models built in this chapter can be utilized to predict the C.U. of tablets obtained from the pilot-scale runs. Implementation of such RTR strategy for C.U. using fast NIR spectroscopy, coupled with extensive tablet sampling helped interrogate greater number of pilot-scale tablet samples, and has been discussed in the next chapter.

Chapter 5. Comparison of sampling methodologies for a blending platform- online blend monitoring, thief sampling, and stratified tablet sampling

5.1. Introduction

Throughout the pharmaceutical industry, process validation programs for the manufacture of tablets have been influenced by the Wolin decision of the US vs. Barr Laboratories [80] lawsuit. The conclusions of this trial addressed problems related to sampling, namely, sample size, outlier testing, and the need to understand and control the performance of blending operations. The decision caused The Food and Drug Administration (FDA) to reexamine and modify its policies on blend uniformity testing, in particular as it pertains to sampling techniques [54]. Eventually, the FDA issued a 'Powder blends and finished dosage units- stratified in- process dosage unit sampling and assessment' draft guidance encouraging industry to implement stratified sampling of compressed tablets. Ten years later, on August 7, 2013, the FDA withdrew this draft guidance, stating it was no longer consistent with current agency thinking [81], and presented several examples of companies that had failed to achieve compliance in blend uniformity. This highlights the persistent need for better tools to characterize blend and tablet homogeneity, which has been addressed in this work. For successful implementation of real time release testing, the utility and accuracy of different PAT sampling methods should be demonstrated. Comparison of these methods to traditional sampling and testing can help justify the move towards real time release testing.

Traditionally, blend homogeneity is assessed using thief sampling [13]. The objective of a sampling methodology is to obtain unbiased, representative blend samples assessing the

true content uniformity of the blend. The problems associated with thief sampling have been discussed in Chapter 3 [50]. Online blend monitoring using Near IR spectroscopy has been established as a fast, non-destructive tool and has been discussed thoroughly in Chapter 3. One of the objectives of blend uniformity analysis is to enable prediction of tablet content uniformity. A perfect blend does not always ensure a perfect product. Introduction of a transfer step during powder handling operation makes a well-blended powder susceptible to segregation [82]. Stratified sampling is the process of selecting locations deliberately from various locations within a lot or batch or from various phases or periods of a process to obtain samples [52]. Garcia *et al.* showed that the total variance for the thief sampling strategy was twice that observed for tablets compressed from the blend [83]. Stratified tablet sampling can help reduce the efforts associated with powder sampling, reduce operator and environmental exposure to potent drugs.

Stratified sampled tablets, when analyzed using fast, online tools like NIR spectroscopy (discussed in chapter 4), can help interrogate hundreds of samples and hence increase the level of scrutiny. It can help detect deficiencies in formulations and manufacturing processes that may have gone undetected (or wrongly assigned) under traditional sampling. API agglomeration is one such problem, which can be detected using extensive blend and tablet sampling. API agglomerates may be created or enhanced during low shear blending operation and can lead to an observed under-potency with occasional detection of super potent tablets [84]. Llusa *et al*. demonstrated the utility of extensive sampling to detect these occasional super-potent samples [85]. Agglomerates can break and reform during different unit operations and the high shear units can be effective in breaking the agglomerates [86]. However, high shear units increase the risk of over

lubrication [24], and extreme caution must be taken to avoid its side effects like reduced tablet strength and slower tablet dissolution.

Powder segregation is another ubiquitous phenomenon in dry- powder handling operations [87]. Achieving blend homogeneity during blending operations can be limited if the blend exhibits a tendency to segregate. Introduction of a transfer step during powder handling operation makes a well-blended powder susceptible to segregation. Such post-blending can be detected by stratified sampling of the resultant tablets [88].

To address the above concerns, an experimental station (pilot-scale) was used, capable of blending and compressing formulations, consisting of a blender, a discharge station, and a tablet press. Blending end-point was detected for this system using online blend monitoring with Near IR spectroscopy. Simultaneously, thief samples were withdrawn and examined to determine their accuracy (or lack thereof). The blends were then used to make tablets, which were tested to determine correlation (or lack thereof) between thief sampling and finished product CU. Tablet calibration model was built and validated using NIR, and was used to scan tablets created from the pilot scale blends and provide information about the distribution of concentration over a large number of tablets. Extensive Content Uniformity studies using tablets were undertaken to provide a rigorous basis for assessing and validating the various thief sampling and PAT methods and determine their relative accuracy and reliability.

5.2. Materials and Equipment

5.2.1. Materials

The materials are given in chapter 3, section 3.2.1.

5.2.2. PAT Platform

The design of the PAT platform is given in chapter 2, section 2.2.2.

5.2.3. Online blend monitoring

The methodology for online blend monitoring was developed in Chapter 3. The blending process was monitored for target blend O2, and the blend end-point was predicted (chapter 3, Figure 3-10) using this methodology.

5.2.4. Thief sampling

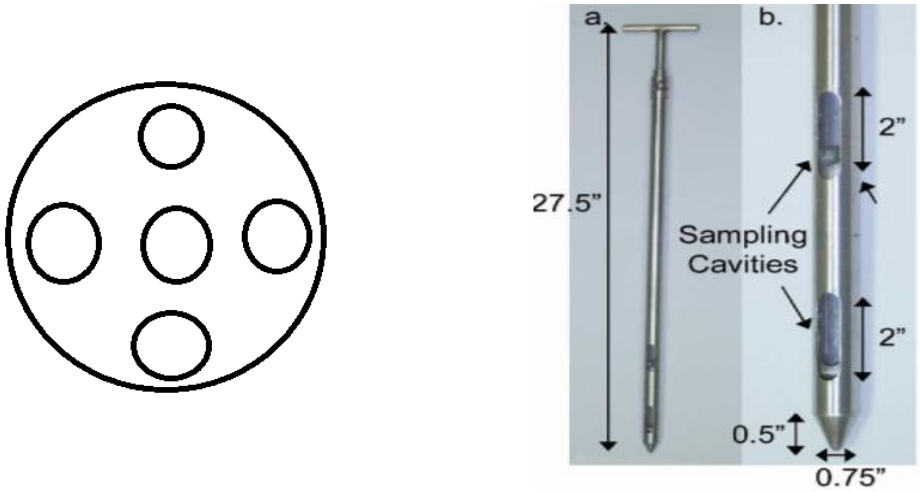

Figure 5-1: Thief sampling locations on the two arms of the V- blender (left). The Globe Pharma thief sampler (right) used for sampling. Outer shell of the thief is closed during insertion. Once the thief is inserted, the probe shell is opened such that the powder flows into the sampling cavities.

After completion of the blending operation, thief samples were withdrawn at twenty different locations for three pilot scale blends- O1, O2 and N. Samples were extracted at 20 sampling positions per blend- (5 spots* 2 heights *2 arms of blender) (Figure 5-1 (a)) using a globe pharma thief sampler (Figure 5-1 (b)). The globe pharma thief sampler is a side-sampling probe with an outer sleeve surrounding an inner pipe. The probe was inserted into the blend, and the sleeve was turned to align the opening in the sleeve with the cavities in the inner pipe to allow powder flow into the cavities [50]. The sleeve was then closed and the probe was removed from the blend. These thief samples were analyzed using HPLC

to determine the drug content in each sample. The HPLC method was described in Chapter 4, section 4.2.4. A 45:40:15 mixture of sodium borate buffer (pH 9), methanol, and acetonitrile was used as mobile phase. The entire approach was to test the utility of thief sampling for blend uniformity characterization. The results were compared to the results from blend uniformity monitoring and with tablet C.U.

5.2.5. Content Uniformity predictions

The methodology for calibration model development and tablet predictions for pilot-scale tablets C.U. using NIR spectroscopy was discussed in Chapter 4. Phenytoin Sodium concentration was predicted for six tablets collected every minute over the entire duration of compaction. An example for assay of blend O2 tablets was shown in Figure 4-9, chapter 4. Similar predictions for tablet C.U. were done for blends O1, N, J and I.

5.3. Results

5.3.1. Comparison of thief sampling and stratified sampling

A test-of –fit for a normal distribution for thief samples and their respective tablets is shown in Figure 5-2. The tablet and thief assay values were plotted against the standardized Z scores, a straight line fit to the data indicates a normal (Gaussian) distribution. The slope of the straight line represents the standard deviation of the distribution function, and the ordinate is equal to the average concentration of the samples. The tablets exhibited average assay of 99%, 93.58%, and 97% for blends O1, O2, and N respectively. The standard deviation for the tablets was observed to be lower as compared to the thief samples for blend O1 and N.

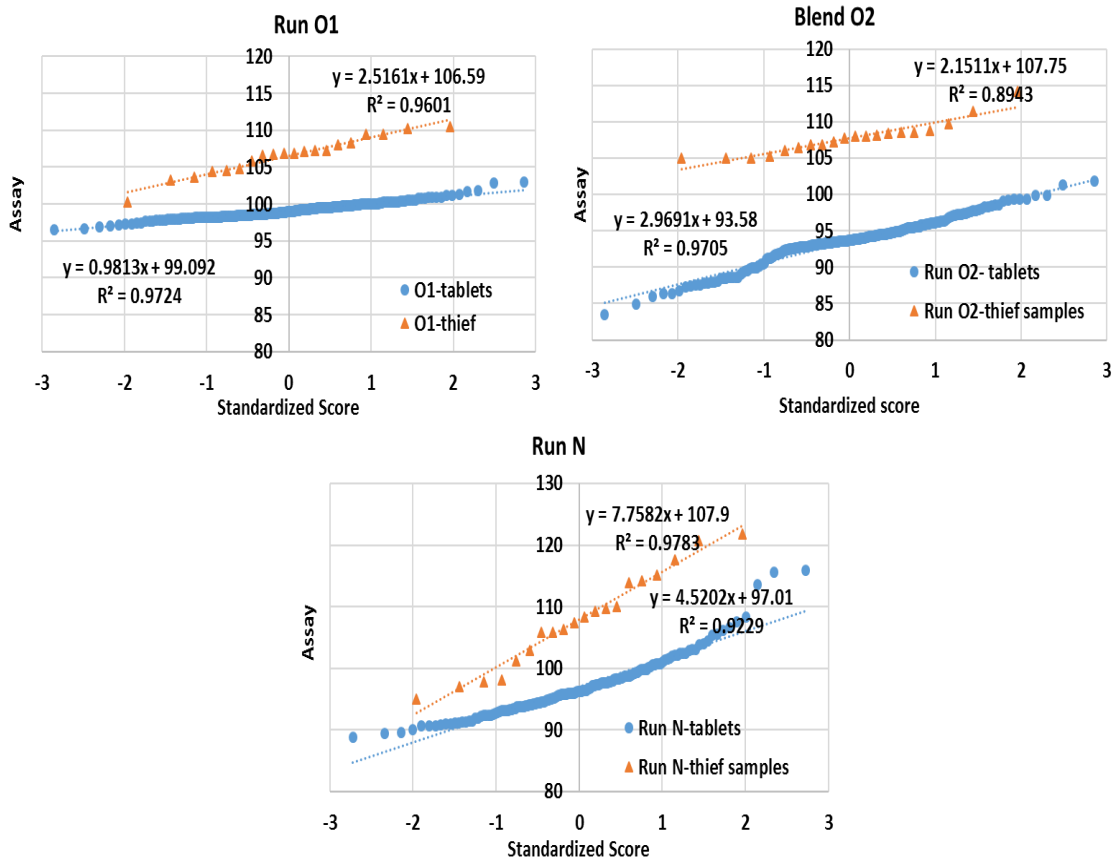

Figure 5-2: Normality plots for thief samples (triangles) and tablets (circles). The intercept on Y-axis is the average assay. The thief samples were observed to be super potent.

All the thief samples were observed to have assay values higher than the label claim, with average assay in the range of 106-108 %. The thief sampler was observed to preferentially sample API compared to the API consistently. A similar situation was observed by Garcia *et al.*, where the over potency of the thief samples was attributed to better flow of API into the thief cavity owing to the larger size of the API particles [89]. They also investigated the role of static charges in sampling bias, and observed that grounding the blender reduced the thief sampling bias and the assay moved closer to the label claim.

To investigate the reasons for the observed thief sampling bias, material cohesion was tested using the shear cell methodology in the FT4 (Freeman Technology, Gloucestershire, UK). The material to be tested was filled into a 25x10 ml vessel and the cohesion values were measured at an applied normal stress of 9 kPa [90]. The API was observed to have a cohesion value of 1.51 (Table 5-1). Wang *et al.* gave a correlation between the cohesion values and the flow function coefficient of the materials [91]. Using this criterion, the API was categorized into 'poor flowing' as compared to the other excipients. Owing to its poor flowability, the chances of the API preferentially flowing into the thief cavity were ruled out.

Table 5-1: Cohesion values obtained from shear cell testing in FT4. The API displayed highest cohesion and poorest flow among the four ingredients

Material	Cohesion at 9 kPa
Phenytoin sodium	1.51
Vivapur MCC	0.40
FF lactose	0.183
Magnesium Stearate	0.682

To further investigate the sampling bias, the blending and sampling experiment was repeated on a smaller scale for the center point O (15% API). The individual ingredients were de-agglomerated by sieving, layered from bottom to top in a 1.87 L V-blender, and blended for 30 minutes. Three thief samples were withdrawn from the blender at different locations. Agglomerates up to 5 mm were evident in the thief samples (Figure 5-3). The agglomerates were sieved out using 45 mesh sieve (0.355 mm opening diameter), the sifted powder was collected on the lower pan and the sieve fractions were analyzed using HPLC. The sifted agglomerates were observed to be 70-80% in API concentration. The

agglomerate mass fraction was in the range of 0.04 to 0.06. The cohesive nature of the API may have led to agglomerate formation. The preferential flow of the relatively larger API agglomerates in the sampling cavity was believed to have caused the observed thief sampling bias.

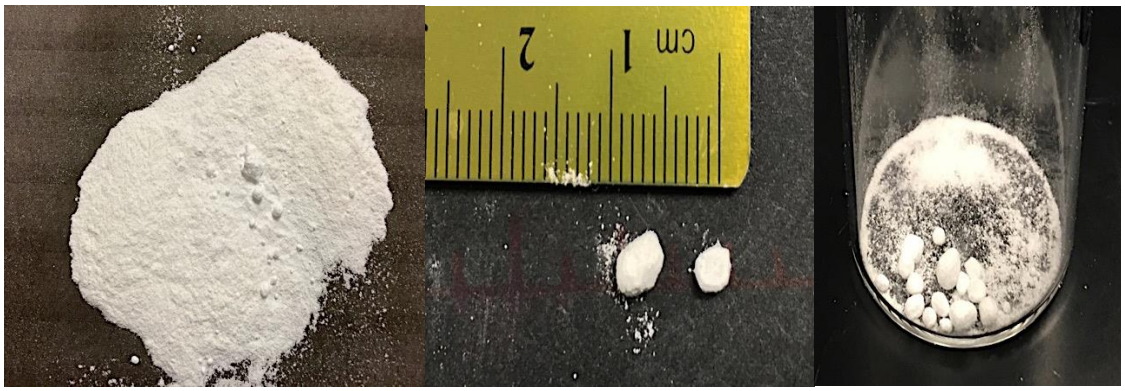

Figure 5-3: Agglomerates observed in thief samples, agglomerate size ranging up to 5 mm.

5.3.1. Stratified sampling can detect agglomeration

The predicted tablet assay values for API are reported in Figure 5-4. Except for blend O2, the average tablet assays for all the sampling points were observed to lie in the 90-110% interval. In the case of blend O2, the tablets were observed to be sub-potent, with an average tablet assay of 93.58%. Blend O2 was mixed the longest (60 min). Material was observed to stick to the walls of the blender after the blend was dispensed out to the tablet press. The residual powder was collected and subjected to HPLC analysis. The samples revealed high API concentration (60- 65%). This could be a possible reason for the observed average sub potency of tablets.

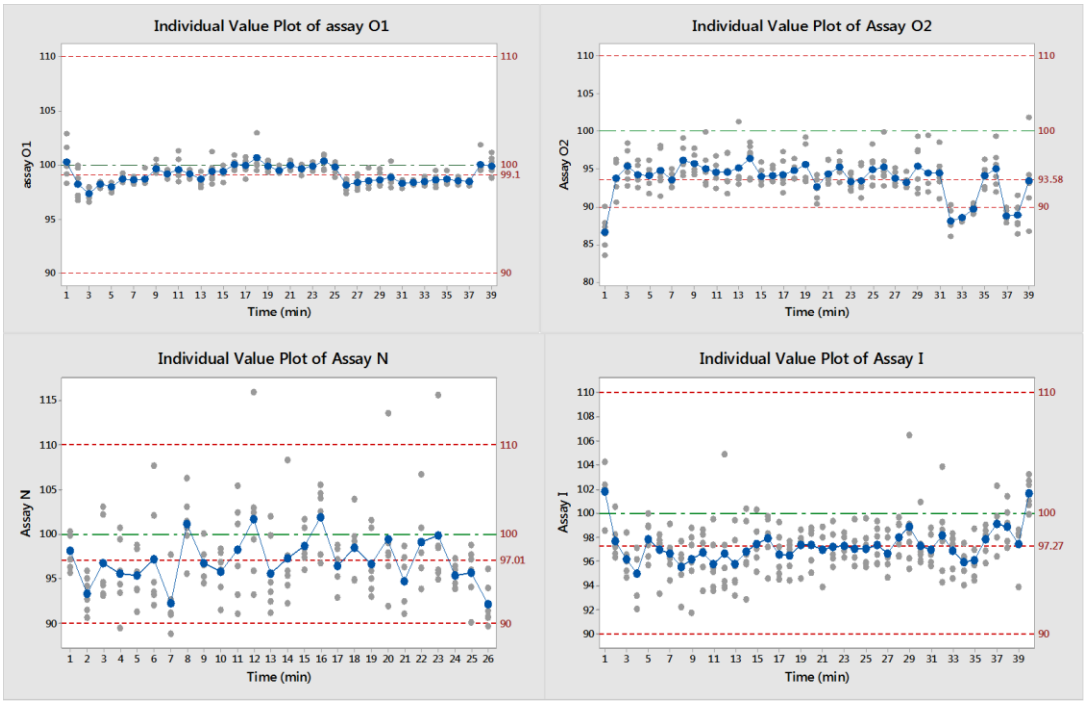

Figure 5-4: Control charts for C.U. for different blends. The average assay for the three blends (O2, N and I) was found to be sub potent and some API was observed to stick to the walls of the blender.

Tablets compacted from blend O2 were observed to exhibit lower assay values towards the end of the compaction run. As mentioned earlier, thief samples were withdrawn at two different heights inside the V-Blender. Analysis of Variance was carried out to examine the effect of sampling height on blend assay (blend O2). The effect of sampling height on thief sample assay was found to be significant (Table 5-2). The samples extracted from the bottom of the blender were observed to exhibit higher assays as compared to the samples at the top.

Table 5-2: Analysis of Variance to examine the effect of height on blend thief assay. The bed height was found to have a significant effect on thief assay

Source	DF	Adj SS	Adj MS	F-Value	P-Value
height	1	34.28	34.277	9.82	0.006
Error	18	62.85	3.492		
Total	19	97.13			

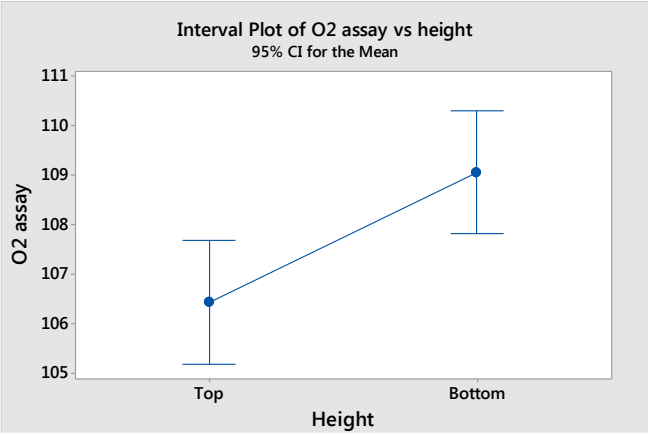

Figure 5-5: Interval plot to examine the effect of sampling height on blend assay. The mean blend assay for the two heights were significantly different.

Because the powder at the top of the blender is discharged onto the tablet press last, the lower thief assay values at the top of the blender could have resulted in the observed sub-potency of the tablets towards the end of the compaction cycle.

5.3.2. Stratified sampling can detect segregation

The tablets compacted from blend J with highest API concentration (18% API) were observed to display two different population distributions with time (Figure 5-6). Stratified sampling was able to detect the gradual increase in the tablet concentration with time and hence detect blend segregation. Unfortunately, no thief sample data was taken for this blend.

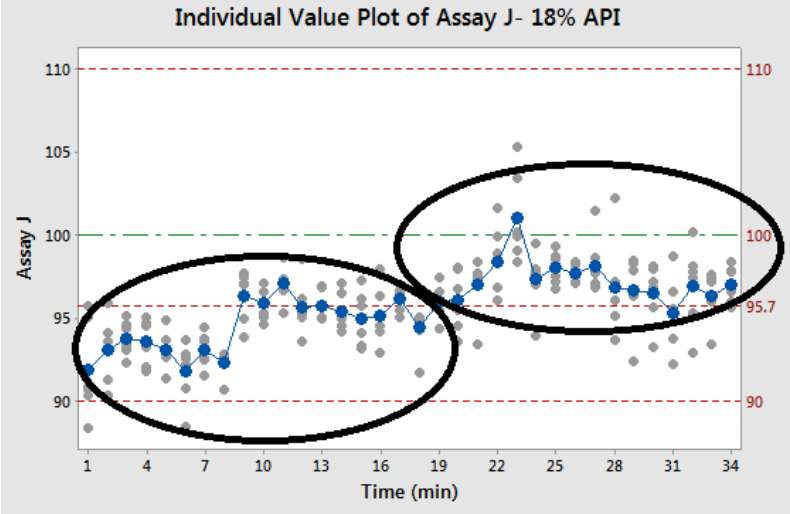

Figure 5-6: Ability of extensive stratified sampling to detect segregation post blending.

Thus an extensive sampling protocol can help detect presence of segregation or agglomeration in tablets.

5.3.3. Comparison of Online blend monitoring with thief sampling

This section involved comparison of the online blend monitoring approach with the traditional thief sampling methodology. A sampling procedure must be designed to account for the dynamics of the mixing process [50]. As discussed, PAT sampling of the blend using online NIR spectrometers has been observed to be an effective method to detect the dynamic progress of blend macro- mixing, and to predict the blend end point. However, the applicability of online blend monitoring to detect blend micro-mixing issues and diagnose the presence of agglomerates has not discussed in the literature.

In our work, the online PAT method was observed to predict the progress of the blending and predict the blend end-point. The presence of API agglomerates in the blend was evident from the thief sample analysis in the previous section. The thief sampling was prone to sampling bias, and hence the measurement was not necessarily representative of

the actual degree of blend uniformity (Figure 5-2). The extensive C.U. sampling of tablets was able to detect the presence of super-potent tablets.

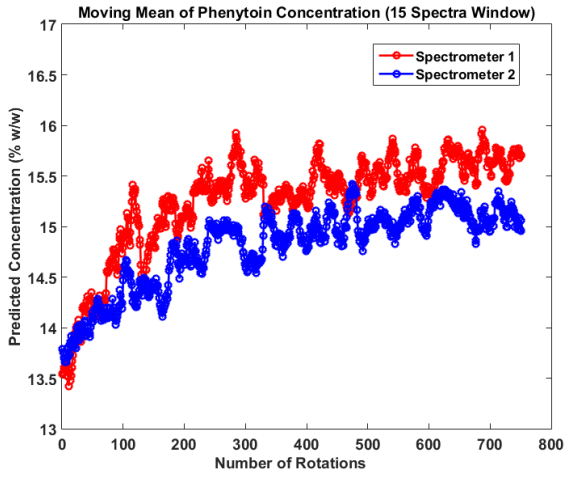

Figure 5-7: a) Online blend monitoring PAT method enabled prediction of blend end point. Cyclic patterns were observed as blending progressed.

Cyclic fluctuations with a certain frequency were observed during online blend monitoring as the blending progressed. These could be the inherent spectrometer fluctuations or could arise from dynamic mixing – demixing phenomenon inside the blender. This issue should be investigated in future work. No correlation or pattern was observed between the formulation parameters and the observed agglomeration or segregation trends.

5.4. Conclusion:

A platform approach was adopted to investigate and compare different sampling methodologies for a direct compaction blend. Sampling bias was observed for the samples taken using the globe pharma thief, where the probe was observed to over sample the blend even when the blend was actually sub-potent. This was explained by the abundance of the API agglomerates and their preferential flow into the sampling cavity.

The online PAT system for blend monitoring was effective in tracking the macro-mixing of the blend. Its utility to detect micro-mixing, including the presence of agglomerates, is under investigation.

The utility of extensive stratified sampling to detect the presence of agglomerates and segregation was studied. Stratified sampling was observed to detect the presence of super potent tablets. An extensive stratified sampling can be of further importance in low- dose products, where agglomerates can occur infrequently and have lower probability of getting captured by limited number of samples. Choosing the right sampling tools and strategies is an important aspect of real time release testing. This work enables implementation and comparison of different PAT sampling techniques as well as traditional methods using a platform approach to determine their reliability and accuracy (or lack thereof).

Chapter 6. The effect of mechanical strain on properties of lubricated tablets compacted at different pressures

6.1. Introduction

Manufacturing pharmaceutical tablets by direct powder compression involves several processes, including die filling, powder densification, compact formation by inter-particle bonding, and tablet ejection and relaxation. These processing steps can have a significant effect on tablet properties, such as tablet porosity, tensile strength and hardness, and dissolution. The work in this chapter forms the basis for understanding the effects of different process parameters on the evolution of tablet structure, and ultimately on tablet hardness and dissolution. Understanding these effects is essential in order to devise strategy for real time release prediction of tablet dissolution using Near IR spectroscopy.

The presence of lubricants in the blend can have a significant effect on tablet properties. It is well known, for example, that tablet tensile strength decreases as lubricant concentration increases. One of the most common lubricants present in pharmaceutical formulations is magnesium stearate (MgSt), and different studies have explained the effect MgSt concentration on tablet properties. Mollan *et al.* [92] observed that the total work put in during compaction decreased with an increase in lubricant concentration, which was attributed to decreased particle cohesiveness. Wang *et al.* [26] demonstrated the detrimental effect of MgSt on tablet hardness and both Wang *et al.* [26] *and* Uzunović *et al.* [22] found a decrease in dissolution as a function of increasing MgSt concentration. The effect that lubricants have on tablet

properties also depends on the excipients present in the formulation and their behavior during compaction [25]. DeBoer *et al.* [93] used SEM imaging to show that MgSt exhibited maximum effect on excipients which underwent plastic deformation without fragmentation and Vromans *et al.* [94] confirmed the effect of magnesium stearate to be dependent on a number of factors, including particle size, flowability and the mechanism of consolidation of the excipients.

In addition, during tablet manufacturing, the powder blend is exposed to different intensities of shear and normal stress, moisture, and temperature fluctuations. For example, in a typical mixing operation, the particles move relative to the mixer blades and vessel walls as well as relative to each other, leading to the dissipation of mechanical energy via frictional work. The shear experienced by the powder blend can also affect tablet properties and quality, particularly tablet hardness and dissolution. In the presence of MgSt lubricant, it is generally accepted that increased shear leads to an increase in MgSt coating of other excipients. In fact, Pingali *et al.* [95] studied SEM images of powder particles and showed that MgSt coated other materials in the blend as shear increased. Using a modified Couette cell, Mehrotra *et al.* were able to show that the relevant variable to quantify the effect of shear is the induced strain, defined as the integral of shear rate with time, which can also be thought as the extent of shear, or as the shear degree. This coating phenomenon also explains the decrease in powder wettability with increasing strain, as observed by Pingali *et al.* [24]. As a result, the amount of lubricant and the strain experienced by the blend

decreases in-vitro dissolution rate. The detrimental effect of excessive shear is generally known as the “over lubrication effect” [96] [97] [24].

If as hypothesized, MgSt is coated onto other particle surfaces, the tablet microstructure should change, depending on formulation and process parameters. The tablet hardness depends not only on tablet porosity, but is also affected by the bonding between the particles. While there is no direct way to estimate the effect of strain on the bonding between the particles, the “work of compaction” approach, which involves studying the energy input during different stages of compaction, has been shown to take into account these effects on tablet microstructure and is also easy to compute. Antikainen *et al.* [98] adopted a similar approach to determine the deformation, fragmentation and elasticity values of different materials satisfactorily. Mollan *et al.* [92] used the force displacement curves to demonstrate the decrease in effects of lubrication on compaction and post compaction properties of maltodextrins. Kottala *et al.* [99] studied material bonding strength between and within the layers of bilayer tablets as a function of material properties, lubricant concentration, and compaction parameters.

However, the effect of total strain on tensile strength and porosity, both in-die as well as after relaxation, and the effect of strain on inter-particle bonding, has not been studied extensively, which is one of the aims of this work. These form the building blocks for the real time release prediction of tablet dissolution.

6.2. Materials and methods

6.2.1. Materials

In all the experiments, the blend formulation consisted of 90% lactose (w/w), 9% acetaminophen, and 1% magnesium stearate (MgSt). We used lactose monohydrate NF as excipient material (Foremost farms, Rothschild, Wisconsin), semi-fine acetaminophen as an active ingredient (Mallinckrodt Inc. Raleigh, NC) and MgSt NF as a lubricant (Mallinckrodt, St. Louis, Missouri, lot: P09247). The mean particle size for lactose, acetaminophen and MgSt were 90 μm, 42 μm, and 38 μm, respectively, and they were sieved to remove any possible agglomerates. Acetaminophen is a model drug widely used in industry. It has poor compressibility, compromising the structural integrity of the resulting compacts. Hence there is a need to study direct compression systems with formulations containing acetaminophen as the active

6.2.2. Experimental Design:

A full factorial design was adopted with 4 levels of shear strain (0,160, 640 and 2560 revolutions of the Couette device [96], see below) and 5 compaction forces (8, 12, 16, 24, 30 kN)

6.2.3. Blending

First, lactose and acetaminophen were layered from bottom to top, and mixed in a 1.87 L V-Blender (Patterson Kelley) at 15 rpm for 15 min. Then, magnesium stearate was added to this pre-blend and mixed for 25 revolutions. The mixing time for the lubricant was kept low and the blender intensifier bar was not operated in order to have minimum exposure to uncontrolled shear in the blender prior to exposing it to controlled shear in the Shearing Device (Couette Cell). Two 1kg blends were made and subsequently divided into 300g samples for the modified Couette shear cell.

6.2.4. Shearing- Couette shear cell

There are different ways to impart shear onto blends; varying the mixing time in a blender is one of them. However, this method is scale dependent and powder in different areas in the blender experience different shear rates. Mehrotra *et al.* [100] suggested a systematic approach to expose the blend to uniform shear by using the Couette shear cell (Chapter 2, Figure 2.3) A similar approach was adopted in this study. The design of the shearing device is explained in (Chapter 2, section 2.2.3). The 300 g samples obtained from the blending procedure were subjected to a controlled uniform shear environment in a modified Couette cell [96]. The shear rate was kept constant at 80 rpm for all the design points. The first sample was not sheared in the cell. Three additional samples were subjected to 160 revolutions (sheared for 2 minutes), 640 revolutions (8 minutes), and 2560 revolution (32 minutes), respectively. These levels have been shown to span the entire range of strain values used in direct compression processes [100]. The terms 'total shear' and 'strain' are used interchangeably in the remainder document.

6.2.5. Tableting

Sheared powder samples were compressed into tablets using a tablet press emulator (Presster™, MCC) and is described in Chapter 2, section2.2.3. 350 mg tablets were made at a nominal force of 8 kN, 12 kN, 16kN, 24 kN, and 30 kN by changing the compaction gap between the punches. The tablet thickness varied from 3.4 mm to 3.0 mm. To reduce tablet variability, the first few tablets were discarded until stable force and mass were obtained.

6.2.6. Tablet porosity measurements:

The volume of the tablets was calculated from the thickness and diameter of the tablets. The porosity was calculated from true density measurements of the individual components obtained from literature (lactose- 1.54 g/cc, Semifine acetaminophen- 1.29 g/cc, magnesium stearate- 1.03 g/cc) and their respective proportions in a single tablet. The measured true density values from Helium Pycnometry (1.55 g/cc, 1.29g/cc and 1.04g/cc for lactose monohydrate, acetaminophen and magnesium stearate respectively) agreed with the reported. The blends and tablets were processed and stored in temperature and humidity-controlled environment where the temperature was maintained at 22^0C and the humidity at 50% RH. None of the materials was known to be hygroscopic and the effect of moisture content on tablet density was neglected. It was assumed that each tablet contained the targeted concentration of individual components. Tablet porosity was measured both during (in- die) and at the end of compaction process (out-of-die). The in-die tablet porosity was calculated from the compaction force-thickness profile, obtained directly from the Presster. A certain amount of axial relaxation was observed when the tablets were taken out of the die. The porosity after relaxation was calculated by measuring the tablet thickness after it was removed from the tablet die. The tablet diameter remained constant at 10 mm and comparatively less relaxation (0.4%) was observed in the radial direction compared to the axial relaxation.

6.2.7. Tensile strength testing

The tensile strength was calculated using the Brazilian disk test [28], where the tablet was subjected to diametrical compression between two parallel plates in the

Scheulinger tensile strength tester. The tablets cracked in brittle form under tensile stress and the maximum crush force was recorded to give the tensile strength as, $s_{max} = (2 * F) / (\pi * D * h)$, where s_{max} is the tensile strength, F is the breaking force, D is the tablet diameter and h is the tablet thickness. As an important detail we note that the tablets from the condition 2560 rev compressed at 30 kN chipped during the procedure and hence were not used.

6.2.8. Work of compaction, plastic and elastic energy calculations:

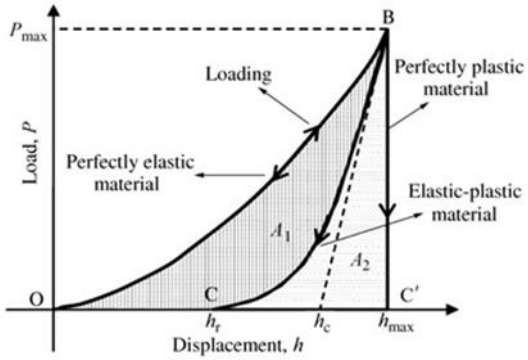

Figure 6-1: Load-displacement curve for compaction. Area under OBC+BCC' gives the total work input (W_{in}). Area under the BCC'- elastic recovered work (WER). Porosity calculated at point O represents the bulk porosity during die fill; porosity calculated at point B represents porosity at maximum compression force and at point C represents final in-die porosity.

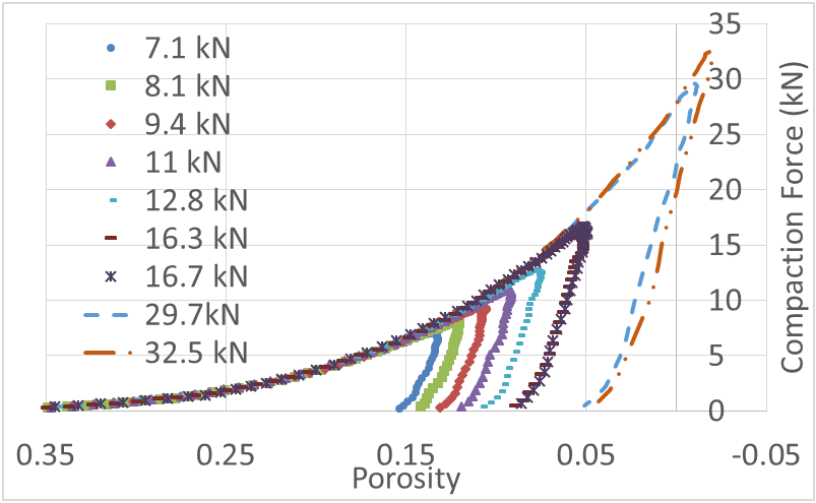

Figure 6-2: An example of the compaction curves obtained during tableting for different maximum compaction forces. Different colors and symbols correspond to different compaction force.

The work of compaction was calculated for each tablet from the force-displacement profile [101]. The total work input (W_{in}) during the compaction process is given by area under the curve- OB as shown in Figure 6-1. As discussed before, the maximum punch displacement (or minimum tablet thickness) was set to obtain the nominal compaction force, but some small variations in compaction force were present. During the decompression phase- curve BC in Figure 6-1, the tablet expands and the elastic energy recovered during unloading (elastic relaxation- EER), is given by the area under the BCC' curve. The force-displacement profiles for tablets made at different compaction forces are displayed in Figure 6-2. The height of the peak changed with respect to the intended maximum compaction force.

6.3. Results and Discussion:

The results are divided into three sections wherein the effect of the process parameters on the porosity and on the tensile strength of the tablets is discussed.

6.3.1. Effect of compaction force and total strain on tablet porosity

Figure 6-3 shows the average porosity of the tablets after relaxation as a function of compaction force for different strain levels. Porosity was measured immediately after ejection. No further relaxation was observed after a week.

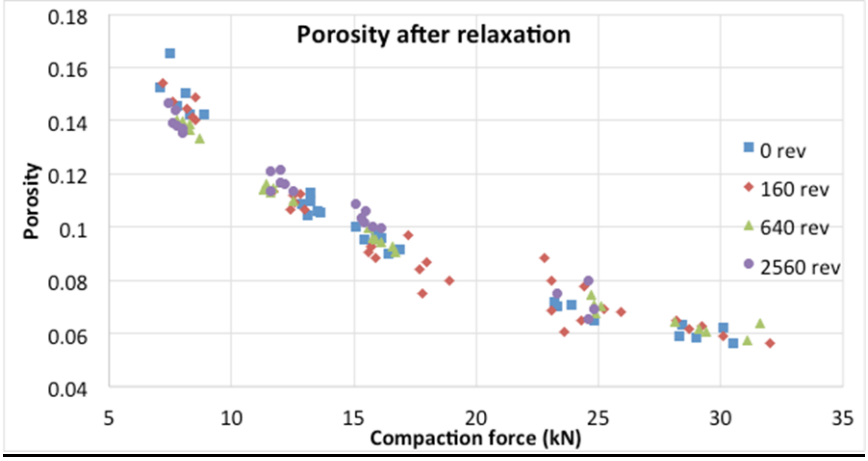

Figure 6-3: Porosity after relaxation of tablets (out-of-die porosity) compacted at 4 strain and 5 force conditions. The tablet porosity decreased with an increase in the compaction force, but blend strain had no discernible effect.

Tablet porosity decreased with an increase in compaction force, as expected. Surprisingly, however, there was no discernible effect of total strain on final tablet porosity. Mehrotra *et al.* observed that the applied strain had a significant effect on blend tapped density [100], which could be expected to affect the porosity of the compacted tablets. However, a response surface regression confirmed that only the compaction force had a statistically significant effect on tablet porosity (see Table 6-1). The residuals were normally distributed as shown in Figure 6-4. To validate this conclusion, the shear effect size was taken into consideration [102]. The shear effect size was equal to 2 times the shear regression coefficient (2*0.003170=0.006340). The 95% shear confidence limit was computed using the t-statistic. For a 95% confidence interval and error degress of freedom (here =13) , the t-statistic was 2.160. Thus the confidence limit was t-statistic*2*SE coefficient= 0.0078, which was

observed to be larger than shear effect. Hence it was concluded that the shear did not have a significant effect for alpha of 0.05.

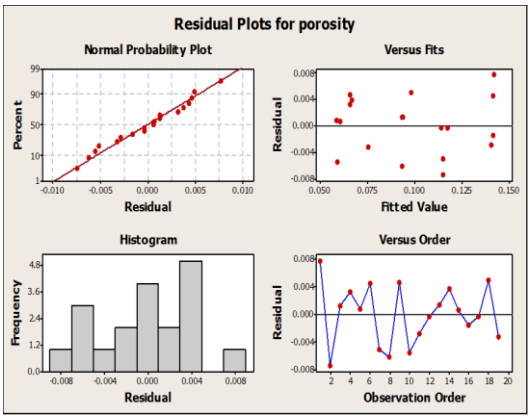

Response Surface Regression: porosity versus shear, force

The analysis was done using coded units.

Estimated Regression Coefficients for porosity

Term	Coef	SE Coef	T	P
Constant	0.082236	0.003563	23.081	0.000
shear	0.003170	0.001811	1.750	0.104
force	-0.038127	0.002302	-16.564	0.000
shear*shear	0.001919	0.003813	0.503	0.623
force*force	0.019573	0.003128	6.257	0.000
shear*force	0.003364	0.002755	1.221	0.244

S = 0.00499576 PRESS = 0.000825334

R-Sq = 98.09% R-Sq(pred) = 95.15% R-Sq(adj) = 97.36%

Figure 6-4: (left) Residual plots for porosity. Shear had no significant effect on tablet porosity. The residuals show no trend with observation order.

Table 6-1: (right) Response surface regression to determine the effect of shear and force on porosity after relaxation. Force had a significant effect on tablet porosity. The effect of shear was not significant.

In contrast, the in-die porosity exhibited a clear trend as a function of the shear strain. Figure 6-5 depicts the evolution of tablet porosity during the compaction process as a function of blend shear, for a compression force of 12 kN. Each curve represents an individual tablet. Similar plots were obtained for the different compaction forces studied here (8, 16, 24, 30 kN).

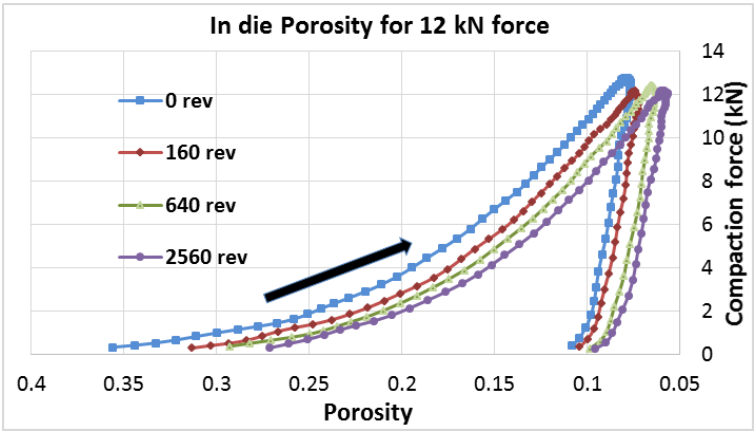

Figure 6-5: Compaction curves in- die for a compaction force of 12kN. The different symbols correspond to different shear-strain levels as indicated. The bulk porosity during die- fill decreased with an increase in strain. The final porosity at the end of the unloading phase was observed to converge for different strain levels. Each curve represents a single tablet.

The compaction curves were also used to calculate the porosity values at different stages of the compaction process. The average porosity at different compaction stages for a nominal compaction force of 12kN as a function of shear strain is presented in Figure 6-6. The bulk porosity during die filling (corresponding to point O in figure 2) was observed to decrease with shear strain, from 36% to 27%, approximately. This was consistent with previous observations, where the particles exposed to higher strain levels packed better during die filling [100]. In addition, the total strain had an effect on porosity at maximum compression (point B in Figure 6-1). The corresponding minimum in-die porosity varied from 6% to 9% (see figure 6). The final in-die porosity post unloading (point C in Figure 6-1), showed less dependence on the shear-strain compared to the die-fill porosity, with porosity close to 10%-12% for tablets at all strain levels. Thus, a clear convergence in the porosity values was observed as a function of shear strain, from initial bed porosities, to the minimum porosities at maximum compression and in-die post unloading porosities. Although most of the axial recovery was observed to occur during the in-die unloading phase, further relaxation was measured after ejection.

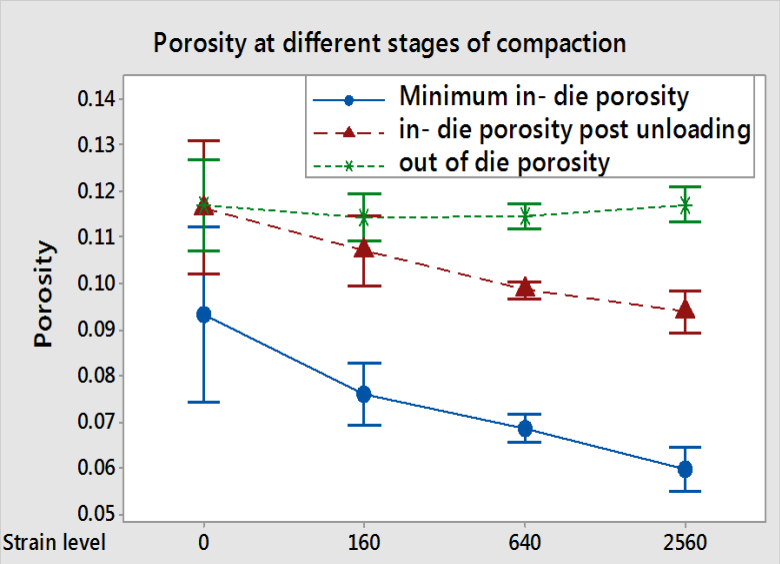

Figure 6-6: Effect of blend shear on porosity at different stages during and post compaction. A part of tablet deformation was recovered during the in- die unloading stage and the remainder was recovered after the tablet was taken out from the die. The recovery was highest for higher strain tablets indicating compromised inter-particle bonding inside the tablet compact.

To gauge the effects of shear on relaxation in-die during the decompression phase, the percentage of apparent axial recovery of each tablet was calculated according the equation:

$$\textbf{Apparent axial recovery in-die} = (\varepsilon - \varepsilon_{min}) * 100 / \varepsilon_{min} \qquad \textbf{Equation 6-1}$$

where ε_{min} is the minimum porosity (at maximum compaction) and ε is the final porosity in- die. The in- die axial recovery during the decompression and ejection phases for compacts made at 12 kN force is plotted inFigure 6-7. with an increase in the strain level, the tendency of the compacts to relax increased from 28% to 60%. For tablets compacted at 8 kN and 16 kN, as strain increased from 0 to 2560 rev the axial recovery increase ranged from 16 to 25% and 70 to 147% respectively. Thus,

the tablets compressed under higher compaction forces were observed to relax more.

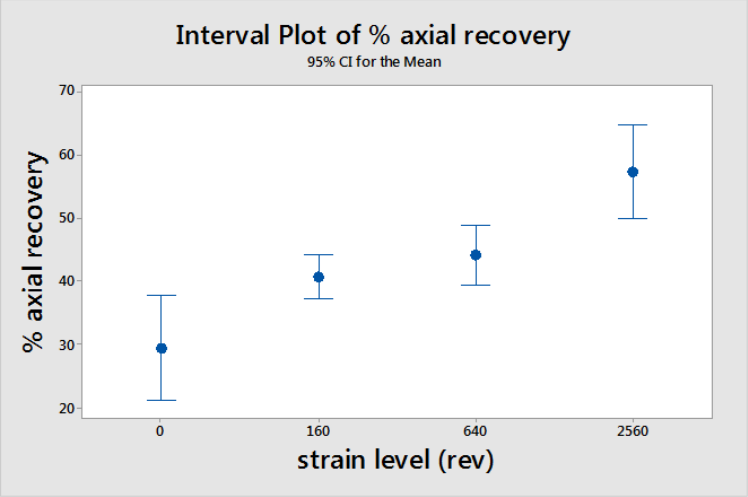

Figure 6-7: Percentage axial recovery in-die as a function of strain for compacts made at 12kN-targeted force. Increase in the strain correlated to an increased tendency of tablets to relax. Axial expansion was greatest for the compacts that were least bonded, which occurred for higher strain level.

Magnesium Stearate acts as a glidant along with being a lubricant. This reduces the particle- particle friction as well as the die wall friction, which leads to efficient packing during die-fill. As far as the effect of force at constant strain was concerned, during the decompression stage, the compacts with lowest porosity (and hence, maximum force) were the ones that showed maximum relaxation.

6.3.2. Work of compaction:

During tablet compaction, the total work input is utilized in both reversible (elastic deformation) and irreversible processes (plastic deformation, fragmentation, and friction) [103]. A fraction of the elastic energy is recovered (EER) during ejection, off-die relaxation, and/or breakage. The rest remains trapped in the tablet in the form of residual stresses, which develop during the loading and unloading process. The

ability of the tablet to store residual stresses depends on the formation of bonds during the consolidation process and their strength. Therefore, the elastic energy recovered is an indication of bond strength.

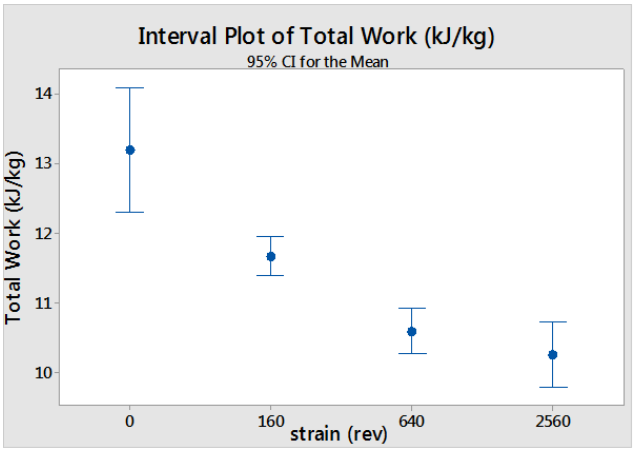

Figure 6-8: Total input work (W_{in}) during compaction (kJ/kg) as a function of total strain. The work decreases with increase in strain.

First of all, let us note here that the total input work (W_{in}, the area under the force-displacement curve) was relatively insensitive to the initial porosity before the compaction process (i.e. porosity during die-fill). On the other hand, the total work input increased with the compaction force, as expected. For a given nominal compaction force, the total work input was observed to decrease with shear strain as shown in Figure 6-8. In addition, the elastic energy recovered per unit total input work increased with shear strain, as shown in Figure 6-9.

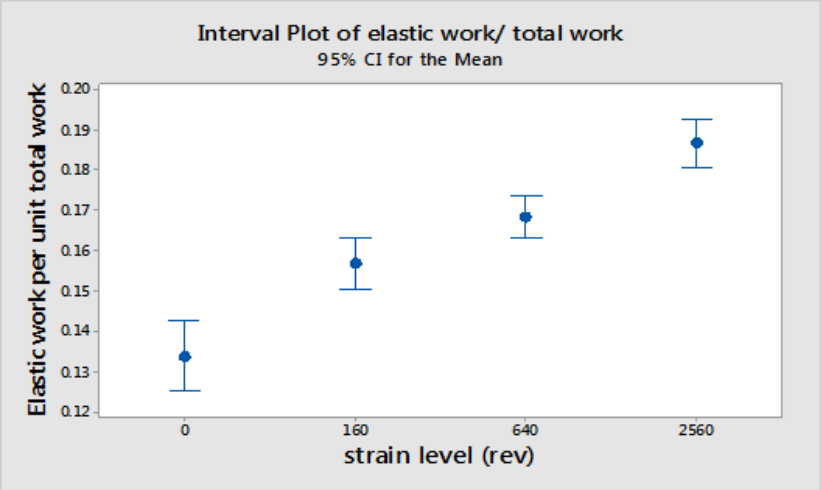

Figure 6-9: Elastic energy recovered (kJ/kg) during in-die unloading per unit total work as a function of total strain. It showed an increase with increase in strain. Weak compacts resulting from insufficient bonding can only store limited amount of elastic energy in the form of residual stresses after ejection, leading to a larger fraction of elastic energy recovered during unload.

The experimental record shows that EER increases with blending strain, which may be attributed to weak particle bonding. As strain increases, the evenly distributed magnesium stearate hinders particle bonding. Hence, the portion of elastic enery recovered shows an increase with increasing strain level as can be seen in Figure 6-9. Similarly, during the unloading phase, the axial expansion of the compact was maximum for particles that were less bonded, which occured for high values of the blending strain. This can be observed from Figure 6-7, where blends that were sheared least exhibited a lesser percentage of axial recovery.

6.3.3. The effect of blend strain and compaction force on tensile strength of tablets

The observed correlation between tablet tensile strength and porosity can help determine the strength and degree of interaction between particles in the compact. In Figure 6-10, the measured tensile strength was presented as a function of porosity.

First of all, the tensile strength was observed to decrease as the porosity of the tablets increased. More important, the tensile strength showed a clear dependence on the shear strain. For a given porosity (or compaction force), the tensile strength of the tablets diminished with increasing shear strain. This confirms that the porosity of the tablets alone was not sufficient to capture the effect of shear strain on the strength of the tablets. In other words, tablets with the same *densification* showed significantly different tensile strengths depending on the shear strain experienced by the blend. This can be attributed to the coating of materials with magnesium stearate, reducing the interparticle contact required for bonding and to create stronger compacts. This is in accordance with Mollan *et al.* where as the total work input during compaction increased, the compacts formed became stronger due to higher amount of energy utilized in the formation of bonds, provided that the die wall friction was minimal [92].

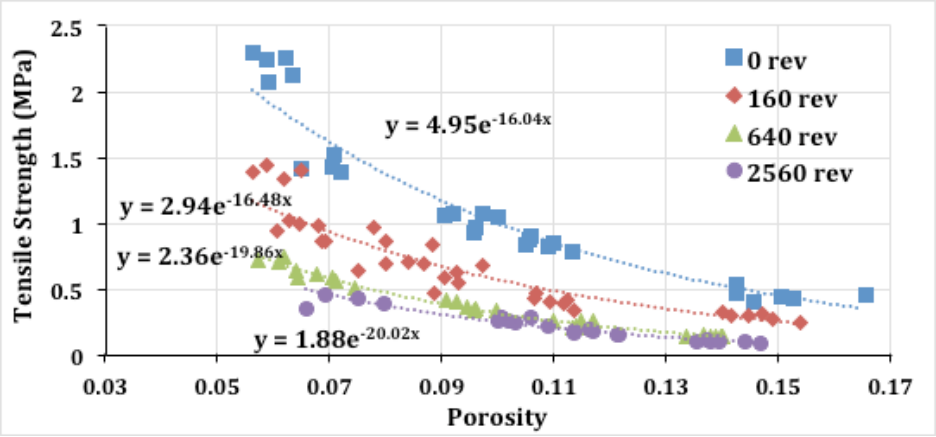

Figure 6-10: Tensile strength as a function of tablet porosity. The tensile strength was affected by both compaction force and strain. Porosity alone was not sufficient to predict tablet hardness. The extent of magnesium stearate coating other ingredients affected bonding between particles, which lead to reduced hardness.

For all shear strain levels, the tensile strength was observed to decay exponentially with porosity (see Figure 6-11 (a)). The tensile strength and porosity profiles were fitted to the Ryskewitch Duckworth equation [104]:

$$s = s_0 \exp(-k_s\, \varepsilon), \qquad \text{Equation 6-2}$$

where s is the tablet tensile strength and ε is the tablet porosity. The fitted parameters are reported in Table 6-2. Interestingly, the effect of shear strain was more significant in the tensile strength at zero-porosity, s_0, with a reduction of 60% with increasing shear strain.

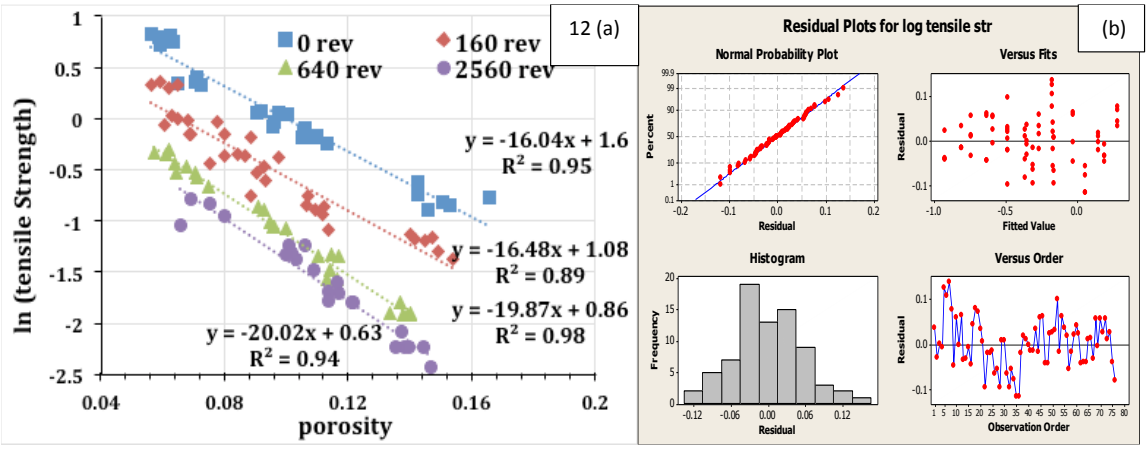

Figure 6-11: a) Tensile strength of the tablets (in logarithmic scale) as a function of the porosity (left). The dotted lines correspond to the fits obtained for different shear-strain levels. b) Residual Plots for log tensile strength (right). The residuals were normally distributed.

Table 6-2: Ryskewitch Duckworth parameters for 12 kN compacts and 4 strain level. The tensile strength at zero porosity decreased with an increase in strain

shear strain level	$\ln(s_0)$	s_0
0	1.5996	4.951052
160	1.0773	2.93674
640	0.8567	2.355375
2560	0.6311	1.879677

Finally, a goodness of fit analysis was performed and a response surface was determined by regression to estimate the linear, quadratic and interaction effects of

shear and force on the natural logarithm of the tensile strength, leading to an R-square of 97.48% (Table 6-3). The data set involved 80 tablets and the residuals were normally distributed (Figure 6-11 (b)), and hence, normality of the data set was not an issue. It was observed that both porosity and compaction force had significant effect on the tensile strength values. Interestingly, the interaction between force and shear appears to be negligible.

Table 6-3: Goodness of fit analysis for response surface regression. Both strain and force had a significant effect on the tensile strength.

Response Surface Regression: ln tensile str versus Force, Shear

The analysis was done using coded units.

Estimated Regression Coefficients for ln tensile str

Term	Coef	SE Coef	T	P
Constant	-1.46061	0.04653	-31.391	0.000
Force	0.74229	0.03006	24.694	0.000
Shear	-0.65009	0.02365	-27.484	0.000
Force*Force	-0.24481	0.04085	-5.993	0.000
Shear*Shear	0.97679	0.04980	19.614	0.000
Force*Shear	0.01134	0.03598	0.315	0.754

S = 0.130485 PRESS = 1.36752

R-Sq = 97.48% R-Sq(pred) = 97.10% R-Sq(adj) = 97.29%

Zuurman *et al.* [105] found similar trend between tablets composed by a filler-binder excipient alone versus same excipient mixed with magnesium stearate. They found that the tablets with magnesium stearate showed a decrease in tensile strength for same porosity. They attributed the effect to decrease in bonding efficiency with magnesium stearate presence. The bonding efficiency between particles was affected by shear, reducing the inter- particle bond strength.

6.4. Conclusions:

Designed experiments were utilized to explore the effect of strain on tablet porosity and hardness. It was concluded that porosity alone was not sufficient to predict tablet tensile strength and that the knowledge of bonding efficiency in tablets was also critical. It was observed that this bonding efficiency indirectly manifested itself in different tablet properties such as tablet porosity during and post compaction, the axial recovery of tablets, the total work of compaction and the elastic work that was recovered during the compaction process. These measurements were used to highlight the role of shear in determining the tablet's hardness.

Strain had, at best, a very small effect on the porosity of the tablets after relaxation. While the initial bed porosities were different, and the porosities at peak compression were also different, the porosity after relaxation was observed to converge. Most of the tablet axial recovery as a fraction of the total recovery happened during the in-die unloading phase. Almost all the additional porosity reduction due to strain was recovered after ejection.

Percentage axial recovery calculations highlighted the differences in the tendencies of tablets to relax with different strain levels. Materials exposed to different shear levels exhibited different tendencies to bond, which ultimately affected the total work input and the recovered elastic energy. The portion of elastic energy recovered during the in-die tablet relaxation showed an increase with increasing strain level. The tensile strength showed an exponential inverse relationship with tablet porosity. Different tensile strength- porosity plots were obtained for tablets made at different strain conditions. Ryskewitch Duckworth equation provided good fit for the data.

The knowledge of the effect of blend strain and compaction force on tablet properties will be exploited in devising the strategy for real time release testing of tablet dissolution both in continuous and batch processing.

Chapter 7. Real Time dissolution prediction of tablets exposed to different degrees of over lubrication in batch process[1]

[1] Work done in collaboration with Eduardo Hernandez
This work can be obtained in the publication: E. Hernandez, P. Pawar, G. Keyvan, Y. Wang, N. Velez, G. Callegari, A. Cuitino, B. Michniak-Kohn, F. J. Muzzio, and R. J. Romañach, "Prediction of dissolution profiles by non-destructive near infrared spectroscopy in tablets subjected to different levels of strain," J. Pharm. Biomed. Anal., vol. 117, pp. 568–576, Jan. 2016.

7.1. Introduction

Performance evaluation of a pharmaceutical product are essential and mandatory to assess and confirm the quality of a drug product that will ultimately be delivered to patients. In the pharmaceutical industry, dissolution testing is a key analytical tool in both drug development and quality control. The data obtained from dissolution tests can be used to detect physical changes in an active pharmaceutical ingredient (API) and formulated product, to establish *in vitro-in vivo* correlations of drug products, and justify post-approval changes [106] [107]. Furthermore, it is useful in identifying critical manufacturing variables, such as mixing time and speed, compaction speed and pressure, and coating parameters. However, as discussed earlier, dissolution testing is a slow, labor-intensive technique and cannot be used for RTRt. In this chapter, the strategy to use Near IR spectroscopy to predict the dissolution profiles of tablets exposed to different levels of mechanical strain during blending is presented. The study follows chapter 6, where the effects of the shear strain and compaction force on tablet properties was investigated in terms of particle bonding, tablet axial recovery, and hardness testing. Near IR reflectance spectroscopy was observed to capture this effect of strain, which ultimately affected tablet

dissolution. This work is aimed towards real time release testing of tablets in batch processing, leading to fast non- destructive prediction of tablet dissolution.

The standard-setting body, the United States Pharmacopoeia (USP) outlines the use USP Apparatus 2 (paddle) for Immediate-release, modified-release, and extended release tablets [108]. Despite its simplicity of design and the ease of use the dissolution apparatus lacks reproducibility, and this has become a concern to the Food and Drugs Administration (FDA) as well as to the pharmaceutical industry. The variability observed in dissolution results often stems from uneven mixing within the dissolution vessels. Studies have shown that tablet position in the vessel, USP Apparatus, and operators have also contributed to variability in drug release profiles [109] and [110]. Additionally, the most significant challenge has been lack of bio-relevance as dissolution methods are often not correlated to *in vivo* performance [111]. Difficulties in having suitable USP calibration tablets, physical-chemical (temperature, particle size, solubility, and polymorphism) and mechanical (position of the aliquot, vibrations, paddle or vessel position) factors can contribute to dissolution variability [112]. Drug release concentration in the dissolution medium is determined with High Performance Liquid Chromatography (HPLC) or Ultraviolet/Visible Spectroscopy (UV/VIS) using solvents with high cost and leading to significant solvent wastes generated in the analysis. However, use of Quality by Design (QbD) has been introduced in the pharmaceutical industry, and efforts have been underway to control the variance observed in the USP Apparatus [113] [114].

Besides formulation parameters, dissolution rate is also affected by process parameters such as tablet press speed and compaction force. As discussed in Chapter 6, one such

process parameter that is often neglected is the total amount of strain that the powder experiences, before it goes into the tablet press. Dissolution performance can be affected by the nature of the process stress within the manufacturing steps (batch or continuous). Studies have been carried out to predict the sources and nature of shear and strain that are related to the process stress in such a continuous process. Vanarase *et al*. explained the effect of number of blade passes (which depend on the residence time and the blade (rpm) and the lubricant feeding point on powder properties for a continuous mixer [115]. Mendez *et al*. investigated the increase in hydrophobicity of tablets and hence dissolution time, owing to the strain exposure in feed frame of tablet press [116]. NIR can be used to investigate effects of such shear strain and thus help predict dissolution of oral solid dosage forms. Near Infrared Spectroscopy (NIRS) gives the opportunity to obtain information on the physical and chemical properties, obtaining a high signal to noise ratio spectrum in one minute and without destroying the unit dose.

Near infrared (NIR) spectroscopy provides information on the physical properties (compaction force, shear, etc.) and chemical composition (content uniformity, water content, etc.) of the sample [117]. This information can be filtered out or maintained, depending on the quality attribute of interest. This is achieved using multivariate data analysis like PCA, PLS, etc. Several researchers have used this kind of approach to evaluate the drug release from the final product. Zannikos *et al*. related the dissolution profiles of carbamazepine tablets exposed to different levels of humidity with NIR spectra [118]. Donoso *et al*. related the NIR diffuse reflectance spectra using linear regression, nonlinear regression and PLS models to predict drug release on theophylline tablets with different

compaction forces at different time points of the dissolution [29]. Freitas *et al*. correlated the dissolution profiles with NIR reflectance spectra using PLS calibration model to predict drug release behavior at different time intervals and for media with different pH [119]. Blanco *et al*. used a single PLS-2 model to predict the dissolution profiles of tablets made at different compaction forces and consisting of different API concentration [120]. PLS-2 gives the opportunity to predict multiple variables in a single calibration model [121]. Otsuka *et al*. used transmission and diffuse reflectance spectra using multivariate regression models to predict dissolution properties in tablets containing indomethacin as active pharmaceutical ingredient (API) [122]. Tabasi *et al*. used PLS to predict dissolution profiles at different time points of tablets with different coating grades [123]. Theses researchers used several PLS calibration models for the selected time point in the dissolution profile. These methods were developed using multiple PLS calibration models at any given time point in the dissolution profile.

This study describes a non-destructive NIR method to predict dissolution profiles based on how shear affects the drug release of tablets with similar drug concentration and compaction force. The importance of characterization of shear in continuous processes, detecting such shear by non-destructive testing, and ultimately predicting tablet dissolution is discussed in this chapter. The authors understand that this is the first study that takes into consideration the shear forces from continuous mixers to develop a non-destructive NIR method to predict dissolution profiles. The non-destructive method has an advantage over the current dissolution test, where it impossible to further evaluate the unit dose when the test fails. With the non-destructive NIR test, the root of cause of the failing unit may be

investigated through multivariate data analysis and by other techniques such as Raman spectroscopy, NIR-Chemical Imaging, Ultrasound or Terahertz [124], [125], and [22] . Following the methodology of this study the authors establish an implementation strategy that can be recommended for continuous manufacturing processes in the pharmaceutical industry.

7.2. Materials & Methods

7.2.1. Materials

The materials are described in chapter 6, section 6.2.1.

7.2.2. Blending and shearing, and tableting process

The blending and shearing procedure was described in Chapter 6, section 6.2.3 and section 6.2.4 respectively. The tableting procedure was described in Chapter 6, section 6.2.5. Tablets compacted at an average force of 24 kN (305 MPa) from the previous study were used for further analysis in this chapter.

7.2.3. Near Infrared Spectroscopy

A Bruker Optics Multipurpose Analyzer (MPA) FT-NIR spectrometer (Billerica, Massachusetts) was used to obtain tablet diffuse reflectance spectra with a resolution of 32 cm^{-1}. The integrating sphere unit was used within the spectral range of 12500 to 3500 cm^{-1}. A total of 256 background and sample scans were averaged. Spectra were obtained from both sides of the tablet.

7.2.4. In- Vitro Dissolution testing

The drug release studies were performed using the USP paddle method, at a rotational speed of 50 rpm in a VK 7010 dissolution apparatus (Varian Inc., Santa Clara, CA). The dissolution medium was composed of 900 ml pH 5.8 Phosphate buffer, and the temperature was maintained at 37.0±0.5^{o}C. Six tablets were each placed in chambers in the dissolution apparatus and ejected into the dissolution vessels simultaneously. Aliquots of the dissolution medium were pumped at 3-minute time intervals using a peristaltic pump VK 810 (Varian Inc., Santa Clara, CA). The medium was then filtered through 35 μm full flow filters prior to detection using a UV spectrophotometer. A wavelength of 243 nm was used to analyze the samples using a Cary 50 UV-Visible spectrophotometer (Varian Inc., Santa Clara, CA). Absorbance values for each tablet were converted to the percent of drug released at each analysis time and used for the calibration model [26].

7.2.5. Multivariate data analysis

Multivariate data analysis was performed using The Unscrambler X 10.2 (Camo, Oslo, Norway). Certain process parameters like compaction pressure affect the physical properties of tablets (example: tablet density). This in turn affects the scattering of radiation and thus affects the near infrared spectrum. Baseline correction was performed to maintain the scattering effects related to physical properties in the spectra. This preprocessing step consisted of setting the first point of the spectra to zero.

After baseline correction, principal component analysis (PCA) and partial least square-2 (PLS-2) were performed on the spectra. A total of 40 spectra obtained from the two sides of 20 tablets were used as calibration set. PCA was used for exploratory data analysis to study the spectral differences arising from the differences in shear.

PLS-2 method was used to develop the calibration model for percent drug released in tablets with differences in strain applied. A PLS-2 model was created to predict dissolution at different time points from 3 to 120 minutes. A total of 40 variables (time points) were used as dependent variables to create the PLS-2 model. Cross-validation (CV) was used for initial method evaluation and as a tool to help in method development. CV groups were established by shear conditions to perform a 'leave one class out' challenge, where one group was left out to be predicted by the model. Table 7-1 summarizes the CV groups. The preliminary model developed with CV, was further challenged with a validation set consisting of 24 spectra from twelve tablets (Table 7-1) that were prepared separately from the calibration tablets. The validation set included tablets spanning over the different strain levels (0, 160, 640, 2560 revolutions). The dissolution profile predictions of the validation set obtained using NIR were compared with the dissolution profiles obtained using the destructive method (USP 2 Apparatus).

Table 7-1 – Calibration and Validation set description for the model.

Set Description	Shear Level (Revolutions)	Number of Tablets	Number of Spectra	Cross Validation Group
Calibration	0	5	10	1
	160	5	10	2
	640	5	10	3
	2560	5	10	4
Validation	0	3	6	N/A
	160	3	6	
	640	3	6	
	2560	3	6	

7.3. Results

7.3.1. In-Vitro Dissolution Testing and Effect of Strain

Figure 7-1 shows the effect of strain on the average dissolution profiles each strain condition. As the strain was increased, the amount and the rate of drug release decreased. This could be an example of over-lubrication due to formation of a magnesium stearate hydrophobic film covering the active ingredient in the formulation [10, 27].

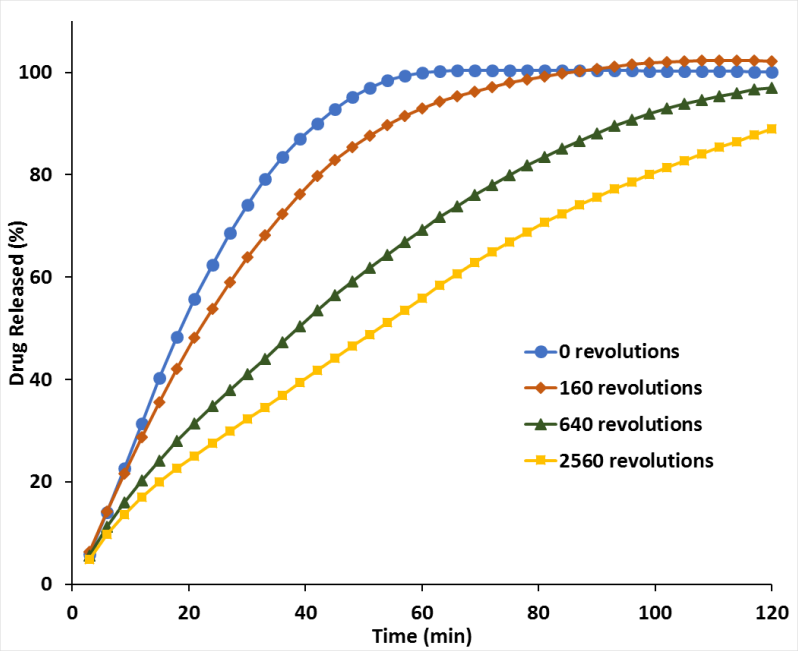

Figure 7-1– Dissolution profiles obtained from USP apparatus 2

7.3.2. Evaluation of NIR spectra, relationship between spectra and dissolution

NIR diffuse reflectance spectra were acquired for tablets. Baseline correction was used to maintain all scattering effects associated with physical properties of tablets before performing any multivariate data analysis. This was done because physical properties of the tablet can affect the dissolution as demonstrated in previous studies, where an increase in the compaction force resulted in an increase in the intensity of NIR diffuse reflectance spectra and dissolution was a function of compaction force [122]. Several studies have shown that light scattering is a function of the physical properties of particles [124], [126],

and [127]. These differences in scattering result in the multiplicative and additive effects observed in the NIR spectra which are usually removed by normalization and derivatives [128]. But baseline correction does not remove multiplicative and additive effects in the spectra, and thus the scattering effects from differences in the physical properties of particles are included in the mode. All spectra obtained in this study showed small but significant variations in the spectral slope from 7000 to 5500 cm^{-1}. Figure 7-2 shows that as strain increased, the spectral slope decreased separating the spectra according to the strain applied. The differences observed in the NIR spectra as the strain was varied indicated the feasibility of developing a calibration model to predict dissolution.

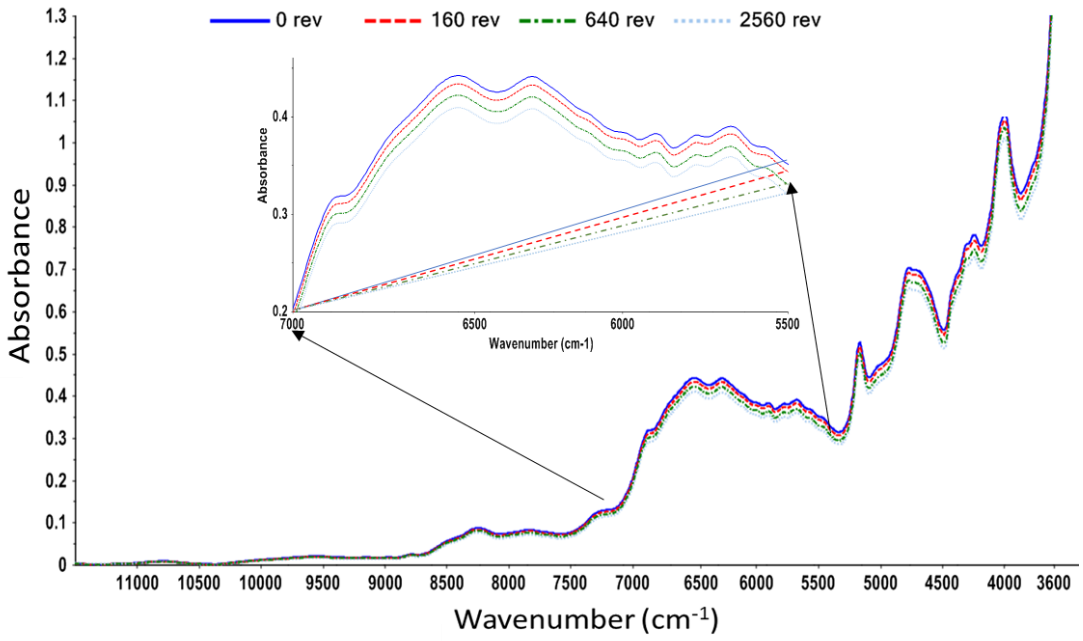

Figure 7-2– NIR spectra for tablets subjected to different levels of strain. Zoom of the spectral region of 7000-5500 cm^{-1} were slope changes are observed.

PCA was used to further investigate the spectral differences observed. The PCA method shows that the first source of variation associated with the samples was the strain applied

since four different groups are observed in Figure 7-3. Four groups were separated along the PC1 with 99% of the variation explained. PC1 loading plot as displayed in Figure 7-4 shows that the spectra varied through the entire spectral region. PCA computes latent variables that are a linear combination of the original manifest variables [129]. The loading plot describes how the principal component is related to the original variables.

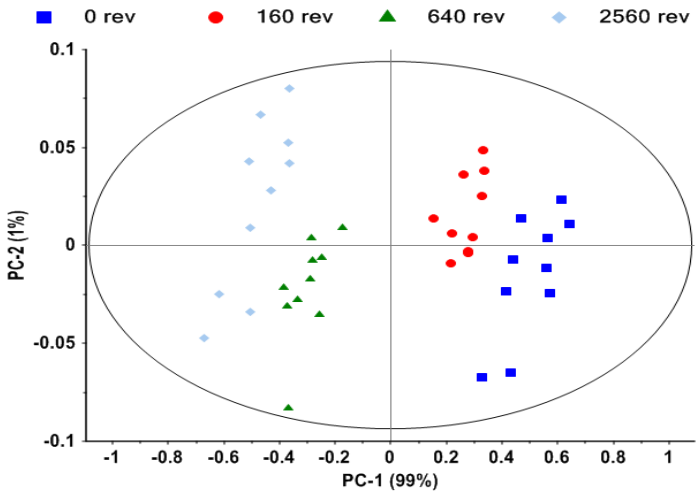

Figure 7-3– PCA score plot of NIR spectra from tablets with different levels of strain.

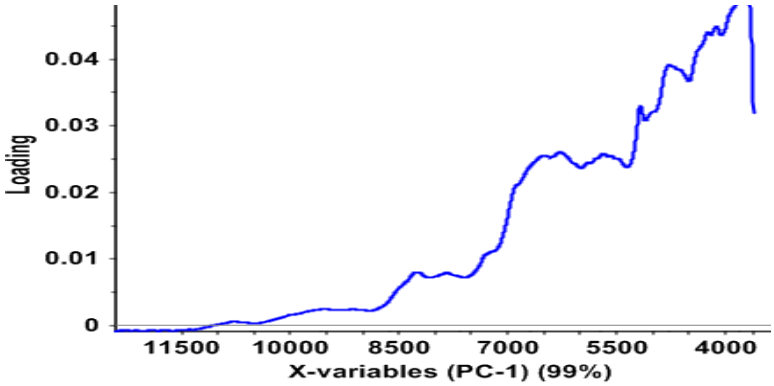

Figure 7-4– Loading plot of PC1

7.3.3. PLS model method evaluation

A PLS-2 calibration model for predicting the drug release was developed relating the spectral differences to the percent drug release values from the dissolution test. The spectra (independent variables) used for the calibration model consisted of tablets compressed at 305 MPa and four different shear levels investigated over the entire spectral range- 11328 to 3614 cm^{-1}. The dependent variables consisted of percent drug release values obtained with the dissolution test every three minutes for the entire 120 minutes dissolution profile. All spectra were mean centered and baseline corrected. Table 7-2 summarized the model evaluation statistics results for 1 to 4 PLS factors for both spectral ranges. The PLS calibration model was developed with two PLS factors. The bias for the leave one class out cross validation results was only 0.59 % for two PLS factors, and only -0.53 % drug release for the validation set tablets in the entire spectral region. The bias is considered low and indicative of excellent accuracy since percent dissolution increases to almost 100%. The results were also evaluated through relative standard error of cross validation or prediction (RSE) as shown below:

$$\boldsymbol{RSE}(\%) = \mathbf{100}\ \boldsymbol{x}\sqrt{\frac{\sum_{i=1}^{n}(y_{pred}-y_{obs})^2}{\sum_{i=1}^{n}(y_{obs})^2}} \qquad \textbf{Equation 7-1}$$

where y_{pred} is the value predicted and y_{obs} is the value for each analysis time in the dissolution profile. Relative Standard Error of cross validation (RSEcv = 8.3%) are based on a leave-one class-out cross validation and Relative Standard Error of Prediction (RSEP = 6.3%) are based on the validation set for the entire spectral range.

Table 7-2– Calibration model evaluation statistic summary for 1 to 4 PLS factors.

PLS Factor	RMSEE	RSEC (%)	BIAS cv	RMSEcv	RSEcv (%)
1	5.26	7.25	-0.568	6.14	8.78
2	4.74	6.23	-0.592	5.97	8.31
3	4.97	6.36	-0.455	6.26	8.66
4	4.48	5.67	-0.491	6.25	8.62

7.3.4. PLS model validation

The validation set included 24 spectra (12 Tablets) of 305 MPa compaction force with four levels of strain applied (Table 7-1). These are completely independent tablets none of which were included in the calibration set. The PCA model was used to project validation set spectra into the score plot space. Figure 7-5 shows the multivariate 95% confidence interval as marked by the ellipse (Hotelling's T^2 test) and the results obtained. All the spectra were within the 95% confidence interval, except for one spectrum from the tablet subjected to 640 revolutions.

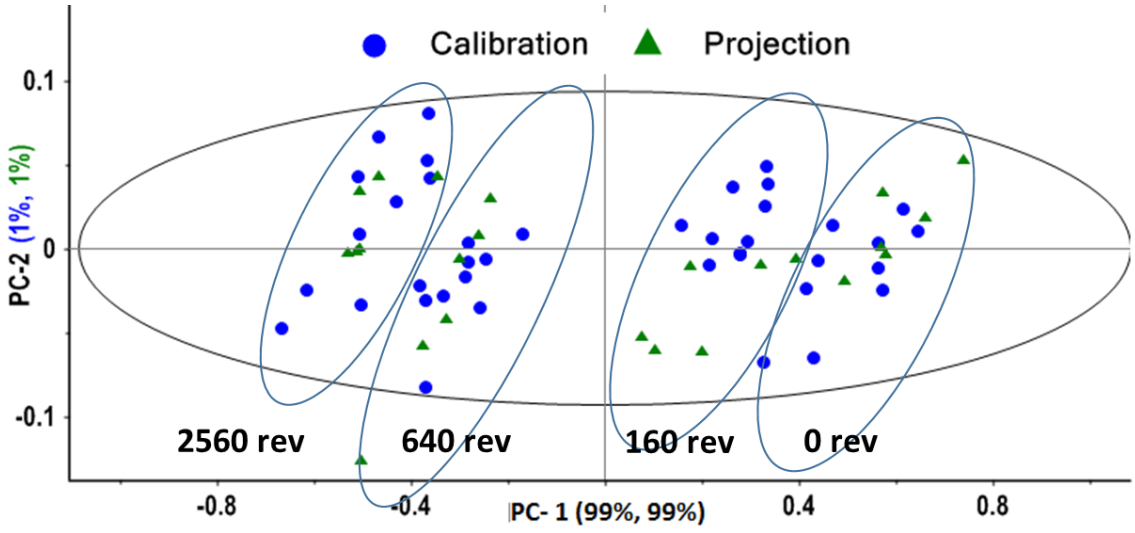

Figure 7-5– Projection of validation set on the PCA scores plot of NIR spectra. Black symbols represent calibration set and white symbols represent validation set.

The PLS-2 calibration model predicted drug release for validation set tablets. Figure 7-6 presents the predictions correlation comparing both dissolution profiles and NIR predictions for the entire spectral range. Predicted dissolution profiles show a high correlation when compared with the reference method achieving a 0.9992 correlation

coefficient for 0 and 160 revolutions, 0.9983 for 640 revolutions and 0.9977 for 2560 revolutions. The accuracy of the prediction of dissolution was evaluated through the use of the RSEP. RSEP for the validation set using the entire spectral region was 6.3%. Table 7-3 summarized the validation set evaluation of the model for both spectral ranges. Minor changes in compaction force and concentration are likely contributing to the variation observed.

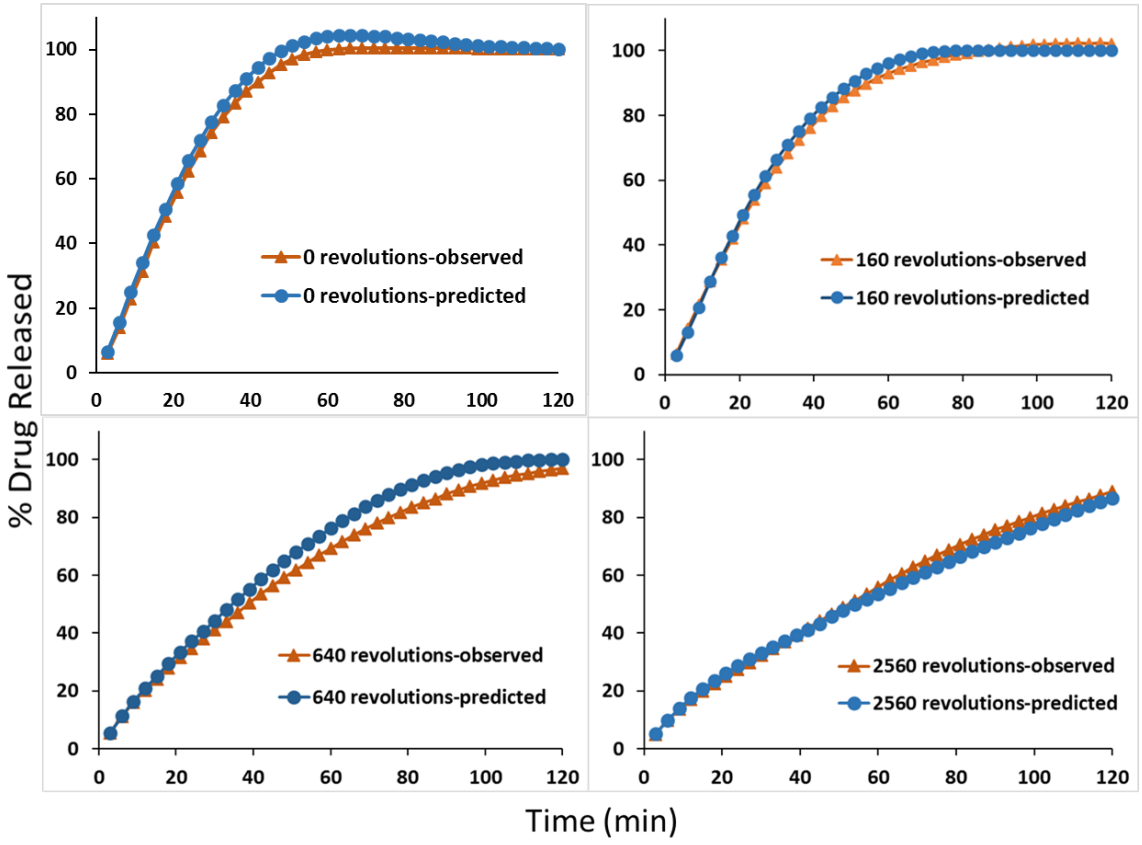

Figure 7-6– Comparison between USP apparatus 2 dissolution profile (observed) and NIR dissolution profiles predicted with 2 PLS factors.

Table 7-3– Validation set results for 2 PLS factors (shear level results and global results). RSEP (%)= relative standard error of prediction, f_2= similarity factor, F= F calculated from ANOVA, R^2= correlation coefficient

PLS Factor	Shear Level (Revolutions)	BIAS TS	RMSEP	RSEP (%)	f_2	F	R^2
2	0	-3.08	4.13	4.68	67	0.622	0.9992
	160	1.53	4.34	5.06	93	0.036	0.9992

	640	5.81	7.29	9.51	75	0.1484	0.9982
	2560	-2.15	3.52	6.06	69	0.3157	0.9977
	Global Results	0.531	4.82	6.33			

7.3.5. Evaluation of dissolution profiles

PCA was also used to compare the dissolution profiles predicted by the NIR method. The independent variables matrix consisted of dissolution values [130], [27]. The PCA scores plot shows four separate groups related to shear level for USP Apparatus 2 values and NIR predictions are shown in Figure 7-7. PC1 explained 94.5% of the variation for this model that corresponded to the variation in strain level. Samples with 0 revolutions and 160 revolutions are close together as expected due to the short time that the sample was exposed to the shear cell. The profiles predicted by NIR also align with the corresponding shear level. Figure 7-7 shows PCA score plot and the projections of the validation set onto the model. The PCA evaluation shows that dissolution profiles predicted by NIR are similar to the dissolution values obtained with the USP Apparatus 2 within the 95% confidence interval.

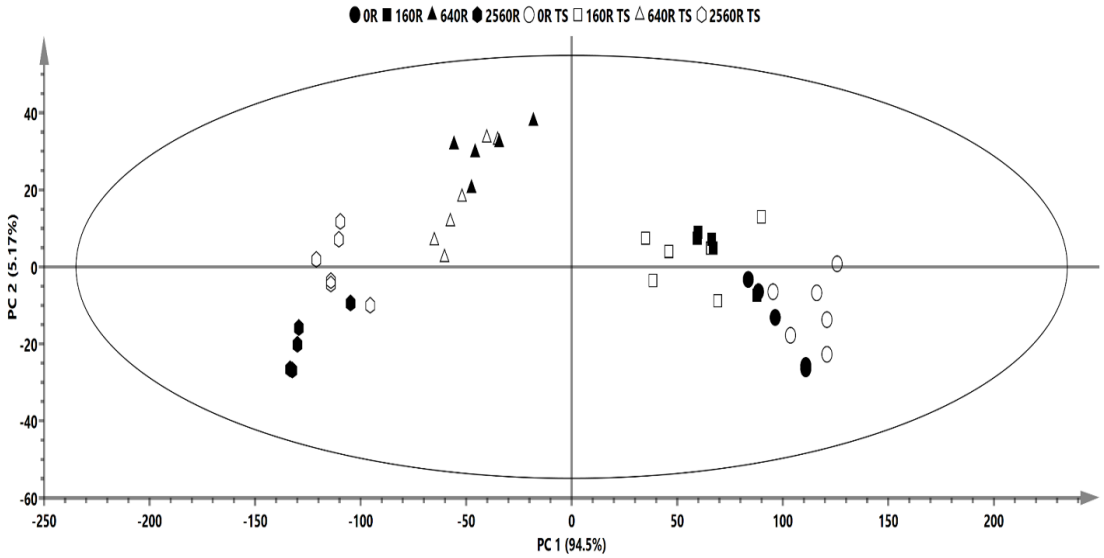

Figure 7-7- Projection of predicted dissolution profiles from results obtained of NIR the PCA scores plot of USP apparatus 2 dissolution profiles. Black symbols USP apparatus 2 dissolution profiles and white symbols represent NIR prediction with 2 PLS factors. (figure taken from: Hernandez *et al.* J. Pharm. Biomed. Anal., vol. 117, pp. 568–576, Jan. 2016)

The similarity factor calculation (f_2) was used to evaluate the similarity between dissolution profiles obtained from the USP Apparatus 2 profiles and NIR prediction profiles. Table 7-3 shows the results of f_2 using the averaged dissolution profiles of the destructive and nondestructive method. If the value of f_2 is greater than or equal to 50, the profiles are considered similar [132] [133]. Results showed that the dissolution profiles obtained from both methods could be considered similar. An analysis of variance (ANOVA) was performed to evaluate whether the two methods are statistically different. The null hypothesis is that the two methods are similar for both spectral ranges. Result shows that F calculated is less than the F_{crit} (F_{crit}= 3.96) for all shear condition using the entire spectral range (Table 7-3). Since the F calculated is less than F_{crit} the null hypothesis is

retained. These results are indicative that both methods are statistically similar at 95% of confidence level.

7.4. Conclusions

This study shows that exposing powders to mechanical strain during blending affected the dissolution behavior of tablets. This effect of blend strain on tablet structure could be picked up using NIR diffuse reflectance spectroscopy. Based on these results NIRS was used in combination with multivariate data analysis to predict dissolution behavior with variation in process conditions. A high correlation was obtained between the destructive test (USP Apparatus 2) and the nondestructive test (NIRS). NIR accurately predicts dissolution using a single PLS model instead of multiple PLS models at each time point. Validation of this methodology can be used for implementation in the quality by design strategy (QbD) and real time release testing (RTRT) in the pharmaceutical industry ensuring product quality.

Chapter 8. Enabling real time release testing by NIR prediction of dissolution of tablets made by Continuous Direct Compression

8.1. Introduction

Recently, pharmaceutical industry has been moving from batch processing to continuous manufacturing (CM). One of the major advantages of CM setup is that intermediate and final product quality can be monitored in real time without interrupting production. In a such a CM line, powder is exposed to different levels of strain generated in the feeders, mill, blender, and feed frame. Vanarase *et al.* observed that the shear generated in the mill led to efficient micro-mixing, and that pairing the mill with a blender provided best possible mixing performance [134]. Portillo *et al*. used two different convective blenders to demonstrate the effect of rotation rate, cohesion, and mixer inclination on the mixing behavior [135]. The total strain developed in a blender depends on the number of blade passes [136] which in turn is affected by the powder properties [134]. Mendez *et al.* [116] observed an increase in hydrophobicity with an increase in feed frame speed in the presence of a lubricant. Osorio *et al.* reported an improvement in blend homogeneity with an increasing amount of Acetaminophen in the blend [137]. Such process and formulation parameters can affect the release of the drug from the tablet.

The drug release is characterized using '*in vitro* dissolution testing', during product development to develop a specification, and then during routine manufacturing for quality control of the solid dosage forms. Despite its widespread use in the pharmaceutical industry, dissolution testing has several shortcomings discussed

previously. There has been a growing interest in the use of NIR for prediction of drug release from tablets obtained from continuous manufacturing.

Cui *et al*. used a single time point to study and predict the drug release as a function of API physical properties [138]. Basalious *et al.* used DOE analysis at two different time points to study the effect of polymeric surfactants and crystallization inhibitors on drug release [139]. Dumarey *et al.* used bi-directional projection to orthogonal structures (O2PLS) on the entire dissolution profile to study the effect of granule and compression variability [140]. Zannikos *et al.* used NIR to predict the dissolution rate for Carbamazepine tablets [118]. Freitas *et al.* used NIR to predict the effect of pH on the drug release at seven different time points, which involved construction of seven different PLS-1 models [119]. Hernandez *et al.* used a Partial least squares-2 approach to predict dissolution of tablets exposed to different levels of mechanical strain [70]. The PLS- 1 model is based on only one Y variable (dissolution at a single time point). Performing several different PLS-1 models for drug released at different time points would be time consuming and hence not practical. The PLS-2 has been used for relating X variables to multiple Y values. Though PLS-2 deals with several X and Y variables at a time, it averages all X and Y variables. It generates only one data set of score and loading vectors, which might not be optimum to quantify relationships between all X and all Y variables.

Principal Component Analysis (PCA) combined with a regression technique can be a simpler alternative to the complex model building approaches described above. Polizzi *et al.* adopted a two-step process, a PCA followed by PLS to predict mechanical properties

of blend compacts from raw materials properties [141]. Xie *et al.* used Principal Component regression to evaluate the relationship between segregation and physical properties of pharmaceutical blends [142]. Sande *et al.* demonstrated superiority of PCA/PCR to simplify the 8 time- point dissolution profiles to two latent variables (Principal components) and established correlations between the formulation and dissolution [143]. Huang *et al.* demonstrated the applicability of PCA to identify the source of variability of dissolution shift upon stability [144].

This work investigates a simpler and an efficient alternative to PLS regression, using Principal Component Analysis combined with Multi linear regression (MLR). NIR spectroscopy yields data of high dimensionality, since each sample is described with hundreds of variables (wavelengths). PCA simplifies the variable space from hundreds or thousands to a few (three to five) latent variables, which capture the major variation in the NIR data. The dissolution profiles on the other hand can be described by a model dependent (Weibull is used here) [145] [146] or a model independent approach [147]. Multi linear regression can be established between the Eigenvalues thus obtained and the observed attributes of interest of the tablet. Such multivariate models enhance process understanding by providing an insight into the process mechanics. MLR models are easy to communicate, simple to construct, and are self-explanatory, since each individual x variable used in the equation can be observed to be related to certain chemical and physical properties of the samples [40].

The case study examined in this work focuses on the effect of process and formulation parameters in a continuous direct compression line on the dissolution profiles. The goal is to predict these profiles in real time.

8.2. Materials and method:

8.2.1. Materials

The same formulation used in 6.2.1 was used here.

8.2.2. Continuous tablet manufacturing via direct compaction:

Tablets were made in a continuous direct compaction line. The setup is described in Chapter 2, section 2.2.4.

8.2.3. Experimental Design:

Two sets of tablets were included in the study- the target (or prediction) set and the calibration set. The prediction set tablets were made at a targeted drug concentration of 9% APAP and a targeted force of 24 kN. The blender speed was kept constant at 200 rpm and the feed frame speed was 25 rpm. The dissolution profiles of these tablets were predicted by utilizing the data obtained from an experimental design built around this targeted condition. The tablets included in this experimental design comprised of the calibration set. The four variables (and their levels) included were: API concentration (low, medium, high), Blender speed (150rpm, 200rpm, 250rpm), feed frame speed (20rpm, 25rpm, 30rpm), and compaction force (8KN, 15KN, 24KN) (Table 8-1). The experimental design consisted of a 3^{4-1} fractional factorial design with additional repeated center points (3 center point runs) resulting into a total of 30 conditions highlighted in

Table 8-2. 6 tablets were analyzed every design point, resulting into a total of 180 (30*6) tablets.

Table 8-1: The four variables included in the design were: API concentration, blender speed, feed frame speed and compression force. Three levels of each variable were examined

Level	API Concentration	Blender speed (RPM)	Feed frame speed (RPM)	Compression force
0	low	150	20	8KN
1	medium	200	25	16KN
2	high	250	30	24KN

Table 8-2: The fractional factorial combinations included in the design. A total of 27 design points with additional repeated center points (3 center points) was included.

	A	B	C	D
1	0	0	0	0
2	0	0	1	1
3	0	0	2	2
4	0	1	0	1
5	0	1	1	2
6	0	1	2	0
7	0	2	0	2
8	0	2	1	0
9	0	2	2	1
10	1	0	0	1
11	1	0	1	2
12	1	0	2	0
13	1	1	0	2
14	1	1	1	0
15	1	1	2	1
16	1	2	0	0
17	1	2	1	1
18	1	2	2	2
19	2	0	0	2
20	2	0	1	0
21	2	0	2	1
22	2	1	0	0
23	2	1	1	1
24	2	1	2	2

25	2	2	0	1
26	2	2	1	2
27	2	2	2	0
28	1	1	1	1
29	1	1	1	1
30	1	1	1	1

8.2.4. Analytical testing of tablets:

The tablets made by the above method were subjected to different at-line tests, described below

8.2.5. At line Near- infrared transmission spectroscopy:

A Bruker Optics Multipurpose Analyzer (MPA) FT-NIR spectrometer (Billerica, Massachusetts) was used to collect tablet spectra in transmission mode. The advantage of using transmittance mode in NIR spectroscopy is that a the light interacts with the entire sample (i.e., the tablet), rather than just its surface, thus helping quantitative determination [66]. The spectral range chosen was from 12500 to 5800 cm^{-1} with a resolution of 32 cm^{-1}. A background and a tablet spectrum were obtained by averaging a total of 256 background scans and sample scans respectively.

8.2.6. Dissolution:

A total of 180 dissolution profiles (30 design points*6 tablets/design point) of the tablets obtained from continuous line were used to build the calibration model. A VK 7010 dissolution apparatus (Varian Inc., Santa Clara, CA) fitted with USP paddles was used to study the drug release. The paddle rotational speed was 50 rpm. The dissolution medium used was phosphate buffer at pH 5.8 and the media temperature was maintained at 37.0±0.5^{o}C. Six tablets were each placed in the dissolution apparatus chambers

containing 900 ml of medium, and were placed into the dissolution vessels simultaneously at the start of the experiment. A peristaltic pump VK 810 (Varian Inc., Santa Clara, CA) was used to pump out aliquots of the dissolution medium at 3-minute time intervals. The medium was then filtered through 35 μm full flow filters prior to detection using a UV spectrophotometer (Varian Inc., Santa Clara, CA) at a wavelength of 243 nm. Absorbance values for each tablet were converted to the percent of drug released at each analysis time.

8.3. Data analysis:

8.3.1. Multivariate data analysis:

The data obtained from the NIR spectrometer was analyzed using Unscrambler X 10.2 (Camo, Oslo, Norway). The data was baseline corrected, where the lowest absorbance value in the spectrum was subtracted from the absorbance values at all the other wavenumbers. This was followed by a Savitzky-Golay first derivative, fitted to a second order polynomial with a total of 11 smoothing points. The algorithm is based on performing a least squares linear regression fit of a polynomial around each point in the spectrum to smooth the data. The second derivative of the fitted polynomial is then calculated. This pretreatment removed the baseline offset between samples and improved the resolution of the peaks that carried the chemical information associated with the concentration of the API.

Principal Component Analysis (PCA) was performed on this pre-treated data (section 2.3.2). The scores (eigenvalues) obtained from the PCA reflected the amount of variance

in the data explained by each Principal Components (PC). These eigenvalues were used for further analysis.

8.3.2. Dissolution data fitting:

The dissolution profiles obtained from the USP dissolution apparatus were analyzed using two approaches: a) model independent approach (parameters: shape, level 1, level 2) and (b) model dependent approach (Weibull parameters: α- and β).

8.3.3. Model independent approach:

In the model independent approach, a dissolution curve is described by calculated parameters without additional need for selecting a mathematical model and adopting a curve-fitting procedure. A previously developed methodology, level-shape analysis, was used. A detailed description of the level-shape analysis can be found elsewhere [147]. The methodology looks at a dissolution curve in terms of level and shape separately. The advantage of this approach is taking into account the auto-correlation in the dissolution profile as time series data. Mathematically, the level of the i^{th} dissolution curve can be defined as the average release percentage across n time points:

$$\overline{y_i} = \Sigma y_{ij} / n$$

while the shape is calculated by performing PCA on the residual matrix for all the averaged dissolution profiles considered. The construction of residual matrix enables to calculate the shape of a profile that is independent of its level. The residual matrix (R) is constructed by subtracting the grand mean (y..), row and column effects ($y_i.$ and $y._j$, respectively):

$$R_{ij} = y_{ij} - y_{..} - (y_{i.} - y_{..}) - (y_{.j} - y_{..})$$

Software JMP 10 (SAS institute, Inc., Cary. NC) was used for level-shape analysis.

8.3.4. Model dependent approach:

DDSolver, an add-in program in Microsoft excel [148], was used to facilitate the modeling of dissolution data using non-linear optimization method. Different dissolution models from the built-in model library were fitted to the above dissolution data and it was observed that the Weibull model best described the dissolution kinetics.

$$\%\ Dissolution = 100 * \{1 - e^{-\frac{(t)^{\beta}}{\alpha}}\}$$

The Weibull model was selected based on high adjusted R-square (~0.989-0.995), the Akaike Information Criteria (AIC) [149], and the Model Selection Criterion (MSC). The higher the MSC, the better is the fit of the model to the data. Generally, a MSC value of more than 2 to 3 indicates a good fit. The MSC obtained from fitting the Weibull model to the dissolution data was approximately in the range of 4.5 to 5, indicating a very good fit.

8.3.5. Multilinear regression between NIR data and dissolution data:

A multivariate linear regression technique (discussed in chapter 2, section 2.3.1) was used to predict the value of more than one response from a set of predictors. The model inputs included the score values from the principal component analysis of the NIR spectrum. The outputs for the model independent approach are the level and shape values for dissolution profiles. Likewise, the outputs for the model dependent approach are the

coefficients (α and β) in the Weibull model. A quadratic response surface model was built and the main effects, two-way interaction, and three- way interaction were included in the model. The four-way interaction was not examined because the fractional factorial design used in the study is unable to distinguish it from the error term. After a preliminary analysis, only those terms that had a significant effect on the model were retained and the final model coefficients were obtained. The predicted dissolution profile can then be reconstructed using the descriptive values from both approaches. Mathematically, the linear regression model for the j^{th} sample unit can be expressed as:

$$Y_j = \gamma_0 + \gamma_1 x_1 + \gamma_2 x_2 + \cdots + \epsilon_j$$

where ϵ is a random error, x is the input predictor, Y is the output to be predicted, and γ are the unknown and fixed regression coefficient.

8.4. Results and Discussion:

As mentioned earlier, data was obtained from two different sets of tablets - the calibration set and the validation (prediction) set. The calibration set consisted of 180 tablets (30 design points*6 tabs/design point). The focus of this work was to demonstrate the feasibility of using the information gleaned from PCA to predict tablet dissolution performance. The results are divided into three sections; Section 3.1 discusses Near IR Spectroscopy data analysis; Section 3.2 focuses on Multi-linear regression between the NIR data and the dissolution parameters, and finally Section 3.3 uses the regression to predict the dissolution profiles for the targeted design point.

8.4.1. Near IR Spectroscopy data analysis:

NIR data was collected over a spectral range of 12500 to 5800 cm^{-1}. High absorbance values were recorded as the wavenumber decreased beyond 6919 cm^{-1}. Further pre-processing of the data indicated that results for wavenumber from 6919 to 5200 were noisy and carried very little information. In addition, the first few wavenumbers from 12500 cm^{-1} to 11996 cm^{-1} were observed to contribute very little information to the pre-processed spectra. The final range chosen was from 11996 to 6919 cm^{-1}.

As is commonly the case, a baseline offset was observed to be present in the NIR absorbance data. The offset was removed by subtracting the lowest intensity in the spectra (which occurred at highest wavenumber) from all the other variables for each sample vector. This treatment was useful in removing the effect of scattering on the NIR signal [150]. The effect of compaction force and API concentration were evident on the baseline corrected NIR absorbance spectra (Figure 8-1). It was observed that the absorbance decreased with an increase in the compaction force. As a side note, the process parameters and the concentration conditions reported on each of the graphs in the following sections are targeted conditions. They represent the targeted design conditions during the continuous manufacturing run.

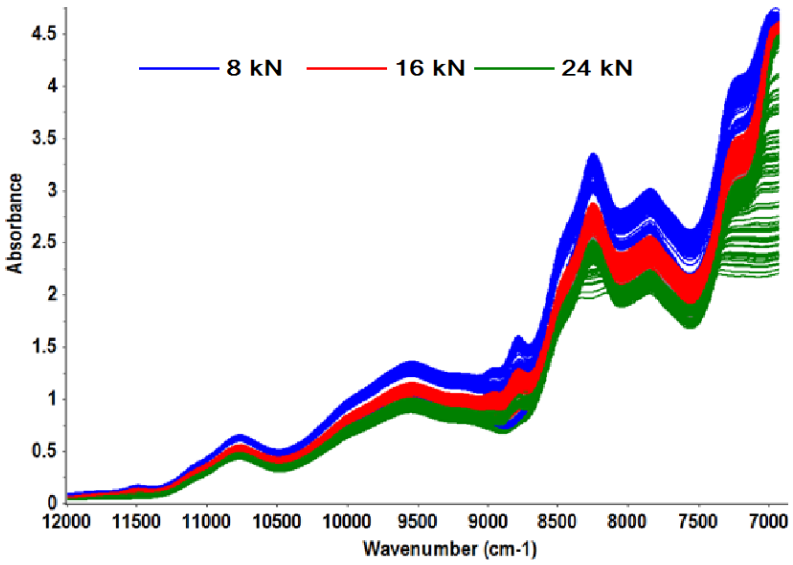

Figure 8-1: Effect of compaction force on the baseline corrected absorbance data for the DOE tablets. The absorbance was observed to decrease with increasing force. The compression conditions mentioned are the conditions that were targeted.

The concentration effects were further enhanced after a Savitzky- Golay first derivative (second order polynomial, 11-point smoothing) treatment [151]. The noise level, the number of data points, and the sharpness of the features of interest were considered while choosing the smoothing window and the derivative order. The second order polynomial and an 11- point smoothing enhanced the signal-to-noise ratio without compromising on the resolution of the peaks. Dissolution was observed to be affected by both process parameters (here compaction force, blender and feed frame rpm) and the chemical properties (API concentration). Hence, the aim of the pre-treatments was to enhance the contribution of the API concentration simultaneously preserving the effect of compaction force (Figure 8-2 b). Different combinations of pre-treatments including Standard Normal Variate followed by Savitzky Golay first derivative, and baseline correction followed by Savitzky Golay second derivative were tested. Principal Component Analysis was

performed on the data obtained from each of these treatments. The validation set was then projected onto the scores plot obtained from each of these pretreated data. The pre-treatment that explained maximum variance in the validation set was finally chosen. In this case, baseline correction followed by Savitzky Golay first derivative explained 99% variance in the validation set and the results for these pretreatments are reflected in Table 8-3.

Table 8-3: Procedure used for choosing the pre-treatment for NIR data. The pre-treatment that explained maximum variance of the validation set was chosen. The baseline correction treatment followed by Savitzky Golay first derivative explained 99% variation in the validation set and was chosen.

	Explained Variance			
Treatments	PC-1	PC-2	PC-3	Total
SNV	42	4	1	47
SNV+SG11(1)	3	2	17	22
BL+SG 11(1)	99	0	0	**99**

The effect of API concentration was observed in two API peaks 8500-9000 cm^{-1} and 11500 cm^{-1} (Figure 8-2 a). The effect of compaction force was evident through the entire spectrum (Figure 8-2b).

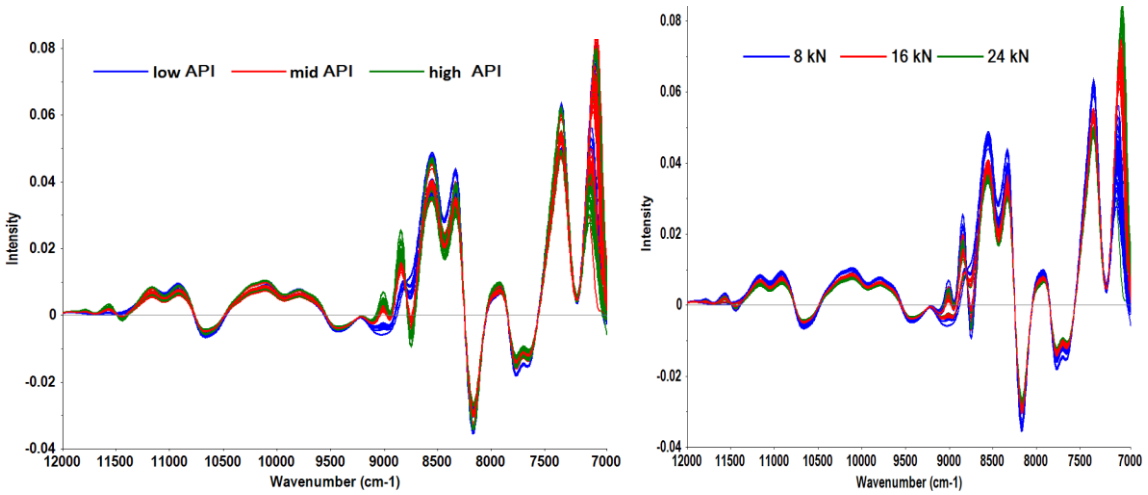

Figure 8-2: Effects of API concentration and compaction force enhanced after pretreatments. a) Trends with respect to API concentration were enhanced and evident in peaks around 8500 and 11500 cm^{-1} (left) b) Trends with respect to changing compaction force were preserved (right).

PCA was performed on the NIR data obtained from the calibration tablets. The PCA algorithm has the capability to separate chemical variations of the API from those of the excipients and from other physical changes [152]. The PCA decomposes the raw data matrix (X) into a structure part and a noise part [153].

$$X = TP^T + E = Structure + Noise$$

The Eigenvalues obtained from PCA carry information about the processing and formulation history of the tablet. The principal components are calculated one at a time and are orthogonal to each other, meaning that after the calculation of the first PC, its contribution is removed from the original X matrix and the next PC is computed.

The PCA on the NIR data yielded three principal components accounting for 100% of the total variation in the data. The first principal component (PC1) explained 85% of the total variance in the data. Three different clusters were observed in the scores plot (Figure 8-3) along the PC1 axis, which grouped according to the compaction force. The forces indicated on the scores plot are targeted forces and the tablets could have experienced compaction pressures in and around the targeted forces. The aim of this work was not to compute the compaction force or the API concentrations of each tablet but to use NIR to extract the information stored in the tablets for dissolution prediction.

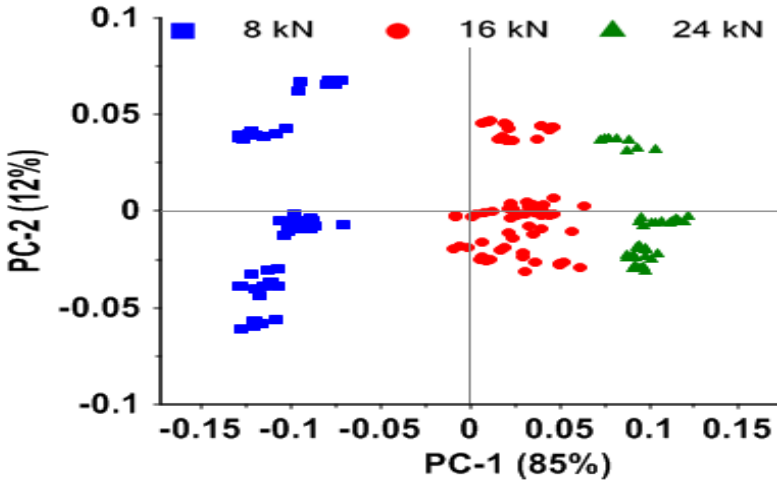

Figure 8-3: Scatter plot of the first two PCs. PC1 explains 85% variation in the data and groups according to increasing compaction force. PC2 accounts for 12%.

To confirm this further, the PC1 scores were plotted against the relative density of the tablets (Figure 8-4). The relative density was proportional to the compaction force of tablets. The PC1 scores displayed a good correlation with the relative density, which confirmed the relation between PC1 and relative density and hence the compaction force.

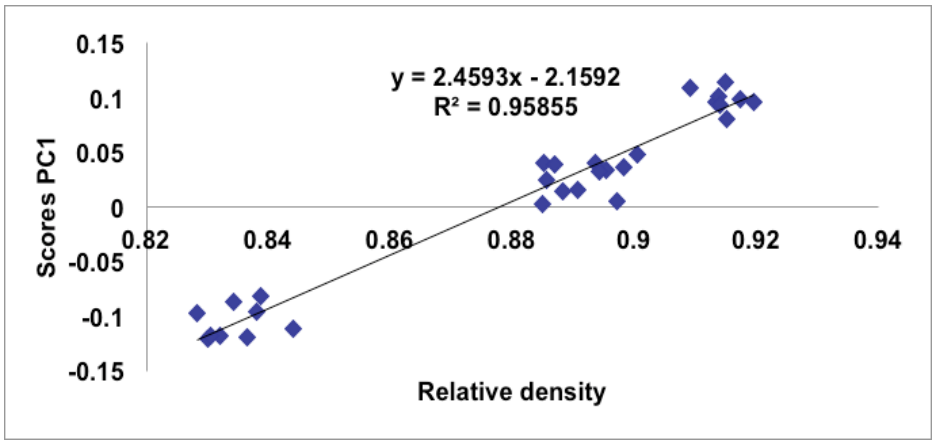

Figure 8-4: PC1 correlates well with the relative density of the compacts, which is related to the compaction force experienced by the tablets. The scores increased as the tablet relative density increased

PC2 explained 12 % of the total variance in the NIR data (Figure 8-5 (a)). Grouping the Eigenvalues with respect to targeted API concentration yielded clusters with decreasing API concentration along PC2 axis. A good correlation was obtained between PC2 Eigenvalues and the observed API concentration (Figure 8-5 (b)). It was observed that tablets could be made at a lower API concentration even in the presence of some uncharacterized variability. However, this approach did not take into account the actual concentration of the API in the tablets, and the final the aim was to predict the dissolution profiles of the tablets using NIR spectroscopy alone.

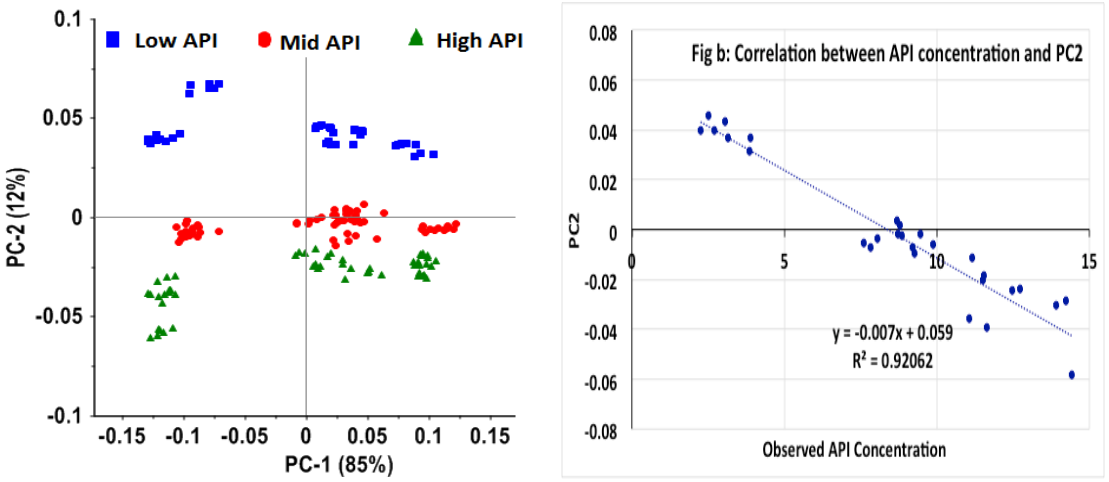

Figure 8-5: The PC2 correlated with the observed API concentration a) Scores plot (left); PC2 captured the changes in API concentration. b) PC2 highly correlated with the observed API concentration in the tablets (right).

The loading plot for PC2 (Figure 8-6) was observed to have peaks in the range of 8500-9000 cm^{-1} and another one in the range of 11500 cm^{-1}. These peaks corresponded to the characteristic peaks for acetaminophen.

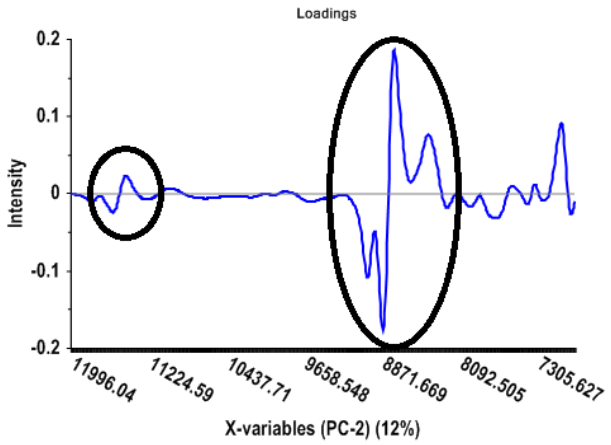

Figure 8-6: The loadings plot showing APAP peaks at 8500-9000 cm^{-1} and 11500 cm^{-1} explaining the specificity of PC2 to API concentration

The chemical or physical meaning of PC3 could not be easily determined. It was more likely related to the amount of shear experienced by the powders throughout the continuous line. The strain experienced by the powder blends lead to the coating of Magnesium Stearate (the lubricant) on other particles, affecting the particle bonding, and hence the internal structure of the tablets [24]. The shear experienced by the powder in the continuous line is known to be affected by the blender speed and the feed frame rotation rate [116] and is also known to have an impact on the micro- mixing on MgSt, which in turn affects tablet dissolution.

As mentioned earlier, the samples consisted of a total of 180 tablets (30 design points*6 tablets/ design point). The Eigenvalues for all the 180 tablets were obtained for each of the principal components (PC1, PC2, PC3). To leverage the tablet-to-tablet variability, the average eigen values for each condition (averaged over 6 tablets each condition) were calculated leading to a total of 30 scores per principal component. These Eigenvalues were further used for Multi-linear regression modeling in section 3.2

8.4.2. Multi-linear regression:

Multi-linear regression was used to examine the relationship between the Eigen values obtained from the PCA and the dissolution parameters obtained either by the model independent (2.3.2.1) or the model dependent approach (2.3.2.2), each of which is discussed in the following sections.

Regression between the PCA scores and the parameters obtained from the model independent approach:

The level was calculated by using the average of individual dissolution profile across all the time points. The shape was calculated by performing a PCA on the residual matrix after the level was subtracted. The principal components were based on the covariance matrix. The first two PCs explained 98.7% of the variability of the dataset as shown in Figure 8-7, and thus two eigenvectors, corresponding to “Shape I” and “Shape II” were calculated, together with their associated Eigenvalues, to represent the shape of dissolution profiles.

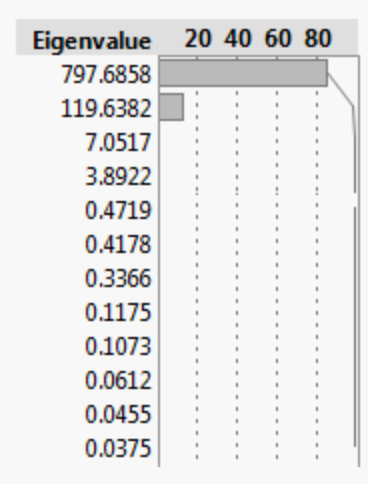

Figure 8-7: PCA on the residual matrix for the calculation of shape of the dissolution profiles. The first two PCs explain most of the variability in the data

After the level and shape parameters for dissolution profiles were obtained, a regression model was fitted between the parameters and regressor variables PC1, PC2 and PC3 (Figure 8-8). The regression model included the main effects, two-way interactions, and three-way interactions. The equation for each of the parameters was calculated from the model estimate. The equation provided a statistically good fit with r-square values of 0.92, 0.89 and 0.90 for level, shape I and shape II predictions respectively ($p<0.001$).

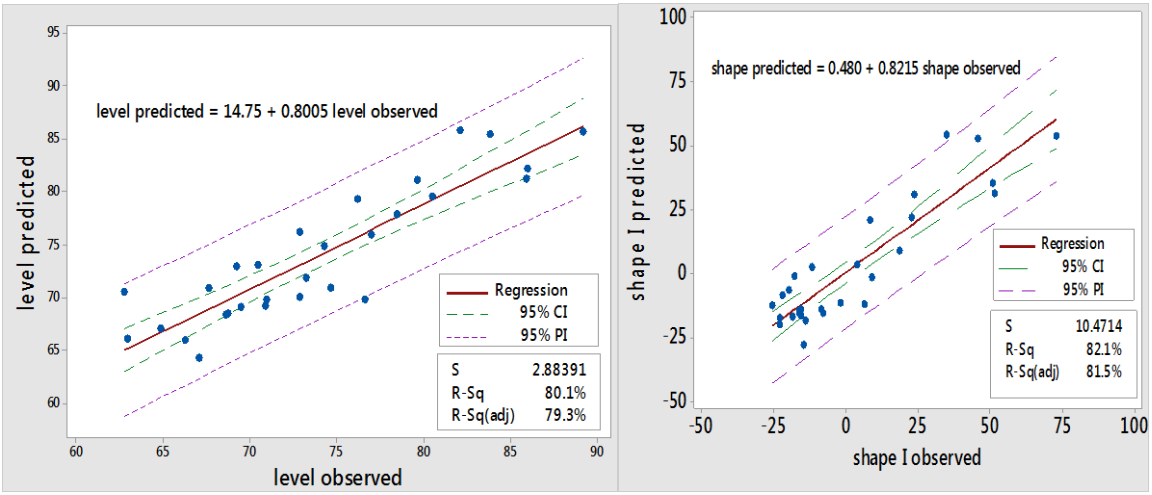

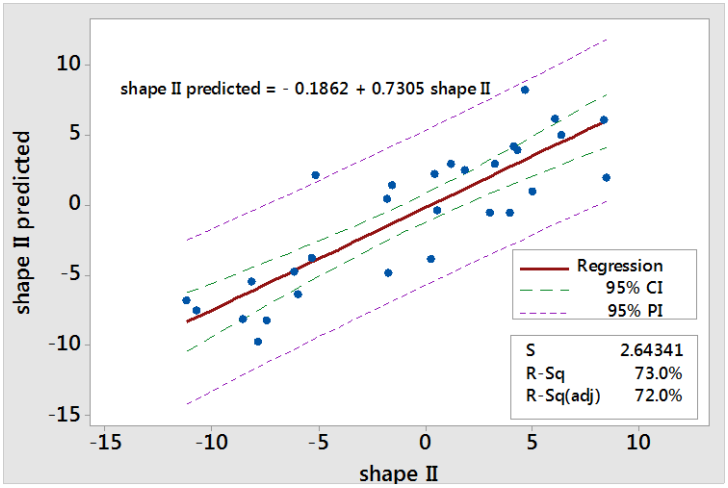

Figure 8-8: Regression model based on level-shape analysis, using average dissolution profile. R-square values of 0.80, 0.82 and 0.73 for level, shape I and shape II predictions respectively suggesting a good fit.

The equations for each of the parameters, level, shape I, and shape II are given in the Appendix section.

Regression between the PCA scores and the parameters obtained from the model dependent approach:

The parameters (α and β) obtained from the model dependent approach were used as the dependent variables. A multilinear regression was built between these dependent variables and the regressor variables: PC1, PC2 and PC3 (Figure 8-9). A good fit was observed for both α and β with an R-square of 0.91 and 0.82 respectively.

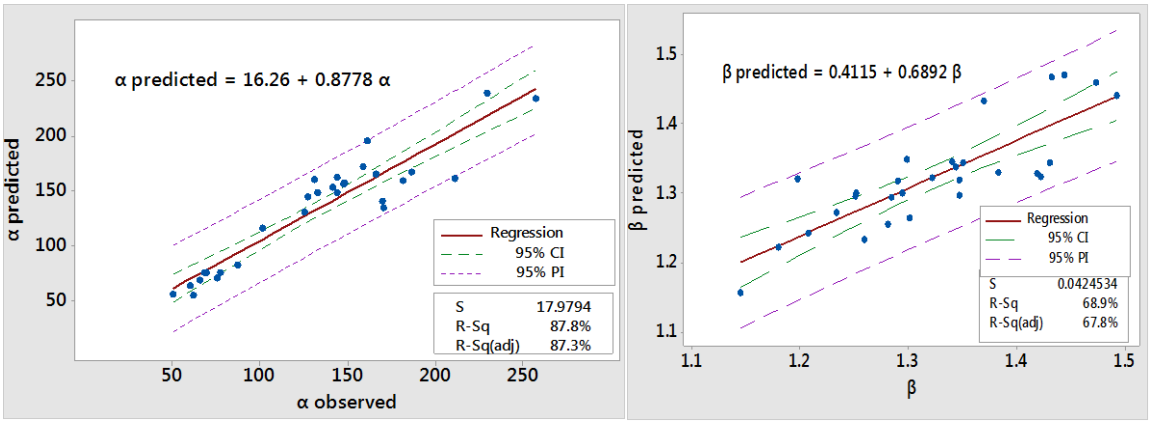

Figure 8-9: Regression based on Weibull model, using averaged dissolution profile. The R-square was 0.87 and 0.69 respectively indicating a good fit.

8.4.3. Internal method validation:

The aim of this section was to test the utility of this approach in predicting the dissolution profiles of an internal validation set. Ten tablets from the 180 tablets that were made in

section 2.2.2 were included in the internal validation set. These tablets were randomly picked from these 180 tablets and covered different conditions with respect to the four input variables-API concentration, compaction force, and blender and feed frame speed. The PCA followed by the regression exercise was repeated for the remainder of 170 tablets where the ten internal validation tablets were kept out. A multi-linear regression was obtained using both model dependent and model independent approaches as described in section 3.2 for these 170 tablets. The dissolution profiles of the remainder ten tablets included in the internal validation set were predicted using the regression models developed.

The internal validation set was projected into the scores plot space as shown in Figure 8-10. All the ten spectra were within the 95% confidence interval as marked by the ellipse (Hotelling's T^2 test)

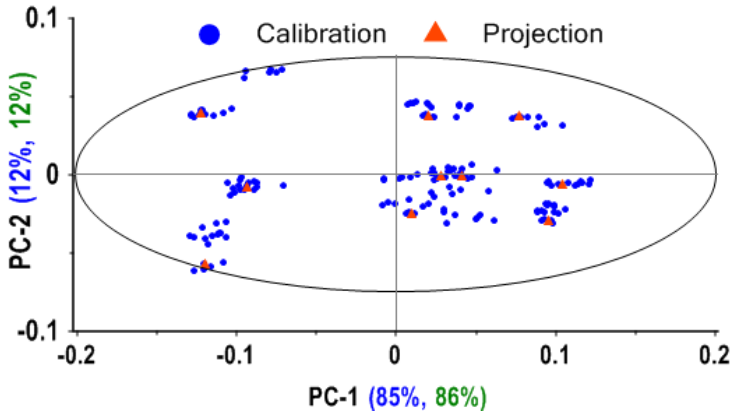

Figure 8-10: Projection of the ten internal validation tablets onto the scores plot of the calibration set consisting of the remainder 170 tablets. The projected tablets were within the 95% Hotelling's ellipse.

The model dependent and independent multi-linear regression equations were then used to predict the dissolution profiles for the validation set tablets. F_1 (difference factor) and f_2 analysis (similarity factor) were used to compare the difference and similarity between the reference and the predicted dissolution profiles [133]. The f_1 and f_2 analysis are a common approach recommended by FDA's Guidance for Industry [132] and is a model-independent approach to define dissolution similarity based on the mean-squared difference between a pair of profiles. A predicted dissolution profile is considered similar to the reference profile if the f_1 value is less than 15 and the f_2 value between the two profiles is not less than 50.

Table 8-4 highlights the f_1 and f_2 values for the ten validation tablets using both the model dependent and model independent approach. An average f_1 value of 6 and f_2 value of 65 was observed for the ten tablets.

Table 8-4: Similarity and difference factor calculations for internal validation set tablets. An average f_1 value of 6 and f_2 value of 65 was observed for the ten tablets.

Sr. No.	Sample name	Model Dependent		Model Independent	
		f_1	f_2	f_1	f_2
1	S1-03-01	4.33	71.29	9.83	55.13
2	S2-06-02	4.24	63.28	5.34	59
3	S3-09-03	6.09	62.7	1.62	64.35
4	S4-12-03	5.21	62.52	5.75	60.72
5	S5-17-07	3.83	75.21	2.89	78.66
6	S6-17-10	7.25	63.01	1.4	89.87
7	S7-18-04	3.93	75.38	1.08	94.37
8	S8-23-07	7.91	61.6	1.16	93.49
9	S9-26-06	9.12	60.1	2.99	68.56
10	S10-27-08	8.17	56.94	3.92	72.80

8.4.4. Prediction of dissolution profiles for the targeted design point (or external validation set):

The targeted design condition was 9% acetaminophen and 24 kN targeted force. This was a completely independent set made in the continuous line on a different day. After the steady state was reached, tablets were sampled from the tablet press outlet. Six of the sampled tablets were analyzed first with NIR and their dissolution profile was predicted using the regression models obtained from the two approaches described in the previous section. The tablets were then subjected to dissolution testing to compare the prediction to the actual results that would be obtained.

The first step was to determine if the targeted tablet spectra was within the defined scope of the model, both with respect to concentration and compaction force. The spectra of the six tablets made under the targeted design condition were projected onto the PCA scores space developed from the calibrations tablets. It was observed that tablets were within the 95% confidence interval given by the Hotelling's ellipse and grouped with the calibration tablets in the area of 9% APAP and closer to the 24 kN range (Figure 8-11). This implies that the projected samples were described well by the calibration model.

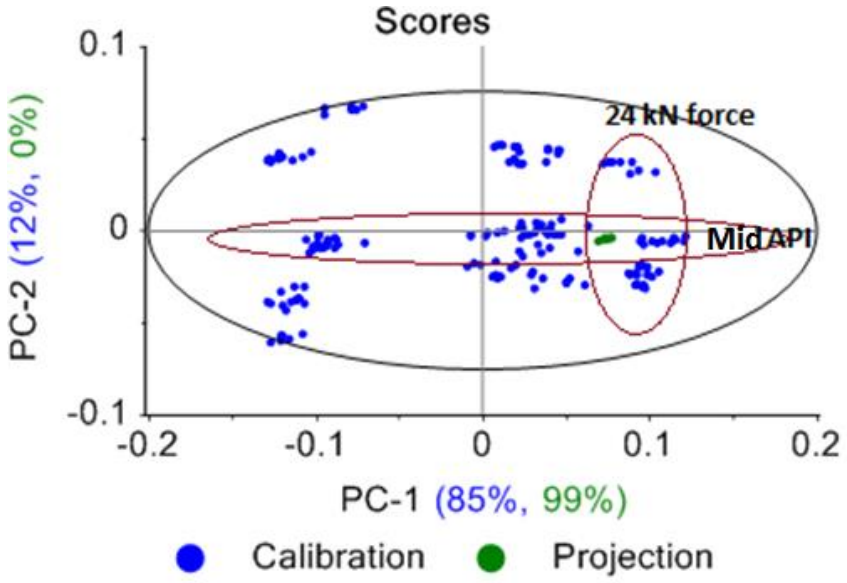

Figure 8-11: Projection of the prediction/ validation set onto the calibration set built from 180 tablets. The projected tablets fell within the 95% Hotelling's ellipse and grouped with the 9% APAP and 24 kN tablets.

The Eigenvalues for the prediction set were obtained from the projection data. The first three Eigenvalues, PC1, PC2, and PC3 of each tablet were used as the regressor variables in the models developed above to predict the dissolution parameters. Once the dissolution parameters were obtained, the dissolution profiles were calculated for each individual tablet. For the model independent approach, based on the level and shape values obtained, the predicted profile is the one that is most similar profile to the available profiles in the calibration sets with respect to level and shape. In the case of the model dependent approach, the Weibull equation was used to construct the entire dissolution profiles.

Figure 8-12 collates the reference and the predicted dissolution profiles for the six individual tablets using the model independent approach. The f_1 value for these tablets was in the range of 3 to 18 and the f_2 value was in the range of 45 to 78. All the six tablets except tablet 2 (f_1=18.6, f_2= 45.44) were considered statistically similar.

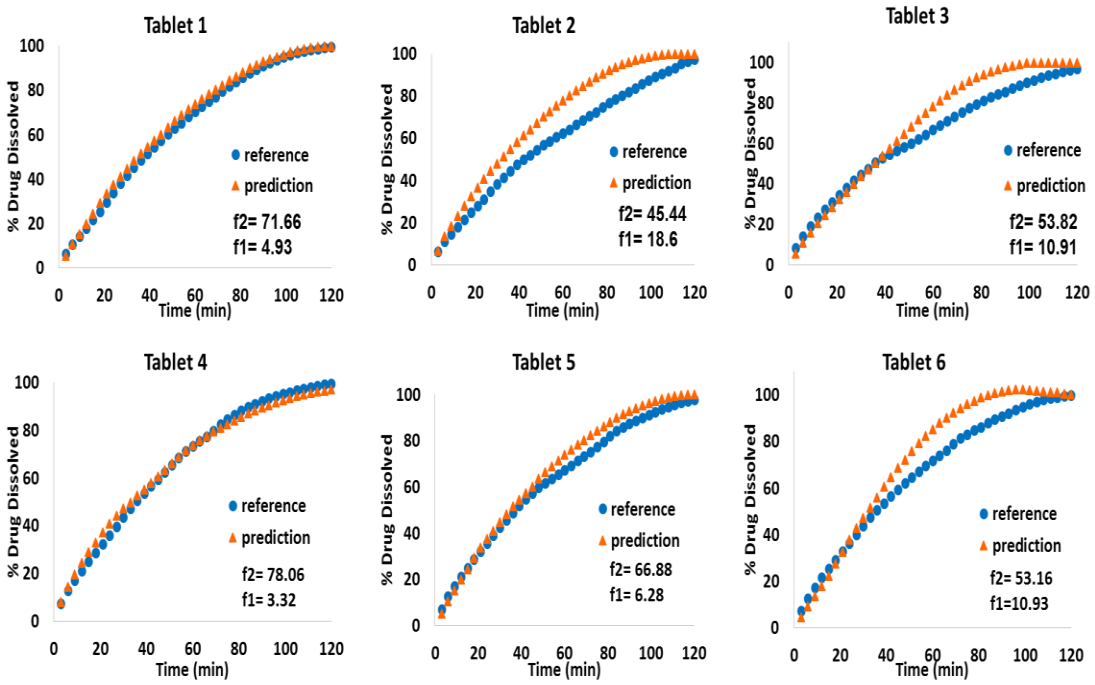

Figure 8-12: Predicting individual dissolution profile from the model independent approach. All the six tablets except tablet 2 (f_2= 45.44) were considered statistically similar as per f_2 analysis.

The dissolution profiles predicted using Model dependent approach (Figure 8-13) gave accurate predictions with a high f_2 values ranging from 75 to 79 with differences between the profiles being smaller than about 10%. The f1 value for these tablets was between 3 to 10.

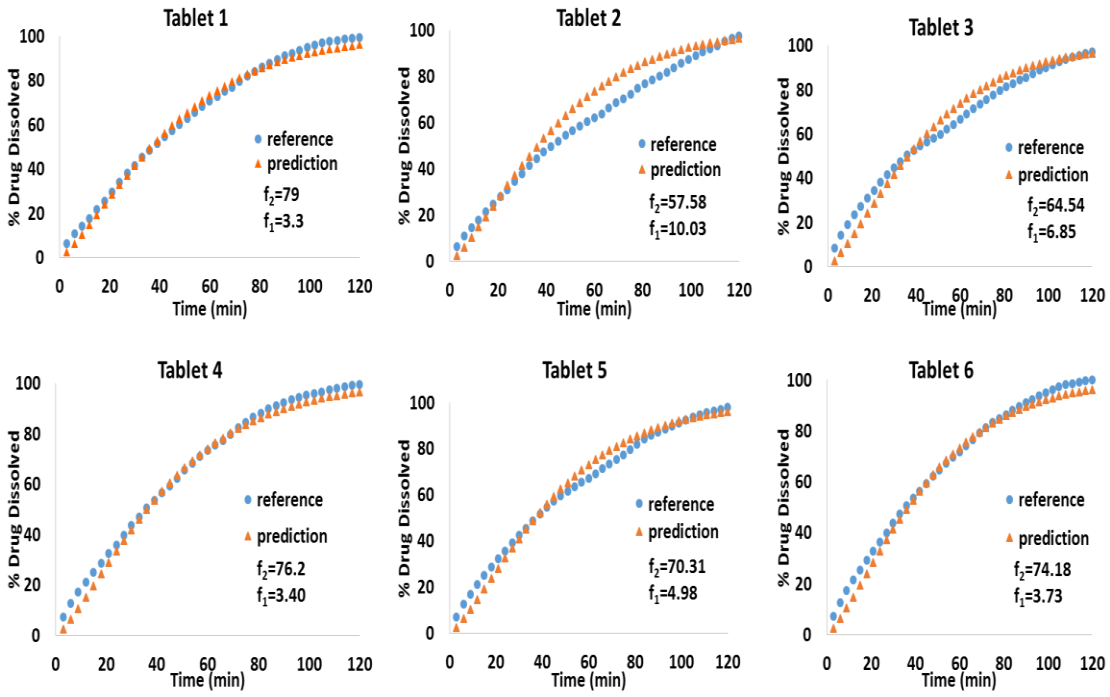

Figure 8-13: Predicting individual dissolution profile from model dependent approach. The similarity factor is greater than 50 indicating a good agreement between the observed and predicted

The way the model-independent approach works is that it finds the most similar profile in the calibration set to the predicted profile (both level and shape). In other words, it cannot create a new profile based on the calibration sets. This approach works in a sense that the predicted profile is similar to the reference. The precision of the prediction requires the calibration sets to be fully comprehensive and diversified for the combination. In our case, the accuracy of the dissolution profile predictions for the model independent approach can be improved by including more tablets in the calibration set spanning a range of conditions. This work confirmed the hypothesis that using NIR it is possible to predict the dissolution profiles.

8.5. Conclusions

This work addressed a challenge in implementing real-time release methods for tablets: the need to predict dissolution profiles. Both a model dependent and a model independent approach for dissolution prediction were examined. A quality-by-design approach was used to predict tablet dissolution profiles nondestructively. Designed experiments were used to understand the impacts of process changes. The established multivariate linear regression model was able to predict the dissolution profile of individual tablets based on its NIR spectrum. A PCA algorithm was used to extract the effect of process and formulation variation from the Near IR data of tablets. The model dependent approach gave better predictions than the model independent approach for the current data set. This was observed to be a fast approach circumventing the need to predict process parameters for any given condition and the need to have a model for every dissolution time point.

Chapter 9. Conclusions and recommendations

Real time quality assurance is a highly desirable goal for both of batch and continuous manufacturing systems. The work presented in this dissertation focused on developing and employing tools for real time release testing in both types of applications. Critical Quality Attributes (CQAs) of blend and direct compression tablets (blend uniformity, tablet content uniformity, and tablet dissolution) were predicted using either real-time measurements (on-line or at-line) or model-based methodologies. A scientific evaluation of different sampling methodologies for RTRt was undertaken and these methods were compared to the traditional sampling approaches. This chapter summarizes the work presented in this dissertation and outlines recommendations for future work.

9.1. Conclusions:

The RTRt work was performed on three different platforms ranging from lab scale batch setup to pilot scale tablet production to direct compaction of tablets using a continuous manufacturing line, discussed in chapter 2. Different data analysis algorithms employed to extract qualitative and quantitative information like PCA, PLS and MLR were discussed. The work discussed in chapters 3,4, and 5 was conducted on a pilot-scale PAT platform equipped with appropriate fixtures to facilitate PAT testing along with withdrawing samples using the traditional approaches. The experiments discussed in chapter 6 and 7 were conducted on a lab-scale blending shearing-compaction platform to evaluate and capture the effect of shear on tablet properties. The final segment of this dissertation discussed in chapter 8 was conducted on a continuous manufacturing platform.

With this background, the first specific aim discussed the implementation of a strategy for blend uniformity monitoring in a batch process (Chapter 3). This was a first published attempt to predict blend end point for a blend containing Phenytoin Sodium, a NTI drug. The calibration model building took into consideration the effects of scale changes, spectrometer differences and the variability introduced by the different excipients on NIR spectra. The effect of baseline differences arising from different spectrometers were reduced by employing data pre-treatments. The mean concentration after 30 minutes of blending predicted using NIR was within 10% of the target dose (15%).

The second specific aim involved developing a RTR strategy to assess content uniformity of tablets obtained by compacting the blends used in the previous aim (chapter 4), and comparing different sampling strategies for the PAT platform (chapter 5). Near IR spectroscopy was found to be an effective tool for expedited C.U. predictions enabling interrogation of a greater number of tablet samples. These extensive tablet C.U. studies provided a rigorous basis for assessing and validating the various thief sampling and PAT methods and determining their relative accuracy and reliability. A bias was observed in the thief samples withdrawn at the completion of the blending operation and the technique was observed to oversample the drug even when the blend was sub- potent. This was explained by the abundance of the API agglomerates and their preferential flow into the sampling cavity. These agglomerates manifested themselves in the form of super-potent tablets, the detection of which was possible owing to the extensive and expedited C.U. sampling and analysis enabled by transmission spectroscopy. The utility of online blend monitoring to detect the blend micro-mixing attributes such as lubricity and degree

of agglomeration was questionable. Choosing the right sampling tools is an important aspect of RTRt and the work in this aim addressed this requirement.

A key component of a meaningful RTR strategy for most products is the ability to predict dissolution utilizing the available on/at-line sensing infrastructure. Dissolution testing typically takes from several minutes to several hours and is therefore not possible to measure it directly online. Therefore, dissolution must be predicted from other measurements (i.e., using a soft-sensing) method. Specific aim 3 focused on developing a RTR strategy for dissolution of tablets made from blends exposed to different strain levels in batch processing (Chapter 6 and 7). The first step towards attaining this goal was to study the effect of strain on tablet properties like tensile strength and porosity, on inter-particle bonding, and the degree of tablet relaxation. Tablets at higher strain levels exhibited maximum axial relaxation, greater recovered elastic energy, and lower tensile strength. This was attributed to the coating of MgSt on different ingredients, compromising the bonding between the particles. Increasing blend shear strain was observed to slow down the rate of drug release from tablets. Near IR diffuse reflectance spectroscopy was observed to pick up the effects of strain on tablet properties. A PLS-2 calibration model was built where the amount of drug released at different time points was used as the dependent variable and the NIR spectra was used as the independent variable. A good agreement between the observed and the predicted dissolution profiles was obtained (f_2, similarity factor values greater than 65).

The fourth and final aim focused on predicting dissolution of tablets obtained from the continuous direct compaction (CDC) line (chapter 8). Four different parameters were

varied in the CDC line throughout the study; API concentration, blender speed, feed frame speed, and compaction force. The RTR approach adopted here was slightly different, where the dissolution profiles were described either using surrogate models (soft sensing) or adopting a model independent modified-PCA approach. The information from the NIR was extracted using PCA and the scores were correlated to the dissolution parameters using MLR models. Individual dissolution profiles could be predicted using this approach with a high correlation between the predicted and the observed dissolution profiles (f_2 values between 75 and 79). This successfully completed the RTR strategy, with the prediction of tablet dissolution profiles using soft sensing combined with at-line Near IR measurements.

9.2. Method Implementation: RTRt for dissolution

The validation results in chapter 7 and 8 demonstrated the feasibility of predicting dissolution profiles based on NIR diffuse reflectance spectra in batch and continuous system. Two different approaches were discussed; a PLS-2 approach, and a 'PCA combined with surrogate model' approach. The PCA combined with surrogate model approach is outlined in Figure 9-1 (left). This approach was easy to implement, describing the dissolution profiles in terms of independent parameters, where the auto correlation between dissolution values at different time points was circumvented. The steps for validation and prediction of a fresh test set using a calibration model are discussed in Figure 9-1 (right). The implementation strategy follows recent European Medicines Agency (EMEA) guidelines that state: "The NIRS method should, as a pre-condition, be able to reject samples that are outside of its defined scope (e.g. out of range, compositionally

incorrect)" [154]. The strategy was implemented by first using PCA to determine whether the spectra were within the defined scope of the model. Thus, PCA was used to determine whether the NIR spectra were similar to those obtained from tablets compressed at a certain force. The second step was to determine whether tablets had the expected drug concentration. This third step predicted the dissolution behavior using the PLS NIR calibration model (chapter 7) or the Multi-linear regression models between the PCA scores and the dissolution parameters (chapter 8). The fourth step compared the NIR predicted dissolution profiles with those obtained from the USP Apparatus 2 dissolution tests. If tablets meet these requirements the batch can be released.

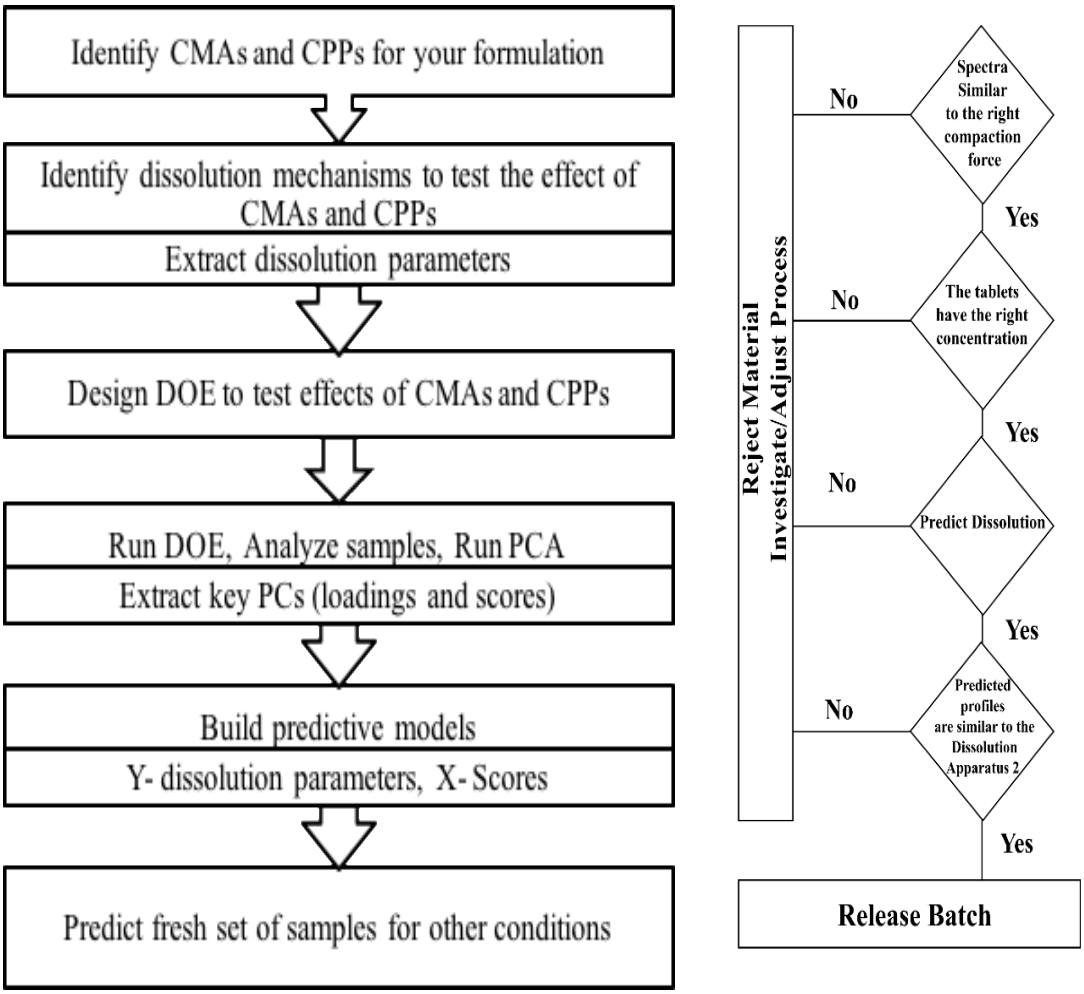

Figure 9-1 –Strategy for dissolution model building using 'tablet NIR and surrogate models (soft sensing)' approach (left). Strategy for prediction of the validation set using the dissolution models (right)- Courtesy: Hernandez *et al*., Prediction of dissolution profiles by non-destructive near infrared spectroscopy in tablets subjected to different levels of strain

9.3. Recommendations for future work

9.3.1. Utilizing the blending platform for different case studies:

Chapter 3,4, and 5 used a blending PAT platform to develop RTR strategies for B.U. and C.U. in batch processing and compare sampling strategies. This strategy was tested for a single API, Phenytoin Sodium. This case study highlighted the presence of API agglomeration and the utility of extensive stratified sampling to detect the agglomerates. Properties of API and excipients can pose potential challenges in developing such platform technologies. Developing effective PAT methodologies for such challenging blends (segregating blends, low potency blends) can help develop representative and robust protocol, and test the potential to repeatedly implement a given PAT system across a manufacturing platform. For such challenging blends, the platform equipped with modern analytical technologies and control models will facilitate development of protocols for effective control during mixing. Process monitoring methods will enable the evaluation of blend uniformity, assay, tendency for segregation, effect of raw material variability, environmental conditions, and other critical parameters associated with achieving the desired state of homogeneity. Investigating different materials will help correlate the "quality" of blends to product critical quality attributes (CQAs) will provide a science-based approach to optimizing blender design, sensor design, mixing protocols, and models for measuring or predicting blend and final product quality. Also, these studies should be carried out using different spectrometers and various chemometric systems to determine instrument dependence of results.

9.3.2. Detection of agglomerates in tablets using Raman Mapping

In chapter 3, 4 and 5, NIR predictions of tablet C.U. yielded results highlighting presence of super potent tablets. As mentioned earlier, for tablets containing a narrow therapeutic index drug, presence of super potent units can have adverse effects on patient health. As highlighted in chapter 5, the presence of drug agglomerates was detected in the blend samples. These blends were further compacted into tablets in a tablet press. The feed frame in tablet press has been observed to exhibit high shear environment which can lead to partial or complete breaking of such agglomerates [116]. As such, tablets need to be studied further to detect and visualize the presence and the degree of agglomeration, if any. This can be accomplished by scanning different tablet layers and obtaining a spatial distribution of API throughout the tablet.

This can be achieved by imaging different layers of the tablet using a chemical imaging system. A primary analysis of some of these super potent tablets was done using mPAT system (H2Optx Inc, San Jose, California) to see if agglomerates were observed in the tablets Figure 9-2. The mPAT system uses Raman Imaging to scan 4mm x 4mm cross section of a tablet. After scanning one layer, a specified thickness of the tablet was shaved off using a ‘pillerator’ attachment, and the new layer of the tablet was scanned again.

Figure 9-2: mPAT LAB+ Pillerator assembly. Enables automatic sectioning of tablets with layer by layer hyperspectral scanning using Raman Spectroscopy

Each of the pixels were analyzed using Classical Least Squares to determine the amount of API and other excipients in them, which was repeated for all the pixels creating a surface image Figure 9-3 (top). These layers were stacked up to obtain a spatial distribution of the API and excipients as shown in Figure 9-3 (bottom). The API is shown in red. Localized clusters of API were observed for one of the super potent tablets.

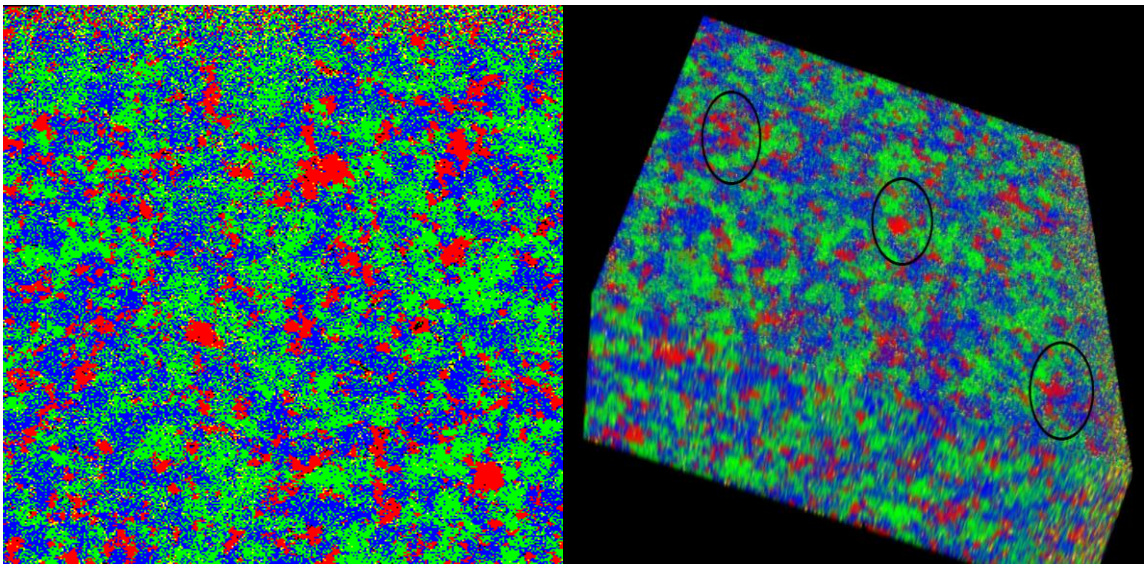

Figure 9-3: Raman imaging for an over-potent (compared to the average) blend O2 tablet. Surface plot of a single layer (left). 3-D stacked plot of 12 layers (right). Agglomerates of Phenytoin Sodium can be observed. Phenytoin-Red, Lactose- Green, MCC- Blue, MgSt- Yellow.

The feasibility of using this tool to locate agglomerates has been discussed here. There are a few issues that need to be addressed. Tablets exhibiting sub-potency should be analyzed and compared to the super potent tablets to determine the differences in the structure and the agglomerates. Efforts must be taken to distinguish and delineate an API agglomerate from the surrounding API pool. The size of the agglomerates should be measured in an effort to quantify the actual amount of API in the agglomerate. An example is shown in Figure 9-4, where the API agglomerates for a tablet containing 12% nominal API are highlighted. The API particles can be categorized based on their size and the agglomerate size can be estimated using this tool. These observations can also be related to the process and the formulation properties to help manufacture better quality tablets.

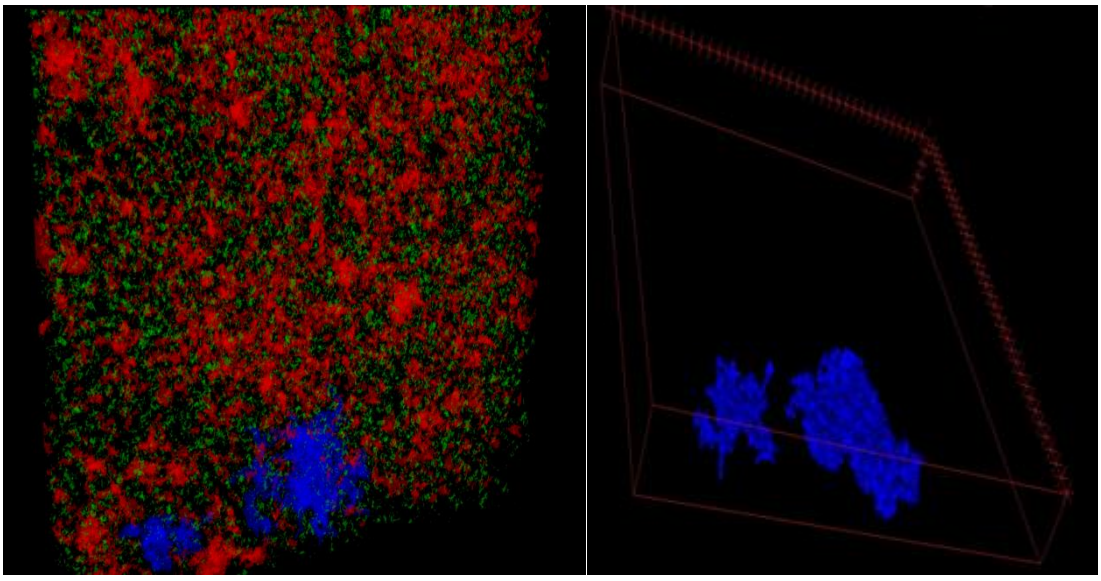

Figure 9-4: Size distribution for API in a tablet containing 12% nominal API concentration. The blue color indicates tablets greater than 250 µ size.

9.3.3. RTRt for dissolution prediction: Investigating different case studies

In an effort to predict dissolution for tablets manufactured in CM systems, only one type of formulation, directly compressed tablets, was examined in chapter 8. This formulation

had relatively simple dissolution behavior, determined primarily by three parameters: tablet porosity, amount of API, and extent of shear experienced by the blend. For such a system, a small number of degrees of freedom are needed to predict dissolution behavior, and both model dependent and model independent methods worked satisfactorily. More complex formulations where drug release might depend on amounts of other ingredients (such as controlled-release polymers and pH modifiers) might require a larger number of factors, and perhaps a more extensive calibration set, but to the extent that the relevant parameters can be tested non-destructively, the methods introduced in chapter 8 are likely to be effective. A broader study involving different formulations should be undertaken, and the merits and demerits of different multivariate methodologies should be examined to predict dissolution in real time. Importantly, once the ability to predict dissolution profiles reliably is properly demonstrated, meeting the remaining requirement for closed-loop quality control, real-time quality assurance, and real-time release should be relatively straightforward.

Appendix I

Multi linear regression equations for dissolution profile parameters:

For model independent parameters:

Level = 74.1239 - 81.658 PC1 + 103.405 PC2 + 30.1696 PC3 + 377.843 PC1*PC2 + 1762.93 PC1*PC3 - 653.277 PC2*PC3 - 38489.1 PC1*PC2*PC3

Coefficients

Term	Coef	SE Coef	T	P
Constant	74.1	0.7	108.247	0.000
PC1	-81.7	13.4	-6.103	0.000
PC2	103.4	25.8	4.015	0.001
PC3	30.2	62.9	0.480	0.636
PC1*PC2	377.8	482.2	0.784	0.442
PC1*PC3	1762.9	1064.2	1.657	0.112
PC2*PC3	-653.3	2311.4	-0.283	0.780
PC1*PC2*PC3	-38489.1	38758.2	-0.993	0.332

Summary of Model

S = 3.65483 R-Sq = 80.05% R-Sq(adj) = 73.40%

\

Shape I = 3.57359 - 330.254 PC1 + 254.108 PC2 + 176.14 PC3 - 1050.08 PC1*PC2 + 6994.8 PC1*PC3 - 2452.04 PC2*PC3 - 109821 PC1*PC2*PC3

Coefficients

Term	Coef	SE Coef	T	P
Constant	4	2	1.45594	0.160
PC1	-330	48	-6.88579	0.000
PC2	254	92	2.75289	0.012
PC3	176	225	0.78142	0.443
PC1*PC2	-1050	1728	-0.60759	0.550
PC1*PC3	6995	3815	1.83369	0.081
PC2*PC3	-2452	8285	-0.29596	0.770
PC1*PC2*PC3	-109821	138926	-0.79050	0.438

Summary of Model

S = 13.1004 R-Sq = 82.15% R-Sq(adj) = 76.19%

Shape II = -0.811668 + 65.2325 PC1 - 100.161 PC2 + 15.1698 PC3 - 566.01 PC1*PC2 - 1989.88 PC1*PC3 + 1310.25 PC2*PC3 + 41747.1 PC1*PC2*PC3

Coefficients

Term	Coef	SE Coef	T	P
Constant	-0.8	0.7	-1.23528	0.230
PC1	65.2	12.8	5.08064	0.000
PC2	-100.2	24.7	-4.05339	0.001
PC3	15.2	60.3	0.25140	0.804
PC1*PC2	-566.0	462.7	-1.22338	0.235
PC1*PC3	-1989.9	1021.2	-1.94862	0.065
PC2*PC3	1310.2	2217.9	0.59076	0.561
PC1*PC2*PC3	41747.1	37190.7	1.12251	0.274

Summary of Model

S = 3.50701 R-Sq = 73.05% R-Sq(adj) = 64.06%

For model dependent parameters:

α = 129.78 + 585.5 PC-1 + 637 PC-2 - 594 PC3 + 9918 PC-1*PC-2 - 3278 PC-1*PC3 + 32418 PC-2*PC3 + 4731 PC-1*PC-2*PC3

Analysis of Variance

Source	DF	Adj SS	Adj MS	F-Value	P-Value
Regression	7	71405.5	10200.8	21.54	0.000
PC-1	1	25578.6	25578.6	54.02	0.000
PC-2	1	8183.8	8183.8	17.28	0.000
PC3	1	1191.0	1191.0	2.52	0.128
PC-1*PC-2	1	5651.6	5651.6	11.94	0.002
PC-1*PC3	1	126.7	126.7	0.27	0.610
PC-2*PC3	1	2627.7	2627.7	5.55	0.028
PC-1*PC-2*PC3	1	0.2	0.2	0.00	0.984
Error	21	9943.4	473.5		
Total	28	81348.8			

Model Summary

R-sq	R-sq(adj)	R-sq(pred)
87.78%	83.70%	80.18%

$\beta = 1.3198 + 0.140\ PC\text{-}1 + 2.242\ PC\text{-}2 - 1.757\ PC3 + 24.76\ PC\text{-}1*PC\text{-}2 + 25.6\ PC\text{-}1*PC3 + 39.8\ PC\text{-}2*PC3 - 978\ PC\text{-}1*PC\text{-}2*PC3$

Analysis of Variance

Source	DF	Adj SS	Adj MS	F-Value	P-Value
Regression	7	0.156565	0.022366	6.65	0.000
PC-1	1	0.001462	0.001462	0.43	0.517
PC-2	1	0.101282	0.101282	30.12	0.000
PC3	1	0.010432	0.010432	3.10	0.093
PC-1*PC-2	1	0.035218	0.035218	10.47	0.004
PC-1*PC3	1	0.007712	0.007712	2.29	0.145
PC-2*PC3	1	0.003953	0.003953	1.18	0.291
PC-1*PC-2*PC3	1	0.008506	0.008506	2.53	0.127
Error	21	0.070610	0.003362		
Total	28	0.227175			

Model Summary

R-sq	R-sq(adj)
68.92%	58.56%

References

[1] "<905> Uniformity of dosage units," United States Pharmacaopeia, USP 29-NF 24.

[2] "Revision Bulletin <701> Disintegration," United States Pharmacopeia (USP), Aug. 2008.

[3] "Guidance for Industry Dissolution Testing of Immediate Release Solid Oral Dosage Forms.," H.H. S., F.D.A, C.D.E. R., Rockville, MD, 1997.

[4] S. L. Lee, T. F. O'Connor, X. Yang, C. N. Cruz, S. Chatterjee, R. D. Madurawe, C. M. V. Moore, L. X. Yu, and J. Woodcock, "Modernizing Pharmaceutical Manufacturing: from Batch to Continuous Production," *J. Pharm. Innov.*, vol. 10, no. 3, pp. 191–199, Mar. 2015.

[5] J. D. Rockoff, "Drug Making Breaks Away From Its Old Ways," *WSJ*. [Online]. Available: http://www.wsj.com/articles/drug-making-breaks-away-from-its-old-ways-1423444049. [Accessed: 01-Mar-2016].

[6] Huiquan Wu, M. A. Khan, and A. S. Hussain, "Process Control Perspective for Process Analytical Technology: Integration of Chemical Engineering Practice into Semiconductor and Pharmaceutical Industries," *Chem. Eng. Commun.*, vol. 194, no. 6, pp. 760–779, Jun. 2007.

[7] J. M. W. Krist V Gernaey, "Introducing mechanistic models in Process Analytical Technology education.," *Biotechnol. J.*, vol. 4, no. 5, pp. 593–9, 2009.

[8] "FDA/ICH. 2006. Guidance for industry. Q8 pharmaceutical development. Available at http://www.fda.gov/cder/guidance/6746fnl.pdf." .

[9] "Process Analytical Technology (PAT) Initiative. U.S. Food and Drug Administration Center for Drug Evaluation and Research Home Page (http:// www.fda.gov/cder/OPS/PAT.htm)." .

[10] A. Drakulich, "Real Time Release Testing." [Online]. Available: http://www.pharmtech.com/real-time-release-testing. [Accessed: 26-Feb-2016].

[11] "Quality Implementation Working Group on Q8, Q9, and Q10 Questions and Answers," ICH, Nov. 2010.

[12] A. P. Ferreira and M. Tobyn, "Multivariate analysis in the pharmaceutical industry: Enabling process understanding and improvement in the PAT and QbD era," *Pharm. Dev. Technol.*, vol. 20, no. 5, pp. 513–527, 2015.

[13] J. Berman, D. E. Elinski, C. R. Gonzales, J. D. Hofer, P. J. Jimenez, J. A. Planchard, R. J. Tlachac, and P. F. Vogel, "Blend uniformity analysis: validation and in-process testing. Technical Report No. 25. PDA (Parenteral Drug association)," *PDA J. Pharm. Sci. Technol. PDA*, vol. 51 Suppl 3, pp. i–iii, S1–99, 1997.

[14] T. Ripley and C. F. Harwood, "Errors Associated with the Thief Probe for Bulk Powder Sampling," *J. Powder Bulk Solids Technol.*, vol. 1, no. 20, pp. 20–29, 1977.

[15] M. Blanco, R. Cueva-Mestanza, and J. Cruz, "Critical evaluation of methods for end-point determination in pharmaceutical blending processes," *Anal. Methods*, vol. 4, no. 9, pp. 2694–2703, Aug. 2012.

[16] T. Shinbrot and F. J. Muzzio, "Nonequilibrium Patterns in Granular Mixing and Segregation," *Phys. Today*, vol. 53, no. 3, pp. 25–30, Jan. 2007.

[17] R. Hogg, "Mixing and Segregation in Powders: Evaluation, Mechanisms and Processes," *KONA Powder Part. J.*, vol. 27, pp. 3–17, 2009.
[18] C. Sajeev, P. R. Jadhav, D. RaviShankar, and R. N. Saha, "Determination of flurbiprofen in pharmaceutical formulations by UV spectrophotometry and liquid chromatography," *Anal. Chim. Acta*, vol. 463, no. 2, pp. 207–217, Jul. 2002.
[19] E. A. Abourashed and I. A. Khan, "High-performance liquid chromatography determination of hydrastine and berberine in dietary supplements containing goldenseal," *J. Pharm. Sci.*, vol. 90, no. 7, pp. 817–822, Jul. 2001.
[20] C. K. Tye, C. (Calvin) Sun, and G. E. Amidon, "Evaluation of the effects of tableting speed on the relationships between compaction pressure, tablet tensile strength, and tablet solid fraction," *J. Pharm. Sci.*, vol. 94, no. 3, pp. 465–472, 2005.
[21] T. Shimizu, Y. Nakano, S. Morimoto, T. Tabata, N. Hamaguchi, and Y. Igari, "Formulation Study for Lansoprazole Fast-disintegrating Tablet. I.
Effect of Compression on Dissolution Behavior," *Chem. Pharm. Bull. (Tokyo)*, vol. 51, no. 8, pp. 942–947, 2003.
[22] A. Uzunović and E. Vranić, "Effect of magnesium stearate concentration on dissolution properties of ranitidine hydrochloride coated tablets," *Bosn. J. Basic Med. Sci. Udruženje Basičnih Med. Znan. Assoc. Basic Med. Sci.*, vol. 7, no. 3, pp. 279–283, Aug. 2007.
[23] K. S. Murthy and J. C. Samyn, "Effect of shear mixing on in vitro drug release of capsule formulations containing lubricants," *J. Pharm. Sci.*, vol. 66, no. 9, pp. 1215–1219, 1977.
[24] K. Pingali, R. Mendez, D. Lewis, B. Michniak-Kohn, A. Cuitiño, and F. Muzzio, "Evaluation of strain-induced hydrophobicity of pharmaceutical blends and its effect on drug release rate under multiple compression conditions," *Drug Dev. Ind. Pharm.*, vol. 37, no. 4, pp. 428–435, Apr. 2011.
[25] P. J. Sheskey, R. T. Robb, R. D. Moore, and B. M. Boyce, "Effects of Lubricant Level, Method of Mixing, and Duration of Mixing on a Controlled-Release Matrix Tablet Containing Hydroxypropyl Methylcellulose," *Drug Dev. Ind. Pharm.*, vol. 21, no. 19, pp. 2151–2165, Jan. 1995.
[26] J. Wang, H. Wen, and D. Desai, "Lubrication in tablet formulations," *Eur. J. Pharm. Biopharm.*, vol. 75, no. 1, pp. 1–15, May 2010.
[27] T. Suzuki and H. Nakagami, "Effect of crystallinity of microcrystalline cellulose on the compactability and dissolution of tablets," *Eur. J. Pharm. Biopharm.*, vol. 47, no. 3, pp. 225–230, May 1999.
[28] H. Mohammed, B. J. Briscoe, and K. G. Pitt, "The interrelationship between the compaction behaviour and the mechanical strength of pure pharmaceutical tablets," *Chem. Eng. Sci.*, vol. 60, no. 14, pp. 3941–3947, Jul. 2005.
[29] M. Donoso and E. S. Ghaly, "Prediction of drug dissolution from tablets using near-infrared diffuse reflectance spectroscopy as a nondestructive method," *Pharm. Dev. Technol.*, vol. 9, no. 3, pp. 247–263, Aug. 2004.
[30] M. P. Freitas, A. Sabadin, L. M. Silva, F. M. Giannotti, D. A. do Couto, E. Tonhi, R. S. Medeiros, G. L. Coco, V. F. T. Russo, and J. A. Martins, "Prediction of drug dissolution profiles from tablets using NIR diffuse reflectance spectroscopy: A

rapid and nondestructive method," *J. Pharm. Biomed. Anal.*, vol. 39, no. 1–2, pp. 17–21, Sep. 2005.

[31] D. Throckmorton, "Examining Drug Shortages and Recent Effort to Address Them," Statement to the House of Representatives, Subcommittee on Health, Committee on Energy & Commerce.

[32] "Current Good Manufacturing Practices for Drugs: Reports, Guidances and Additional Information - Pharmaceutical cGMPS for the 21st Century — A Risk-Based Approach: Second Progress Report and Implementation Plan." [Online]. Available: http://www.fda.gov/Drugs/DevelopmentApprovalProcess/Manufacturing/QuestionsandAnswersonCurrentGoodManufacturingPracticescGMPforDrugs/UCM071836. [Accessed: 28-Feb-2016].

[33] "The New Pharma Factory | Automation World." [Online]. Available: http://www.automationworld.com/batch-manufacturing/new-pharma-factory. [Accessed: 26-Feb-2016].

[34] L. A. and S. H. S. R. of T. W. S. Journal, "New Prescription For Drug Makers: Update the Plants," *WSJ*. [Online]. Available: http://www.wsj.com/articles/SB10625358403931000. [Accessed: 01-Mar-2016].

[35] S. Byrn, M. Futran, H. Thomas, E. Jayjock, N. Maron, R. F. Meyer, A. S. Myerson, M. P. Thien, and B. L. Trout, "Achieving Continuous Manufacturing for Final Dosage Formation: Challenges and How to Meet Them. May 20–21, 2014 Continuous Manufacturing Symposium," *J. Pharm. Sci.*, vol. 104, no. 3, pp. 792–802, Mar. 2015.

[36] A. Mehrotra, M. Llusa, A. Faqih, M. Levin, and F. J. Muzzio, "Influence of shear intensity and total shear on properties of blends and tablets of lactose and cellulose lubricated with magnesium stearate," *Int. J. Pharm.*, vol. 336, no. 2, pp. 284–291, May 2007.

[37] A. U. Vanarase and F. J. Muzzio, "Effect of operating conditions and design parameters in a continuous powder mixer," *Powder Technol.*, vol. 208, no. 1, pp. 26–36, Mar. 2011.

[38] P. M. Portillo, A. U. Vanarase, A. Ingram, J. K. Seville, M. G. Ierapetritou, and F. J. Muzzio, "Investigation of the effect of impeller rotation rate, powder flow rate, and cohesion on powder flow behavior in a continuous blender using PEPT," *Chem. Eng. Sci.*, vol. 65, no. 21, pp. 5658–5668, Nov. 2010.

[39] K. H. Esbensen, D. Guyot, F. Westad, and L. P. Houmoller, *Multivariate Data Analysis - in Practice: An Introduction to Multivariate Data Analysis and Experimental Design*. Multivariate Data Analysis, 2002.

[40] "Wiley: Process Analytical Technology: Spectroscopic Tools and Implementation Strategies for the Chemical and Pharmaceutical Industries, 2nd Edition - Katherine A. Bakeev." [Online]. Available: http://www.wiley.com/WileyCDA/WileyTitle/productCd-047072207X.html. [Accessed: 27-Nov-2015].

[41] P. Geladi and B. R. Kowalski, "Partial least-squares regression: a tutorial," *Anal. Chim. Acta*, vol. 185, pp. 1–17, 1986.

[42] P.-C. Chiang and H. Wong, “Incorporation of physiologically based pharmacokinetic modeling in the evaluation of solubility requirements for the salt selection process: a case study using phenytoin,” *AAPS J.*, vol. 15, no. 4, pp. 1109–1118, Oct. 2013.
[43] N. Madhavi and B. Sudhakar, “Formulation and Evaluation of Phenytoin Sodium Sustained Release Matrix Tablet,” *J. Bioequivalence Bioavailab.*, vol. 04, no. 07, 2013.
[44] P. J. Neuvonen, “Bioavailability of phenytoin: clinical pharmacokinetic and therapeutic implications,” *Clin. Pharmacokinet.*, vol. 4, no. 2, pp. 91–103, Apr. 1979.
[45] R. Gugler, C. V. Manion, and D. L. Azarnoff, “Phenytoin: pharmacokinetics and bioavailability,” *Clin. Pharmacol. Ther.*, vol. 19, no. 2, pp. 135–142, Feb. 1976.
[46] H. Sekikawa, J. Fujiwara, T. Naganuma, M. Nakano, and T. Arita, “Dissolution Behaviors and Gastrointestinal Absorption of Phenytoin in Phenytoin-Polyvinylpyrrolidone Coprecipitate,” *Chem. Pharm. Bull. (Tokyo)*, vol. 26, no. 10, pp. 3033–3039, 1978.
[47] J. N. Barnes and K. L. Rascati, “Switching of Antiepileptic Drug Formulations,” *J. Pediatr. Pharmacol. Ther. JPPT*, vol. 15, no. 2, pp. 64–65, 2010.
[48] D. H. Rosenbaum, A. J. Rowan, L. Tuchman, and J. A. French, “Comparative bioavailability of a generic phenytoin and Dilantin,” *Epilepsia*, vol. 35, no. 3, pp. 656–660, Jun. 1994.
[49] G. Borgheini, “The bioequivalence and therapeutic efficacy of generic versus brand-name psychoactive drugs,” *Clin. Ther.*, vol. 25, no. 6, pp. 1578–1592, Jun. 2003.
[50] F. . Muzzio, C. . Goodridge, A. Alexander, P. Arratia, H. Yang, O. Sudah, and G. Mergen, “Sampling and characterization of pharmaceutical powders and granular blends,” *Int. J. Pharm.*, vol. 250, no. 1, pp. 51–64, Jan. 2003.
[51] J. T. Carstensen and C. T. Rhodes, “Sampling in Blending Validation,” *Drug Dev. Ind. Pharm.*, vol. 19, no. 20, pp. 2699–2708, Jan. 1993.
[52] T. P. Garcia, M. K. Taylor, and G. S. Pande, “Comparison of the performance of two sample thieves for the determination of the content uniformity of a powder blend,” *Pharm. Dev. Technol.*, vol. 3, no. 1, pp. 7–12, Feb. 1998.
[53] FDA, “Guidance for Industry: PAT - A Framework for Innovative Pharmaceutical Development, Manufacturing, and Quality Assurance,” Food and Drug Administration, 2004.
[54] “Guidance for Industry Powder Blends and Finished Dosage Units — Stratified In-Process Dosage Unit Sampling and Assessment.”
[55] D. J. Wargo and J. K. Drennen, “Near-infrared spectroscopic characterization of pharmaceutical powder blends,” *J. Pharm. Biomed. Anal.*, vol. 14, no. 11, pp. 1415–1423, Aug. 1996.
[56] Z. Shi, R. P. Cogdill, S. M. Short, and C. A. Anderson, “Process characterization of powder blending by near-infrared spectroscopy: Blend end-points and beyond,” *J. Pharm. Biomed. Anal.*, vol. 47, no. 4–5, pp. 738–745, Aug. 2008.
[57] H. Wu, M. Tawakkul, M. White, and M. A. Khan, “Quality-by-Design (QbD): An integrated multivariate approach for the component quantification in powder blends,” *Int. J. Pharm.*, vol. 372, no. 1–2, pp. 39–48, May 2009.

[58] P. A. Hailey, P. Doherty, P. Tapsell, T. Oliver, and P. K. Aldridge, "Automated system for the on-line monitoring of powder blending processes using near-infrared spectroscopy. Part I. System development and control," *J. Pharm. Biomed. Anal.*, vol. 14, no. 5, pp. 551–559, Mar. 1996.

[59] S. S. Sekulic, J. Wakeman, P. Doherty, and P. A. Hailey, "Automated system for the on-line monitoring of powder blending processes using near-infrared spectroscopy: Part II. Qualitative approaches to blend evaluation," *J. Pharm. Biomed. Anal.*, vol. 17, no. 8, pp. 1285–1309, Sep. 1998.

[60] O. Berntsson, L.-G. Danielsson, B. Lagerholm, and S. Folestad, "Quantitative in-line monitoring of powder blending by near infrared reflection spectroscopy," *Powder Technol.*, vol. 123, no. 2–3, pp. 185–193, Mar. 2002.

[61] E. T. S. Skibsted, H. F. M. Boelens, J. A. Westerhuis, D. T. Witte, and A. K. Smilde, "Simple assessment of homogeneity in pharmaceutical mixing processes using a near-infrared reflectance probe and control charts," *J. Pharm. Biomed. Anal.*, vol. 41, no. 1, pp. 26–35, Apr. 2006.

[62] A. S. El-Hagrasy, H. R. Morris, F. D'Amico, R. A. Lodder, and J. K. Drennen, "Near-infrared spectroscopy and imaging for the monitoring of powder blend homogeneity," *J. Pharm. Sci.*, vol. 90, no. 9, pp. 1298–1307, Sep. 2001.

[63] O. Berntsson, L.-G. Danielsson, M. O. Johansson, and S. Folestad, "Quantitative determination of content in binary powder mixtures using diffuse reflectance near infrared spectrometry and multivariate analysis," *Anal. Chim. Acta*, vol. 419, no. 1, pp. 45–54, Aug. 2000.

[64] J. G. Osorio and F. J. Muzzio, "Evaluation of resonant acoustic mixing performance," *Powder Technol.*, vol. 278, pp. 46–56, Jul. 2015.

[65] S. S. Sekulic, H. W. Ward, D. R. Brannegan, E. D. Stanley, C. L. Evans, S. T. Sciavolino, P. A. Hailey, and P. K. Aldridge, "On-line monitoring of powder blend homogeneity by near-infrared spectroscopy," *Anal. Chem.*, vol. 68, no. 3, pp. 509–513, Feb. 1996.

[66] P. Merckle and K. A. Kovar, "Assay of effervescent tablets by near-infrared spectroscopy in transmittance and reflectance mode: acetylsalicylic acid in mono and combination formulations," *J. Pharm. Biomed. Anal.*, vol. 17, no. 3, pp. 365–374, Jul. 1998.

[67] M. Otsuka and I. Yamane, "Prediction of tablet properties based on near infrared spectra of raw mixed powders by chemometrics: Scale-up factor of blending and tableting processes," *J. Pharm. Sci.*, vol. 98, no. 11, pp. 4296–4305, Nov. 2009.

[68] M. Blanco, M. Bautista, and M. Alcalà, "API Determination by NIR Spectroscopy Across Pharmaceutical Production Process," *AAPS PharmSciTech*, vol. 9, no. 4, pp. 1130–1135, Nov. 2008.

[69] P. Pawar, E. Hernandez, S. Rodriguez, S. Lysenko, F. J. Muzzio, and R. J. Romañach, "The Effect of Shear Applied During a Pharmaceutical Process on Near Infrared Spectra," *Appl. Spectrosc.*, vol. 70, no. 3, pp. 455–466, 2016.

[70] E. Hernandez, P. Pawar, G. Keyvan, Y. Wang, N. Velez, G. Callegari, A. Cuitino, B. Michniak-Kohn, F. J. Muzzio, and R. J. Romañach, "Prediction of dissolution profiles by non-destructive near infrared spectroscopy in tablets subjected to

different levels of strain," *J. Pharm. Biomed. Anal.*, vol. 117, pp. 568–576, Jan. 2016.
[71] G. E. Ritchie, R. W. Roller, E. W. Ciurczak, H. Mark, C. Tso, and S. A. MacDonald, "Validation of a near-infrared transmission spectroscopic procedure: Part B: Application to alternate content uniformity and release assay methods for pharmaceutical solid dosage forms," *J. Pharm. Biomed. Anal.*, vol. 29, no. 1–2, pp. 159–171, Jun. 2002.
[72] J. Philip, I. J. Holcomb, and S. A. Fusari, "Phenytoin," in *Analytical Profiles of Drug Substances*, vol. 13, K. Florey, Ed. Academic Press, 1984, pp. 417–445.
[73] S. H. Atwell, V. A. Green, and W. G. Haney, "Development and evaluation of method for simultaneous determination of phenobarbital and diphenylhydantoin in plasma by high-pressure liquid chromatography," *J. Pharm. Sci.*, vol. 64, no. 5, pp. 806–809, May 1975.
[74] "United States Pharmacopeia and National Formulary USP-29 NF 24. The United States Pharmacopeial Convention, Inc., Rockville, MD, 2007," p. 1722.
[75] M. V. Velasco and A. R. Rajabi-Siahboomi, "Tablet lubrication: Problems and perspectives," *Pharm. Technol.*, Dec. 1998.
[76] L. Roblot-Treupel and F. Puisieux, "Distribution of magnesium stearate on the surface of lubricated particles," *Int. J. Pharm.*, vol. 31, no. 1–2, pp. 131–136, Jul. 1986.
[77] M. Perrault, F. Bertrand, and J. Chaouki, "An investigation of magnesium stearate mixing in a V-blender through gamma-ray detection," *Powder Technol.*, vol. 200, no. 3, pp. 234–245, Jun. 2010.
[78] A. T. Serajuddin and C. I. Jarowski, "Influence of pH on release of phenytoin sodium from slow-release dosage forms," *J. Pharm. Sci.*, vol. 82, no. 3, pp. 306–310, Mar. 1993.
[79] G. Morin and L. Briens, "The Effect of Lubricants on Powder Flowability for Pharmaceutical Application," *AAPS PharmSciTech*, vol. 14, no. 3, pp. 1158–1168, Jul. 2013.
[80] *United States of America vs. Barr Laboratories Inc. Civil action for the District of New Jersey, February 1993.* .
[81] "Federal Register/ vol.78, NO.152, p. 48175-48176, August 7, 2013/Notices."
[82] "Sampling: A Vital Process in Evaluating Blending and Segregation Problems | Powder/Bulk Solids." [Online]. Available: http://www.powderbulksolids.com/article/sampling-vital-process-evaluating-blending-and-segregation-problems. [Accessed: 12-Mar-2016].
[83] T. Garcia, B. Elsheimer, and F. Tarczynski, "Examination of Components of Variance for A Production Scale, Low Dose Powder Blend and Resulting Tablets," *Drug Dev. Ind. Pharm.*, vol. 21, no. 18, pp. 2035–2045, Jan. 1995.
[84] T. P. Garcia, A. Carella, and V. Pansa, "Identification of factors decreasing the homogeneity of blend and tablet uniformity," *Pharm. Technol.*, vol. 28, no. 3, pp. 110–122, 2004.
[85] M. Llusa and F. Muzzio, "A Quantitative Method for Modeling Blend Composition Distributions in the Presence of Agglomerates," *J. Pharm. Innov.*, vol. 2, no. 1–2, pp. 51–64, Oct. 2007.

[86] M. Llusa, K. Sturm, O. Sudah, H. Stamato, D. J. Goldfarb, H. Ramachandruni, S. Hammond, M. R. Smith, and F. J. Muzzio, "Effect of High Shear Blending Protocols and Blender Parameters on the Degree of API Agglomeration in Solid Formulations," *Ind. Eng. Chem. Res.*, vol. 48, no. 1, pp. 93–101, Jan. 2009.
[87] F. J. M. A Alexander, "Segregation patterns in V-blenders," *Chem. Eng. Sci. - CHEM ENG SCI*, vol. 58, no. 2, pp. 487–496, 2003.
[88] X. He, X. Han, N. Ladyzhynsky, and R. Deanne, "Assessing powder segregation potential by near infrared (NIR) spectroscopy and correlating segregation tendency to tabletting performance," *Powder Technol.*, vol. 236, pp. 85–99, Feb. 2013.
[89] T. P. Garcia, S. J. Wilkinson, and J. F. Scott, "The development of a blend-sampling technique to assess the uniformity of a powder mixture," *Drug Dev. Ind. Pharm.*, vol. 27, no. 4, pp. 297–307, Apr. 2001.
[90] R. E. Freeman, J. R. Cooke, and L. C. R. Schneider, "Measuring shear properties and normal stresses generated within a rotational shear cell for consolidated and non-consolidated powders," *Powder Technol.*, vol. 190, no. 1–2, pp. 65–69, Mar. 2009.
[91] Y. Wang, S. Koynov, B. J. Glasser, and F. J. Muzzio, "A method to analyze shear cell data of powders measured under different initial consolidation stresses," *Powder Technol.*, vol. 294, pp. 105–112, Jun. 2016.
[92] M. J. Mollan Jr. and M. Çelik, "The effects of lubrication on the compaction and post-compaction properties of directly compressible maltodextrins," *Int. J. Pharm.*, vol. 144, no. 1, pp. 1–9, 1996.
[93] A. H. De Boer, G. K. Bolhuis, and C. F. Lerk, "Bonding characteristics by scanning electron microscopy of powders mixed with magnesium stearate," *Powder Technol.*, vol. 20, no. 1, pp. 75–82, May 1978.
[94] H. Vromans, G. K. Bolhuis, and C. F. Lerk, "Magnesium stearate susceptibility of directly compressible materials as an indication of fragmentation properties," *Powder Technol.*, vol. 54, no. 1, pp. 39–44, Jan. 1988.
[95] K. Pingali, R. Mendez, D. Lewis, B. Michniak-Kohn, A. Cuitiño, and F. Muzzio, "Mixing order of glidant and lubricant – Influence on powder and tablet properties," *Int. J. Pharm.*, vol. 409, no. 1–2, pp. 269–277, May 2011.
[96] M. Llusa, *Towards Scientific Manufacturing: The Effects of Shear Rate, Strain, and Composition on the Properties of Blends and Tablets*. ProQuest, 2008.
[97] H. Abe and M. Otsuka, "Effects of lubricant-mixing time on prolongation of dissolution time and its prediction by measuring near infrared spectra from tablets," *Drug Dev. Ind. Pharm.*, vol. 38, no. 4, pp. 412–419, Apr. 2012.
[98] O. Antikainen and J. Yliruusi, "Determining the compression behaviour of pharmaceutical powders from the force–distance compression profile," *Int. J. Pharm.*, vol. 252, no. 1–2, pp. 253–261, Feb. 2003.
[99] N. Kottala, A. Abebe, O. Sprockel, J. Bergum, F. Nikfar, and A. M. Cuitiño, "Evaluation of the performance characteristics of bilayer tablets: Part I. Impact of material properties and process parameters on the strength of bilayer tablets," *AAPS PharmSciTech*, vol. 13, no. 4, pp. 1236–1242, Dec. 2012.
[100] A. Mehrotra, M. Llusa, A. Faqih, M. Levin, and F. J. Muzzio, "Influence of shear intensity and total shear on properties of blends and tablets of lactose and cellulose

lubricated with magnesium stearate," *Int. J. Pharm.*, vol. 336, no. 2, pp. 284–291, May 2007.
[101] T. Iqbal, B. J. Briscoe, S. Yasin, and P. F. Luckham, "Continuous stiffness mode nanoindentation response of poly(methyl methacrylate) surfaces," *Chin. J. Polym. Sci.*, vol. 31, no. 8, pp. 1096–1107, May 2013.
[102] B. Thompson, "Effect sizes, confidence intervals, and confidence intervals for effect sizes," *Psychol. Sch.*, vol. 44, no. 5, pp. 423–432, May 2007.
[103] S. Patel, A. M. Kaushal, and A. K. Bansal, "Compression physics in the formulation development of tablets," *Crit. Rev. Ther. Drug Carrier Syst.*, vol. 23, no. 1, pp. 1–65, 2006.
[104] "Discussion of Ryshkewitch Paper by Winston Duckworth*," *J. Am. Ceram. Soc.*, vol. 36, no. 2, pp. 68–68, Feb. 1953.
[105] K. Zuurman, K. Van der Voort Maarschalk, and G. K. Bolhuis, "Effect of magnesium stearate on bonding and porosity expansion of tablets produced from materials with different consolidation properties," *Int. J. Pharm.*, vol. 179, no. 1, pp. 107–115, Mar. 1999.
[106] J. B. Dressman, G. L. Amidon, C. Reppas, and V. P. Shah, "Dissolution Testing as a Prognostic Tool for Oral Drug Absorption: Immediate Release Dosage Forms," *Pharm. Res.*, vol. 15, no. 1, pp. 11–22, Jan. 1998.
[107] "In Vitro Dissolution Testing for Solid Oral Dosage Forms," *Part. Sci.*, vol. 5, 2010.
[108] "FIP Guidelines for Dissolution Testing of Solid Oral Products," vol. 5, no. 14, 1997.
[109] J. Kukura, J. L. Baxter, and F. J. Muzzio, "Shear distribution and variability in the USP Apparatus 2 under turbulent conditions," *Int. J. Pharm.*, vol. 279, no. 1–2, pp. 9–17, Jul. 2004.
[110] J. Kukura, P. E. Arratia, E. S. Szalai, and F. J. Muzzio, "Engineering tools for understanding the hydrodynamics of dissolution tests," *Drug Dev. Ind. Pharm.*, vol. 29, no. 2, pp. 231–239, Feb. 2003.
[111] Z. Gao, T. W. Moore, A. P. Smith, W. H. Doub, and B. J. Westenberger, "Studies of variability in dissolution testing with USP apparatus 2," *J. Pharm. Sci.*, vol. 96, no. 7, pp. 1794–1801, Jul. 2007.
[112] M. Röst and P.-O. Quist, "Dissolution of USP prednisone calibrator tablets: effects of stirring conditions and particle size distribution," *J. Pharm. Biomed. Anal.*, vol. 31, no. 6, pp. 1129–1143, Apr. 2003.
[113] "Guidance for Industry: Q8(R2) Pharmaceutical Development, USDHHS, FDA, CDER, CBER, ICH, Rockville, MD, US," vol. 1–25, 2009.
[114] V. Gray, G. Kelly, M. Xia, C. Butler, S. Thomas, and S. Mayock, "The Science of USP 1 and 2 Dissolution: Present Challenges and Future Relevance," *Pharm. Res.*, vol. 26, no. 6, pp. 1289–1302, Jan. 2009.
[115] A. U. Vanarase and F. J. Muzzio, "Effect of operating conditions and design parameters in a continuous powder mixer," *Powder Technol.*, vol. 208, no. 1, pp. 26–36, Mar. 2011.

[116] R. Mendez, F. J. Muzzio, and C. Velazquez, "Powder hydrophobicity and flow properties: Effect of feed frame design and operating parameters," *AIChE J.*, vol. 58, no. 3, pp. 697–706, 2012.
[117] M. Alcalà, M. Blanco, J. C. Menezes, P. M. Felizardo, A. Garrido, D. Pérez, E. Zamora, C. Pasquini, and R. J. Romañach, "Near-Infrared Spectroscopy in Laboratory and Process Analysis," in *Encyclopedia of Analytical Chemistry*, John Wiley & Sons, Ltd, 2006.
[118] P. N. Zannikos, W. I. Li, J. K. Drennen, and R. A. Lodder, "Spectrophotometric prediction of the dissolution rate of carbamazepine tablets," *Pharm. Res.*, vol. 8, no. 8, pp. 974–978, Aug. 1991.
[119] M. P. Freitas, A. Sabadin, L. M. Silva, F. M. Giannotti, D. A. do Couto, E. Tonhi, R. S. Medeiros, G. L. Coco, V. F. T. Russo, and J. A. Martins, "Prediction of drug dissolution profiles from tablets using NIR diffuse reflectance spectroscopy: A rapid and nondestructive method," *J. Pharm. Biomed. Anal.*, vol. 39, no. 1–2, pp. 17–21, Sep. 2005.
[120] G. T. M. Blanco M. Alcalá, "Determination of dissolution profiles in intact pharmaceutical tablets by NIR spectroscopy," *J. Process Anal. Technol.*, vol. 3, pp. 25–29, 2006.
[121] V. A. Lozano, J. M. Camiña, M. S. Boeris, and E. J. Marchevsky, "Simultaneous determination of sorbic and benzoic acids in commercial juices using the PLS-2 multivariate calibration method and validation by high performance liquid chromatography," *Talanta*, vol. 73, no. 2, pp. 282–286, Sep. 2007.
[122] M. Otsuka, H. Tanabe, K. Osaki, K. Otsuka, and Y. Ozaki, "Chemoinformetrical evaluation of dissolution property of indomethacin tablets by near-infrared spectroscopy," *J. Pharm. Sci.*, vol. 96, no. 4, pp. 788–801, Apr. 2007.
[123] S. H. Tabasi, V. Moolchandani, R. Fahmy, and S. W. Hoag, "Sustained release dosage forms dissolution behavior prediction: a study of matrix tablets using NIR spectroscopy," *Int. J. Pharm.*, vol. 382, no. 1–2, pp. 1–6, Dec. 2009.
[124] J. Ropero, Y. Colón, B. Johnson-Restrepo, and R. J. Romañach, "Near-infrared chemical imaging slope as a new method to study tablet compaction and tablet relaxation," *Appl. Spectrosc.*, vol. 65, no. 4, pp. 459–465, Apr. 2011.
[125] A. Żarów, B. Zhou, X. Wang, R. Pinal, and Z. Iqbal, "Spectroscopic and X-Ray Diffraction Study of Structural Disorder in Cryomilled and Amorphous Griseofulvin," *Appl. Spectrosc.*, vol. 65, no. 2, pp. 135–143, Feb. 2011.
[126] S. M. Short, R. P. Cogdill, P. L. D. Wildfong, J. K. Drennen, and C. A. Anderson, "A near-infrared spectroscopic investigation of relative density and crushing strength in four-component compacts," *J. Pharm. Sci.*, vol. 98, no. 3, pp. 1095–1109, Mar. 2009.
[127] M. J. Barajas, A. R. Cassiani, W. Vargas, C. Conde, J. Ropero, J. Figueroa, and R. J. Romañach, "Near-infrared spectroscopic method for real-time monitoring of pharmaceutical powders during voiding," *Appl. Spectrosc.*, vol. 61, no. 5, pp. 490–496, May 2007.
[128] T. Næs, *A User-friendly Guide to Multivariate Calibration and Classification*. NIR Publications, 2002.

[129] H. Martens and M. Martens, “Multivariate Analysis of Quality. An Introduction,” *Meas. Sci. Technol.*, vol. 12, no. 10, p. 1746, 2001.
[130] R. M. Maggio, P. M. Castellano, and T. S. Kaufman, “A new principal component analysis-based approach for testing ‘similarity’ of drug dissolution profiles,” *Eur. J. Pharm. Sci. Off. J. Eur. Fed. Pharm. Sci.*, vol. 34, no. 1, pp. 66–77, May 2008.
[131] R. M. Maggio, P. M. Castellano, and T. S. Kaufman, “PCA-CR analysis of dissolution profiles. A chemometric approach to probe the polymorphic form of the active pharmaceutical ingredient in a drug product,” *Int. J. Pharm.*, vol. 378, no. 1–2, pp. 187–193, Aug. 2009.
[132] “FDA. Guidance for Industry: Dissolution Testing of Immediate Release Solid Oral Dosage Forms.” 1997.
[133] V. P. Shah, Y. Tsong, P. Sathe, and J.-P. Liu, “In Vitro Dissolution Profile Comparison—Statistics and Analysis of the Similarity Factor, f2,” *Pharm. Res.*, vol. 15, no. 6, pp. 889–896, Jun. 1998.
[134] A. U. Vanarase, J. G. Osorio, and F. J. Muzzio, “Effects of powder flow properties and shear environment on the performance of continuous mixing of pharmaceutical powders,” *Powder Technol.*, vol. 246, pp. 63–72, Sep. 2013.
[135] P. M. Portillo, M. G. Ierapetritou, and F. J. Muzzio, “Effects of rotation rate, mixing angle, and cohesion in two continuous powder mixers—A statistical approach,” *Powder Technol.*, vol. 194, no. 3, pp. 217–227, Sep. 2009.
[136] F. J. M. Aditya U. Vanarase, “Effect of operating conditions and design parameters in a continuous powder mixer,” *Powder Technol.*, vol. 208, no. 1, pp. 26–36, 2011.
[137] J. Osorio and W. J. Engisch, “Bulk and Micro-Scale Characterization of Continuous Powder Blending Integrated with an Multi-Point in-Line NIR As a PAT Tool,” presented at the AIChE Annual Meeting 2012, 2012.
[138] Y. Cui, X. Song, M. Reynolds, K. Chuang, and M. Xie, “Interdependence of drug substance physical properties and corresponding quality control strategy,” *J. Pharm. Sci.*, vol. 101, no. 1, pp. 312–321, Jan. 2012.
[139] E. B. Basalious, W. El-Sebaie, and O. El-Gazayerly, “Application of pharmaceutical QbD for enhancement of the solubility and dissolution of a class II BCS drug using polymeric surfactants and crystallization inhibitors: development of controlled-release tablets,” *AAPS PharmSciTech*, vol. 12, no. 3, pp. 799–810, Sep. 2011.
[140] M. Dumarey, D. J. Goodwin, and C. Davison, “Multivariate modelling to study the effect of the manufacturing process on the complete tablet dissolution profile,” *Int. J. Pharm.*, vol. 486, no. 1–2, pp. 112–120, May 2015.
[141] M. A. Polizzi and S. García-Muñoz, “A framework for in-silico formulation design using multivariate latent variable regression methods,” *Int. J. Pharm.*, vol. 418, no. 2, pp. 235–242, Oct. 2011.
[142] L. Xie, H. Wu, M. Shen, L. L. Augsburger, R. C. Lyon, M. A. Khan, A. S. Hussain, and S. W. Hoag, “Quality-by-design (QbD): effects of testing parameters and formulation variables on the segregation tendency of pharmaceutical powder measured by the ASTM D 6940-04 segregation tester,” *J. Pharm. Sci.*, vol. 97, no. 10, pp. 4485–4497, Oct. 2008.

[143] S. A. Sande and K. Dyrstad, “A Formulation Development Strategy for Multivariate Kinetic Responses,” *Drug Dev. Ind. Pharm.*, vol. 28, no. 5, pp. 583–591, Jan. 2002.
[144] J. Huang, C. Goolcharran, and K. Ghosh, “A Quality by Design approach to investigate tablet dissolution shift upon accelerated stability by multivariate methods,” *Eur. J. Pharm. Biopharm. Off. J. Arbeitsgemeinschaft Für Pharm. Verfahrenstechnik EV*, vol. 78, no. 1, pp. 141–150, May 2011.
[145] J. Siepmann and F. Siepmann, “Mathematical modeling of drug dissolution,” *Int. J. Pharm.*, vol. 453, no. 1, pp. 12–24, Aug. 2013.
[146] P. Costa and J. M. Sousa Lobo, “Modeling and comparison of dissolution profiles,” *Eur. J. Pharm. Sci.*, vol. 13, no. 2, pp. 123–133, May 2001.
[147] Y. Wang, R. D. Snee, G. Keyvan, and F. J. Muzzio, “Statistical comparison of dissolution profiles,” *Drug Dev. Ind. Pharm.*, pp. 1–12, Aug. 2015.
[148] Y. Zhang, M. Huo, J. Zhou, A. Zou, W. Li, C. Yao, and S. Xie, “DDSolver: An Add-In Program for Modeling and Comparison of Drug Dissolution Profiles,” *AAPS J.*, vol. 12, no. 3, pp. 263–271, Apr. 2010.
[149] K. P. Burnham and D. R. Anderson, *Model Selection and Multimodel Inference: A Practical Information-Theoretic Approach*. Springer Science & Business Media, 2003.
[150] K. R. Beebe, R. J. Pell, and M. B. Seasholtz, *Chemometrics: a practical guide*. Wiley, 1998.
[151] A. Savitzky and M. J. E. Golay, “Smoothing and Differentiation of Data by Simplified Least Squares Procedures.,” *Anal. Chem.*, vol. 36, no. 8, pp. 1627–1639, Jul. 1964.
[152] W. Li, L. Bagnol, M. Berman, R. A. Chiarella, and M. Gerber, “Applications of NIR in early stage formulation development. Part II. Content uniformity evaluation of low dose tablets by principal component analysis,” *Int. J. Pharm.*, vol. 380, no. 1–2, pp. 49–54, Oct. 2009.
[153] K. H. Esbensen and P. Geladi, “2.13 - Principal Component Analysis: Concept, Geometrical Interpretation, Mathematical Background, Algorithms, History, Practice,” in *Comprehensive Chemometrics*, S. D. B. T. Walczak, Ed. Oxford: Elsevier, 2009, pp. 211–226.
[154] “Guideline on the use of near infrared spectroscopy by the pharmaceutical industry and the data requirements for new submissions and variations, EMEA, CHMP, CVMP, QWP, London, U.K.,” vol. 1, no. 28, 2014.